



UNIVERSITÀ
DEGLI STUDI
FIRENZE

PhD in
Scienze Biomediche

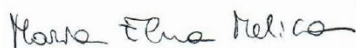
CYCLE XXXIV

COORDINATOR Prof. Fabrizio Chiti

**Glomerular crescents derive from hyperplasia of
single progenitors and a drug enhancing their
differentiation into podocytes attenuates crescentic
glomerulonephritis**

Academic Discipline (SSD) MED/14

Doctoral Candidate
Dr. Melica Maria Elena



(signature)

Supervisor
Prof. Romagnani Paola



(signature)

Coordinator
Prof. Chiti Fabrizio

(signature)

Years 2018/2021

Summary

1. Introduction	1
1.1 Glomerulonephritis.....	1
1.2 Non-proliferative glomerulonephritis.....	2
1.3 Proliferative glomerulonephritis.....	5
1.4 Glomerular crescent	7
1.5 Fibrocellular and fibrous crescents.....	8
1.6 Periglomerular inflammation and ruptures of Bowman’s capsule.....	9
1.7 Origin of the crescents in the glomerulus.....	9
1.8 Phenotypic characteristics of glomerular epithelial parietal cells.....	11
1.9 Phenotypic characteristics of glomerular epithelial parietal cells . Errore. Il segnalibro non è definito.	
1.10 Functional characteristics of PEC: renal progenitor cells.....	14
1.11 Role of PEC in the genesis of glomerular pathologies	23
1.12 Molecular pathways of parietal epithelial cell hyperplasia in crescentic glomerulonephritis	26
1.12.1 CD44 and CD9	26
1.12.2 Glucocorticoids	28
1.12.3 Heparin-binding epidermal growth factor-like growth factor	28
1.13 Therapeutic strategies in use for the treatment of RPGN	29
2. Study design.....	30
3. Materials and methods.....	32
3.1 Human kidney biopsies	32
3.2 Animal studies.....	32
3.3 Transgenic mouse models	33
3.4 Genotyping.....	35
3.5 Blood urea nitrogen measurement.....	36
3.6 Albumin and Creatinine excretion measurement.....	36
3.7 Transcutaneous measurement of glomerular filtration rate.....	36
3.8 Histological analysis	37
3.9 Immunofluorescence and confocal microscopy	37
3.10 Optical tissue clearing and confocal 3D reconstruction	39
3.11 STED microscopy and slit diaphragms density quantification	40
3.12 Clone frequency analysis	40
3.13 Calculating observed and theoretical distribution of crescent colors.....	41
3.14 Crescent quantification and podocyte regeneration.....	42

3.15 Analysis of glomerular damage in kidney sections upon optical tissue clearing.....	43
3.16 Single cell RNA sequencing	43
3.17 Bioinformatic Analysis on mouse samples.....	45
3.18 Bioinformatic Analysis on human samples	46
3.19 Differentiation of murine bone marrow-derived macrophages.....	47
3.20 Generation of necrotic soups.....	48
3.21 Stimulation of bone marrow-derived macrophages.....	49
3.22 Flow cytometry analysis of macrophages.....	49
3.23 ELISA.....	49
3.24 RPC cultures	50
3.25 MTT assay.....	50
3.26 Annexin-V/ Propidium Iodide staining and cell cycle analysis.....	50
3.27 <i>In vitro</i> differentiation.....	51
4 Results.....	53
4.1 Crescents derive from Pax2+ progenitors of the Bowman capsule.....	53
4.2 Crescents originate from clonal expansion of single Pax2+ progenitors.....	54
4.3 Panobinostat attenuates crescentic glomerulonephritis	58
4.4 Panobinostat promotes the generation of new podocyte	61
4.5 Panobinostat improves 3D glomerular structure and restores slit diaphragm integrity .	70
4.6 Delayed treatment with panobinostat maintains renoprotective capacity and avoids chronic kidney disease	73
4.7 Expansion within crescents of a PEC subset expressing CD133 and stratifin associates with patient outcome	76
4.8 Panobinostat inhibits RPC proliferation and promotes their differentiation into podocytes also in humans.....	84
5. Discussion.....	88
References	94

1. Introduction

Crescentic glomerulonephritis encompasses a group of diverse disorders characterized by the presence of massive hyperplasia of parietal epithelial cells (PEC) as the main histopathological lesion at kidney biopsy (1, 2). It is associated with a rapid decline in kidney function referred to altogether as rapidly progressive glomerulonephritis (1, 2). Anti-neutrophil cytoplasmic antibody-associated small-vessel vasculitis is the most frequent underlying diagnosis (3), but rapidly progressive glomerulonephritis also occurs with cryoglobulinemic vasculitis, anti-glomerular basement membrane (GBM) disease (4), lupus nephritis, and other forms of immune complex glomerulonephritis. Crescents involving more than 50% of glomeruli associate with poor prognosis in terms of kidney function and patient survival.

1.1 Glomerulonephritis

The term glomerulonephritis encompasses a number of immune-mediated disorders that cause inflammation in the glomerulus and other compartments of the kidney. The pathogenesis of these diseases is very complex and still not fully understood; it derives from a number of factors:

- different endogenous and exogenous processes can cause this type of disease, for example phenomena of autoimmunity, cancer and ultrastructural abnormalities within the kidney, but also both bacterial and pharmacological infections.
- the genetic factor that determines a great individual variability in the susceptibility to the development of these diseases also plays an important role in the pathogenesis.
- there are complex cytokines between soluble factors (chemokines and growth factors)

and the cells of the kidney itself that cause inflammation within the glomerulus.

- Renal damage is a progressive damage and this is due to the contribution of non-specific factors such as hypertension and proteinuria.

Inflammation of the glomeruli in these pathologies can lead to the development of a nephrotic syndrome and a nephritic syndrome. Nephrotic syndrome, characterized by the presence of plasma proteins in the urine (proteinuria), is caused by the loss of podocytes on the glomerular filtration membrane due to inflammation of the glomeruli; Furthermore, a minor protein causes, especially of the albumen, is excreted with this relative blood pressure of the oncosis and consequent edema.

Nephritic syndrome, characterized by the presence of blood in the urine, in dysmorphic red blood cells (hematuria), is particularly caused by the destruction of the epithelial barrier following inflammation of the cells lining the glomerulus.

Glomerulonephritis are divided into two broad categories: proliferative and nonproliferative and their diagnosis is very important since the outcome of the disease and treatment differ in the different subtypes (5).

1.2 Non-proliferative glomerulonephritis

In the context of non-proliferative diseases, altered number of cells in the glomerulus is not reported and these forms normally cause nephrotic syndrome:

- **Focal Segmental Glomerulosclerosis (FSGS):** Focal segmental glomerulosclerosis is characterized by systemic hypertension, renal failure, steroid resistance, and glomerular sclerolytic lesions. Hyalinosis affects only a portion (segmental glomerulosclerosis) less than 50% (focal glomerulosclerosis) of the glomeruli and the first to be affected are the juxtamedullary ones. At the glomerular level there is an accumulation of hyaline acellular subendothelial material and the typical detachment of podocytes from the basement

membrane (Fig. 1) (6). Focal segmental glomerulosclerosis can occur in association with other factors (secondary focal segmental glomerulosclerosis), including drugs or drugs of abuse. In focal segmental glomerulosclerosis, because both the electrical charge and the anatomical structure of the ultrafiltration barrier are altered, proteinuria is typically nonselective, with filtration of both high-molecular-weight proteins (eg, Ig) and of low molecular weight proteins such as albumin. The kidneys tend to be small in size (7).

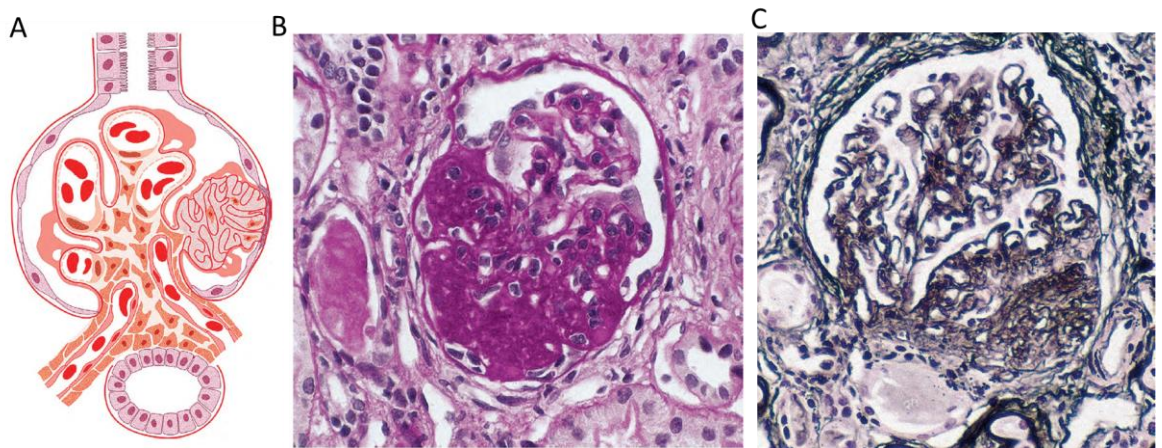


Fig. 1. Focal segmental glomerulosclerosis (FSGS). (A) A scheme representing the sharply defined segmental sclerosis present in the FSGS, defined as obliteration of capillary loops and increased matrix, without deposits and with diffuse foot process effacement by electron microscopy. Adhesions can also be present. (B-C) Two representative images of sclerotic lesion of FSGS stained with periodic acid Schiff (PAS) (B) or Jones silver stain (C) are shown, both reporting an increased mesangial matrix and obliteration of capillary lumina involving the majority of the glomerulus. The uninvolved portion of the glomerulus has mild increase in mesangial matrix. The adjacent tubule shows atrophy and a proteinaceous cast (x 400) (Fogo AB, Diagnostic Atlas of Renal Pathology 2nd Ed).

Focal segmental glomerulosclerosis can present in several variants that can be distinguished based on the results of the observation of the renal biopsy and whose recognition can have a prognostic value as the various forms are differently associated with the rate of progression towards renal disease at the stage terminal prognosis. The most common variants are:

- **Collapsing glomerulopathy (CGP):** is a morphological variant of the focal segmental glomerulosclerosis characterized by collapse of segmental and global glomerular capillaries, marked hypertrophy and hyperplasia of the podocytes and severe tubulointerstitial disease (Fig. 2). The cause of this disorder is unknown, but nearly identical pathological findings are present in idiopathic collapse glomerulopathy and human immunodeficiency virus (HIV) associated nephropathy (8). CGP is most commonly described in African Americans and individuals with recent African ancestry. The disease is rapidly progressive and often presents with sudden onset of renal failure and nephrotic range proteinuria (24-hour proteinuria greater than 3.5 grams) (9).

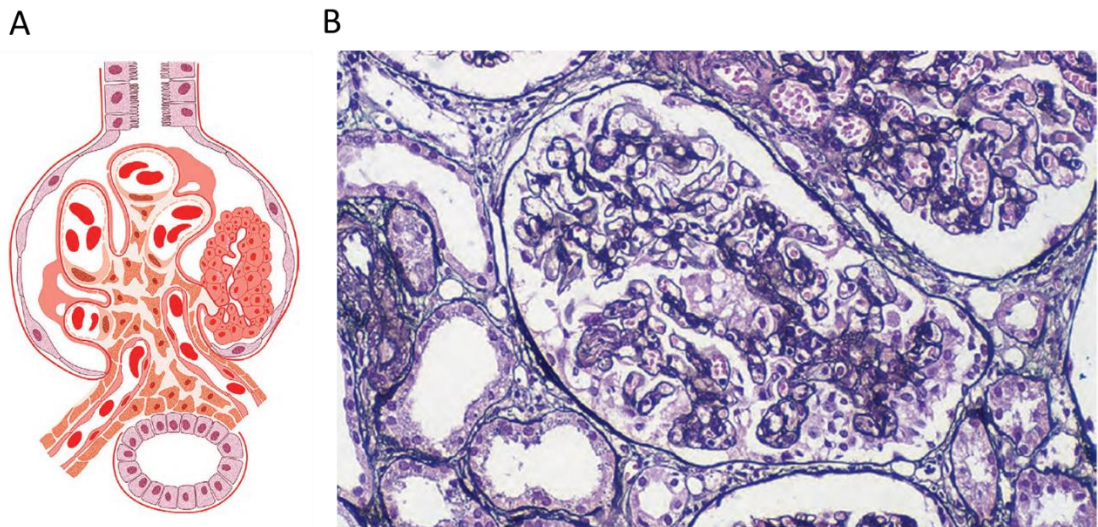


Fig. 2. Collapsing glomerulopathy. (A) Scheme representing the segmental or global collapse of the capillary tuft with overlying visceral epithelial cell hyperplasia; often prominent protein droplets are present. The collapse may be global, or more segmental. (B) Representative kidney biopsy manifestation of collapsing glomerulopathy (Jones silver stain, x400) (Fogo AB, Diagnostic Atlas of Renal Pathology 2nd Ed).

- **Glomerular tip lesion (GTL):** a particular form of FSGS, it is a distinctive histopathological lesion that occurs in patients with idiopathic nephrotic syndrome. GTL

is a segmental glomerular lesion defined by its characteristic location at the origin of the proximal tubule and showing both intracapillary and extracapillary changes. In this type of pathology, a small portion of the glomerular skein located on the tubular pole expands by means of endocapillary foam cells with vacuolized cytoplasm or acellular hyaline material, usually accompanied by the formation of adhesions between the affected glomerular segment and the Bowman's capsule or membrane basal tubular (Fig. 3). In the renal biopsy sections, involvement of most of the glomeruli is observed. The overlying podocytes are typically swollen and hyperplastic, containing cytoplasmic vacuoles (10).

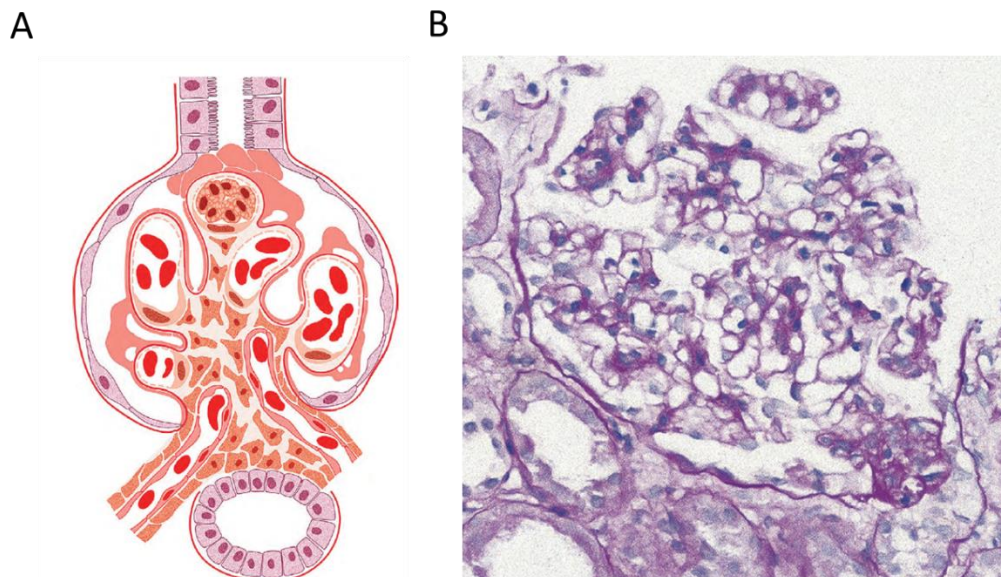


Fig. 3. Focal segmental glomerulosclerosis (FSGS), tip lesion. (A-B) A scheme (A) and a representing PAS stained renal section (B) reporting main pattern of tip lesion manifestation. The localized sclerotic lesion that only involves the proximal tubular pole of the glomerulus is defined as the tip variant of FSGS. Often endocapillary proliferation with foam cells and overlying visceral epithelial cell hyperplasia are reported. Foot processes are diffusely effaced, without deposits (periodic acid Schiff, x100) (Fogo AB, Diagnostic Atlas of Renal Pathology 2nd Ed).

1.3 Proliferative glomerulonephritis

Proliferative glomerulonephritis, on the other hand, is characterized by an increase in the number of cells in the glomerulus. These forms usually present with reduced urine

production with traces of haematuria associated with hypertension (nephritic syndrome). These diseases in many cases progress to end-stage renal disease (ESRD) within a limited period of time, from weeks to years, which varies depending on the disease under consideration.

- **Rapidly progressive glomerulonephritis (RPGN):** also known as crescentic GN, is characterized by a rapid and progressive deterioration of renal function (usually a 50% decrease in glomerular filtration rate (GFR) within 3 months). In RPGN we see the formation of typical crescent-shaped lesions within the glomerulus and this was observed in 50-75% of the total glomeruli examined within kidney biopsies (7). The formation of the "crescent" is favored by the passage of fibrin inside the Bowman's capsule following a greater permeability of the glomerular basement membrane. Fibrin stimulates the proliferation of endothelial cells in the Bowman's capsule and attracts immune cells, such as monocytes. The rapid growth and fibrosis of the crescentic lesions compresses the capillaries, which leads to kidney failure within weeks to months (Fig. 4). RPGNs can be classified into 3 types based on the immunofluorescence pattern they exhibit. Representing approximately 20% of the RPGN, type I RPGN is characterized by the presence of autoantibodies directed against the glomerular basement membrane (GBM). It is also called 'anti-GBM glomerulonephritis'. The antibodies are directed against a particular protein present in GBM, type IV collagen, in particular the non-collagenic region of its $\alpha 3$ chain (11). Type II RPGN is caused by the deposition of immune complexes, which account for 25% of RPGN cases. Therefore, any disease of the immune system involving the glomerulus, if severe enough, can evolve into RPGN; these diseases include systemic lupus erythematosus, acute proliferative glomerulonephritis and IgA nephropathy (11). Also known as pauci-immune RPGN, type III RPGN accounts for 55% of RPGNs and exhibits neither immune complex deposition nor anti-GBM antibodies.

However, the glomeruli are damaged indefinitely, probably through activation of neutrophils in response to ANCA (anti-neutrophil cytoplasmic antibodies) (11).

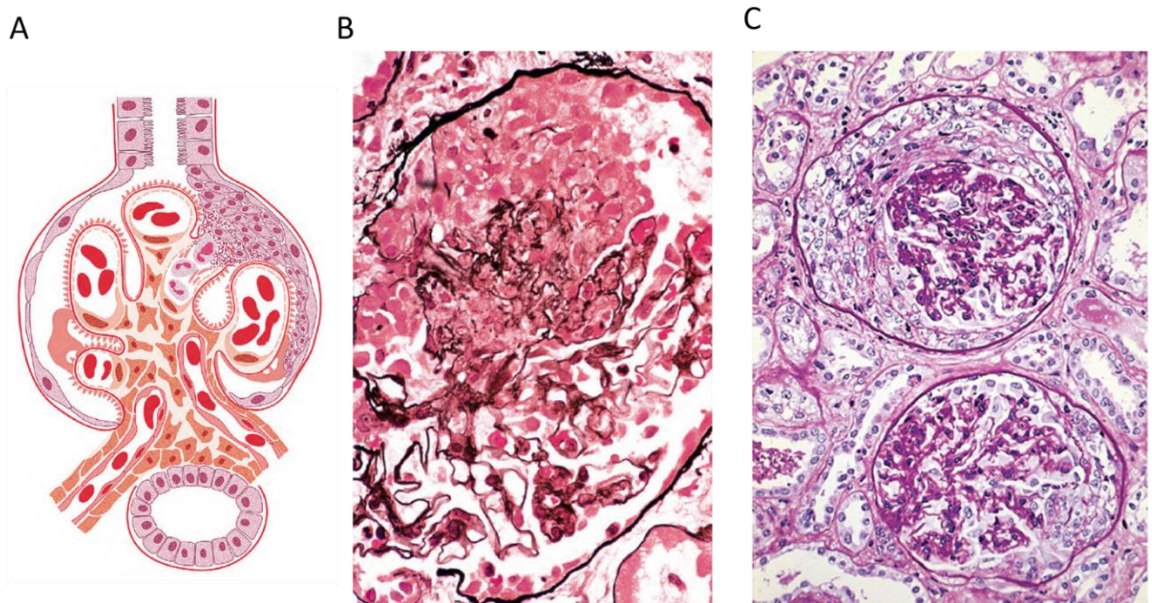


Fig. 4. Rapidly progressive glomerulonephritis. (A) Representative scheme reporting main pattern of Rapidly progressive glomerulonephritis. A segmental necrosis with a break of the glomerular basement membrane, and fibrinoid necrosis and polymorphonuclear leukocytes in this area, with a cellular crescent. (B) Representative glomerulus with the right half completely preserved, while the left half shows glomerular basement membrane ruptures, with corrugation and cellular crescent (Jones silver stain, x400). (C) Representative kidney biopsy showing glomeruli with crescentic lesions (periodic acid Schiff,) (Fogo AB, Diagnostic Atlas of Renal Pathology 2nd Ed).

1.4 Glomerular crescent

The term 'glomerular crescent' is used for hyperplastic lesions involving 10% or more of the circumference of Bowman's capsule. Crescents can be composed of a variable mixture of cells, fibrin, and fibrous matrix (12). A composition of more than 75% cells and fibrin and less than 25% fibrous matrix is referred to as 'cellular crescent', a composition of more 25–75% cells and fibrin and the remainder fibrous matrix is a 'fibrocellular crescent', and more than 75% fibrous matrix and less than 25% cells and fibrin is a 'fibrous crescent' (12). Diagnostic kidney biopsies reveal the occasional

presence of crescents in a wide range of glomerular disorders but crescents are the predominant histopathological lesions found in severe forms of rapidly progressive glomerulonephritis (RPGN), frequently in association with acute or subacute renal failure, also referred to as ‘crescentic glomerulonephritis’ (CGN). However, RPGN and CGN are only descriptive clinical or morphological terms, respectively, and no diagnoses (13). Only integrating all results from clinical phenotyping, standard laboratory tests, and specific immunological exams can ultimately clarify the diagnosis underlying CGN. As such, crescent formation is the consequence of diverse upstream pathomechanisms that fuel into shared cellular responses (1).

1.5 Fibrocellular and fibrous crescents

Multilevel growth of PEC can be associated with an epithelial–mesenchymal transition-like change in cell phenotype characterized by a loss of polarization and release of extracellular matrix towards all directions. The histomorphological hallmark of this process is a gradual coating of PEC with extracellular matrix leading to honeycomb-like structures within Bowman’s space (14). The expanding extracellular matrix can make up a majority of the crescent area, whereas the cellular components succumb, that is, a fibrous crescent. These structures are considered irreversible in terms of a potential recovery of single nephron GFR, and the nephron ultimately undergoes atrophy and phagocytic clearance accompanied and followed by interstitial fibrosis. This sequence of events argues against interstitial fibrosis being a suitable target for therapeutic intervention as reducing interstitial fibrosis in this setting neither recovers lost nephrons nor their function (1).

1.6 Periglomerular inflammation and ruptures of Bowman's capsule

Glomerular crescents can be accompanied by a strong periglomerular inflammatory response, potentially triggered by proinflammatory mediators released from activated parietal epithelial cells across Bowman's capsule. Indeed, immune cells more easily adhere and transmigrate from the low flow, low shear stress, postcapillary venules rather than from the high flow, high pressure glomerular capillaries. Particularly animal models of RPGN show prominent periglomerular T-cell infiltrates but Bowman's capsule forms a barrier preventing T cells from entering the glomerulus and contributing fibrous organization of crescents and nonrecoverable injury (15). Indeed, Bowman's capsule acts as an active immunologic shield that protects the glomerular integrity in glomerulonephritis. In contrast, the well-described role of T-cell subsets to experimental CGN may rather relate to extrarenal roles in regulating systemic (auto-) immunity upstream to renal manifestations (16-18). Ruptures of Bowman's capsule are sometimes seen, which allows periglomerular immune cells to populate the crescent (19).

1.7 Origin of the crescents in the glomerulus

The formation of crescents is a fairly simple and immediate element to be recognized within a kidney biopsy. On the other hand, it has been much more complicated to determine the origin and the composition of these cellular hyperproliferations and over the years several theories have emerged to identify the molecular actor responsible for the phenomenon (20); over time, three possible cellular candidates for the formation of these lesions have been identified: podocytes, macrophages and parietal epithelial cells of Bowman's capsule (PEC).

Podocytes are specialized cells of the glomerular filtration membrane, responsible for maintaining the slit diaphragm. To investigate their possible involvement in crescent formation, Thorner and co-workers conducted a study that showed expression of the nestin protein in the crescent. Nestin, a marker of cell migration and proliferation, within a mature kidney is associated only with podocytes and metanephric blastema, which gives rise to the podocytic lineage. Expression of this protein was also observed within the crescents (50% of the total), however not all cells labeled expressed podocyte markers (20); in fact, inside the lesion, the podocytes are present by differentiation from other cell types with stem characteristics, which do not present cellular markers typical of the podocytic cell subtype (nephrin, podocin and synaptopodin) (21) or because they are incorporated during the hyperproliferation that leads to the formation of the crescent. From these observations it can be concluded that the podocyte contributes to the formation of the lesion but cannot be considered as the cell originating the crescent.

A second hypothesis has placed macrophages at the center of attention, identifying them as entities capable of causing increasing lesions. In vivo studies, in models of rapidly progressive glomerulonephritis in rats, have shown that inside the crescent there is a large inflammatory component consisting mainly of monocytes and macrophages (40% of the total cells) and these cells proliferate directly in place, not being recalled by the mechanisms of immunity following damage. However, macrophages, while playing an important role in the growth of the crescent, are not responsible for its creation, intervening only secondarily and worsening the degree of the lesion (22).

Excluding the first two theories, more recent studies concluded that probably a third type of cell was responsible for the formation of crescents within the glomerulus; these cells are the parietal epithelial cells (PEC) of Bowman's capsule.

In support of the latter theory, lineage tracing studies in transgenic mice clearly document that the cellular crescents develop from the parietal epithelial cells (PEC) residing along

the inner aspect of Bowman's capsule (23). The cell of origin may be a subset of less differentiated PEC that maintained an immature progenitor-like phenotype with a higher capacity for hyperplastic expansion (24). Adjacent podocytes may become part of the crescent but do not contribute to the primary lesion (23). The functional consequence of crescent formation is a decline in single nephron glomerular filtration rate (GFR) for two reasons. First, the increasing intra-glomerular mass increases the counter-pressure that together with oncotic pressure counterbalances arterial filtration pressure. Already slight increases in counter-pressure will cease the physiological net filtration pressure across the glomerular filtration barrier of 10mmHg and may endorse the collapse of the glomerular tuft (25). Second, once a glomerular crescent involves and obstructs the urinary pole, the entire nephron no longer contributes to total GFR (26). However, the fortunate clinical course of some patients with severe CGN suggests that cellular crescents are reversible lesions. Indeed, treatment with steroids and cyclophosphamide elicits anti-inflammatory and antiproliferative effects not only on the immune system but also on hyperplastic epithelial lesions. Whether cells of a cellular crescent are cleared by detachment and shedding of cells into the urine or by apoptosis and phagocytic clearance in situ is not known (1).

1.8 Phenotypic characteristics of glomerular epithelial parietal cells

In recent years, there has been a crescentic interest in the scientific community for parietal epithelial cells of the Bowman's capsule both for their biology and for their diversity. Just 20 years ago, PEC were considered as a simple monolayer of epithelial cells that served as a lining in the Bowman's capsule and as a fundamental component of crescent lesions (27); in fact, it was not known the existence of distinct subpopulations of PEC even within

healthy kidneys and that these subsets had different roles in glomerular pathologies, considering both the crescent and non-crescent ones. The characterization of these cells is evolving rapidly, spurred by exciting new discoveries regarding their morphology, function, molecular phenotype and cellular responses.

PEC are defined anatomically as the epithelial cells that line the Bowman's capsule; they are continuous with neighboring podocytes and proximal tubular cells in areas where Bowman's capsule reflects on the glomerular basement membrane at the glomerular hilum and on the basement membrane of the proximal renal tubule. The different subpopulations of PEC can be classified on the basis of their location with respect to the glomerular vascular pole and the tubular pole; in fact, three fundamental microdomains have been identified within the Bowman capsule: the peripolar region, the central medial extension and the peritubular region (27).

In the peripolar region, located near the vascular pole, there are cells called peripolar cells, identifiable by their large size and granular appearance that they show under the electron microscope. Although their functions remain largely unknown, they are considered transition cells capable of expressing both typical PEC markers and podocyte markers. These cells, in humans, contribute to increasing the total number of podocytes during embryonic development from infancy to adulthood. Given the spatial proximity between PEC and podocytes and their common embryological ancestor, it is not surprising that a subset of these cells also express mature phase podocyte proteins (27).

The central medial extension is instead the residence of the classic flat PEC (fPEC); express typical markers such as claudin, Pax2, keratin 8 in both mice and humans (28). In humans, flat PEC also express stem cell markers such as CD133 and CD24 that are upregulated in diseases leading to conspicuous loss of podocytes, where this population likely replaces lost podocytes allowing for damage regeneration (29). In healthy mice, on

the other hand, these cells express and are specifically labeled with Csk (Src inhibiting protein kinase (30).

In the third microdomain of Bowman's capsule, the peritubular region, PEC are labeled as cuboidal cells (cPEC); they share morphological characteristics with proximal tubular cells and this can be traced to the fact that in rodents it is common for proximal tubular cells to colonize a portion of Bowman's capsule, a feature pathologists refer to as "Bowman's capsule tubularization". on the other hand, this phenomenon is rare and affects 2% to 3% of human glomeruli at random histological sectioning, which occurs mainly in males. At the junction between cuboidal and flat PEC there is a transition intermediate population called iPEC (31); this type of cells are always present even if the phenomenon of tubularization of the Bowman's capsule does not occur (Fig. 5).

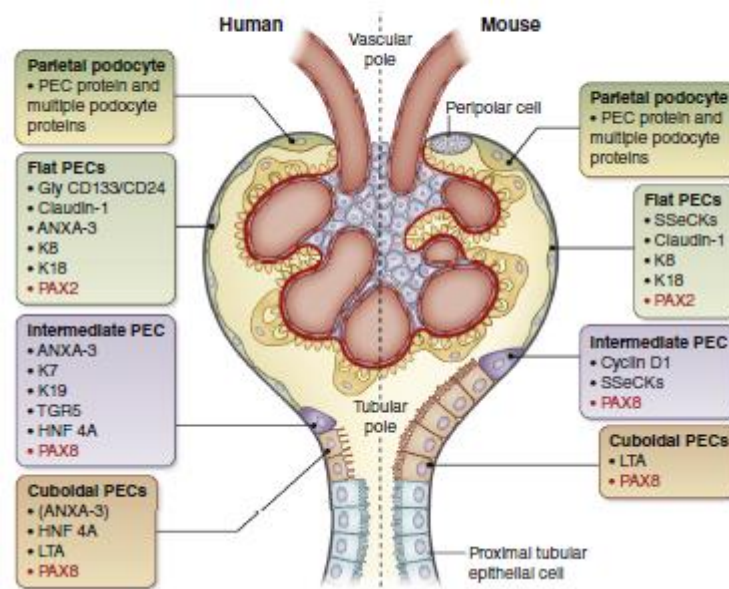


Fig. 5. Heterogeneity of PEC.

Diagram showing the different subpopulations of PEC along the Bowman's capsule (blue) in humans (left) and mice (right), defined by the histological aspect and the markers used to identify them; D'Agati Kidney International, 96(1), 16–19.

In conclusion, observing these 3 subpopulations of PEC (cuboidal, flat and intermediate) by means of lineage tracing experiments, it emerged that these are not static cells but can make a transition between the different subtypes; in fact cPEC can convert to the iPEC phenotype, but not for example to the flat phenotype (fPEC) (32).

1.10 Functional characteristics of PEC: renal progenitor cells

From a functional point of view, among the PEC can be distinguished a subpopulation of cells with a high proliferative potential and with characteristics of stem cells, called renal progenitors. The regenerative capacity of the kidneys was already known from the early 2000s, but stem cells within these organs had not yet been identified (33). In 2001, 3 papers were published demonstrating the recruitment of circulating peripheral blood cells for the regeneration and repair of acute and chronic kidney damage in the transplanted kidney. The authors highlighted the presence of a stem cell population among the recruited cells capable of generating mature tubular cells, endothelial cells, myofibroblastic cells and mesangial cells (33). It was not clear which stem cell population between hematopoietic stem cells (HSCs) and mesenchymal stem cells (MSCs) contributed to the repair of the damage. In 2003 the works of Lin *et al.* and by Kale *et al.* showed how, in the first case the HSC cells, and in the second the MSC cells, had been recruited into the murine kidney after induced ischemic damage and localized tubular regions in the lesion, where they differentiate into tubular epithelial cells (34-35). Two years later the study by Duffield and collaborators showed that the regeneration of the tubular epithelium in the ischemic kidney occurs independently of stem cells derived from the bone marrow and that the regenerative capacity is intrinsic to the organ itself (36). In 2004, Oliver and colleagues proposed the renal papilla as the site of renal stem cells, given the early formation of this area during embryonic development and the higher level of

hypoxia present in the internal marrow than in the cortex (37). They administered bromodeoxyuridine (BrdU) to rats and mice for two months to look for cells with a low replication rate, which were identified in the papillary interstitium and some tubules. However, Oliver and colleagues failed to isolate positive BrdU cells *in vitro* and to characterize them.

In 2006, Sagrinati and colleagues described for the first time a population of multipotent progenitors (Renal Progenitor Cells, RPC) in the adult human glomerulus, characterized by the co-expression of two surface markers: CD24, specific to the metanephric mesenchyme during embryonic and renal development and CD133, specific for adult tissue stem cells. The double positive population was identified near the urinary pole of Bowman's capsule and was isolated and extensively characterized. Flow cytometric analyzes showed the presence of other surface markers, such as CD106, CD105 and CD44, while no endothelial or podocyte markers were highlighted. Analysis of mRNA expression showed almost negligible levels of renal differentiation markers, reinforcing the idea of the undifferentiated nature of these cells. The proliferative and clonogenic potential of CD24+CD133+ cells were very high, especially when compared with CD24-CD133- cells, and was confirmed by the expression of Bmi-1 and Oct4, transcription factors responsible for the maintenance of stemness. Furthermore, the CD24+CD133+ population showed multipotency capacity: cells were able to differentiate towards tubular, osteogenic, adipocytic and neurogenic lineages (38). Subsequent work describes CD24+CD133+ renal progenitor cells as a heterogeneous and hierarchical population, organized in a precise sequence within the Bowman's capsule, with a differentiative potential towards the podocytic and tubular lineage. Three cell populations with different characteristic have been identified within Bowman's capsule. Cells located in the urinary pole that express both CD24 and CD133 but not podocalyxin (PDX) or other podocytic markers (CD24 + CD133 + PDX- cells) can differentiate into both tubular and podocyte

lines. Conversely, cells located between the urinary and vascular poles, which express markers of both progenitors and podocytes (CD24 + CD133 + PDX + cells), are able to regenerate only the podocytes (39). Finally, the cells located at the vascular pole of the capsule have a phenotype similar to that of the mature podocyte (CD24-CD133-PDX +), with which they also share functional characteristics of post mitotic cells: they are therefore not able to give rise to clones and they can be kept in culture for only a few days, according to their nature as terminal differentiated cells (39) (Fig. 6).

To test the ability of these cells to participate in the repair of renal damage, Sagrinati and Ronconi in their study used a model of acute kidney injury from rhabdomyolysis in SCID mice, induced by an intramuscular injection of glycerol and a mouse model of damage. renal induced by adriamycin respectively. At the peak of damage, two human cell populations, one CD24-CD133- and one CD24+CD133+ (PEC), were labeled with a red dye (PKH26) and subsequently injected intravenously into the tail of SCID mice with glycerol damage. Ten days later the animals were sacrificed, the kidneys were recovered and sections of the kidneys were analyzed for the presence of labeled cells. The presence of labeled cells was never found in the kidneys of control mice injected with CD24-CD133- cells, while in mice that received the infusion with CD24+CD133+ cells they were found in the cortical and medulla of the kidney. Most of the injected PEC were located within the tubules where they differentiated and also expressed markers typical of different portions of the nephron, and sometimes some cells have also been identified in the interstitium and glomeruli. Furthermore, these cells once inside the kidney significantly improve kidney damage both morphologically and functionally. This study therefore led to the demonstration that renal progenitors are multipotent cells, capable of differentiating into different types of renal cells (38-39).

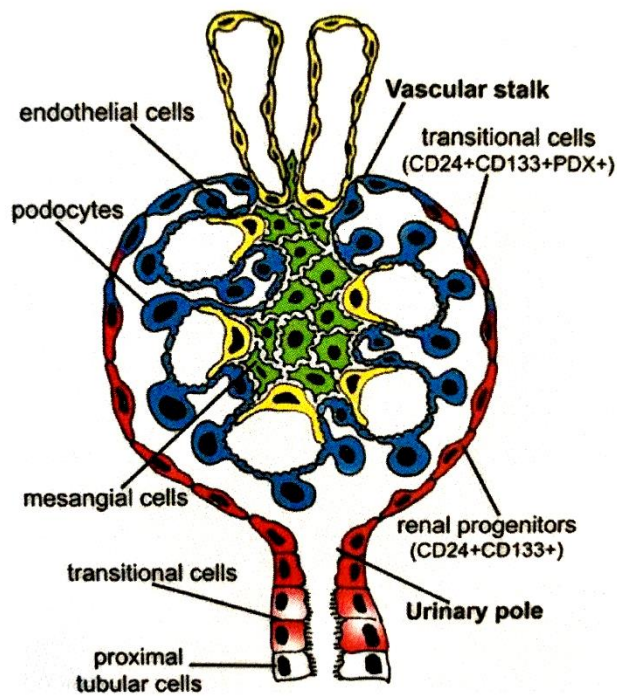


Fig. 6. Hierarchical distribution of renal progenitors in adult glomeruli

The CD24+CD133+ renal progenitors (red) are found in the urinary pole and are in close contiguity with the podocytes (blue) at one end (vascular pole) and with the renal tubular cells (white) at the other end. A transitional cell population (CD24+CD133+PDX+, red/blue) has intermediate characteristics between those of renal progenitors (red) and podocytes (blue) and is located between the urinary pole and the vascular pole. At the level of the vascular pole of the glomerulus, the transition cells are in contiguity with cells that lack expression of progenitor markers but express podocyte markers and have phenotypic characteristics of differentiated podocytes (blue). Endothelial cells (yellow) and mesangial cells (green) are also represented; Romagnani, *Stem Cells*, 2009;27(9): 2247-2253.

The study conducted by Angelotti and collaborators demonstrated that the CD133+CD24+ renal progenitors can be further separated into subpopulations, functionally distinct based on the surface expression of the vascular cell adhesion molecule 1 (VCAM1), also known as CD106. CD133+CD24+CD106+ cells were located in the urinary pole of Bowman's capsule, while a distinct population of scattered CD133+CD24+CD106- cells was found in the proximal tubule and distal convoluted tubule. CD133 + CD24 + CD106 + cells showed a high proliferation rate and the ability to differentiate both towards the podocyte and tubular lineage. In contrast,

CD133+CD24+CD106- cells showed a lower proliferative capacity and showed a phenotype purely committed to the tubular line. It also emerged from this study that both types of progenitors once injected into immunodeficient mice (SCID) showed great resistance to apoptosis and that they are able to integrate into the kidney and generate new tubular cells leading to an improvement in renal function (40) (Fig. 7).

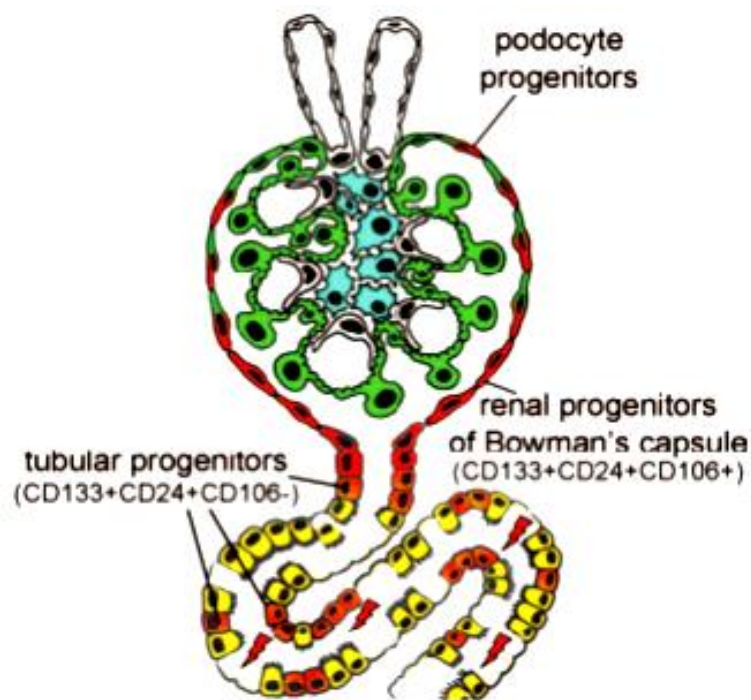


Fig. 7. Schematic representation of the response of renal progenitors following damage. Following acute kidney injury, differentiated (yellow) tubular cells that are exposed to damaging agents die, while scattered (orange) tubular progenitors survive due to their resistance to death. These tubular progenitors can proliferate and differentiate to replace dead cells. Angelotti et al., Stem Cells 2012; 30: 1714-1725

The results obtained from these studies hypothesize that CD24+CD133+ cells may provide a new potential source for renal regeneration, both the multipotency of the progenitors and their organ-specific identity.

To test these hypotheses, a way to track the fate of renal progenitor cells *in vivo* had to be found. To test the possible recruitment of podocytes by the parietal epithelial cells (PEC) of Bowman's capsule after the S-shaped phase of glomerular development, Moeller and Smith used a triple transgenic mouse model to label PEC and transition cells. The *pPEC-rtTA/LC1/R26R* model was induced at the age of 6 weeks, at the end of nephrogenesis, with administration of doxycycline for 14 days. In response to doxycycline, cells express the specific promoter of PEC (podocalyxin promoter) express the reverse transactivator of tetracycline (rtTA), which binds the responsive element of tetracycline (TRE) as well as to the gene expression of luciferase (LC1) and of Cre recombinase. Cre recombinase extrudes the neomycin cassette onto the Rosa26 reporter by activating transcription of the LacZ gene, expressing β galactosidase. The authors observed that approximately 10% of podocytes were positive for the gene tag, even 12 weeks after induction, thus demonstrating that visceral epithelium is recruited from transitional cells and PEC even after the termination of glomerular development (41). These results support the data obtained with *in vivo* lineage tracing model in the previously cited works by Sagrinati and Ronconi.

In order to obtain experimental models that would allow to better characterize the behavior and functions specifically of renal progenitors, it was necessary to identify this cellular subpopulation of PEC also in mice. However, this proved very difficult as the mouse does not show CD133 expression; therefore, it was necessary to identify a marker that identified these cells in the mouse. In this regard, in 2015 the study by Lasagni and collaborators showed that a subpopulation of murine renal progenitors was characterized by the expression of a regulatory region of the transcription factor Pax2, a fundamental regulator for the development of the population of embryonic progenitors during development of the kidney in vertebrates. Pax2 is co-expressed together with CD133 in adult human renal stem cells and therefore it has been hypothesized that this protein may

be used to identify and to trace the renal progenitors present on the Bowman's capsule in mice, as it represents a true marker of stemness (29). To trace the murine RPC, the authors exploited a new lineage tracing model, the inducible triple transgenic *Pax2.rtTA,TetO.Cre,R26.Confetti* mouse model, in which a yellow, green, red or cyan fluorescent protein is expressed stochastically. under the control of the Pax2 gene promoter, enabling the tracking of individual Pax2-expressing cells and their progeny.

Since Pax2 can also be expressed by podocyte precursors during renal development, but is lost during their differentiation into mature podocytes and remains present only on Bowman's capsule stem cells in the postnatal kidney (42), puppies were induced with doxycycline by administering the inducer to their mothers during the nursing period for different periods of time after birth. These experiments showed that Pax2 was expressed only by some cells scattered within the tubular structures of the nephron and by the renal progenitors of the Bowman's capsule, and also showed that about 8% of the podocytes present within the glomeruli of the kidneys. of adult mice are recruited from Pax2 + cells during postnatal glomerular development, as found in the 2009 work by Moeller group (29, 41). Subsequent studies have also shown that, in later stages of development, marked podocytes, derived from the differentiation of cells present on the epithelium of the Bowman's capsule, were present inside the glomeruli. however, these podocytes were stained with different fluorescent proteins of the Confetti reporter, suggesting that they are not the result of the clonal expansion of a single progenitor but are derived from the differentiation and migration of multiple progenitor cells within the same glomerulus (29).

Once the physiological regeneration of podocytes was verified, the authors evaluated whether Pax2+ cells could play a role in podocyte regeneration following glomerular injury, inducing adriamycin nephropathy in *Pax2.rtTA mouse models; TetO.Cre; mT / mG*. The injury was induced at the age of 5 weeks with the administration of doxycycline

for 10 days. After induction, Pax2⁺ cells express the green fluorescent protein (GFP), while all other cells will be colored red because they will only express the TomatoRed gene. After damage, approximately one third of the lost podocytes were regenerated in mice with remission of proteinuria, and intraglomerular Pax2⁺ cells were observed around the tuft and showed expression of podocyte markers WT1, podocin and synaptopodin,; whereas in mice with persistent proteinuria Pax2⁺ cells were not detected or were observed within intraglomerular hyperplastic lesions. This experimental model allowed the authors to trace the fate of Pax2⁺ cells and to demonstrate how the remission or progression of glomerular damage depends on a balance between a more or less efficient differentiation of renal progenitor cells into podocytes. To evaluate whether the differentiation of RPC into podocytes could represent a possible therapeutic strategy for the remission of glomerular diseases, Lasagni and collaborators performed a screening of molecules that could favor the podocyte differentiation of renal progenitors. Among the molecules analyzed, emerged BIO, the GSK3 inhibitor that was capable to promote the *in vitro* and *in vivo* differentiation of human RPC toward a podocyte phenotype. BIO acts by increasing the endogenous differentiation effect of retinoic acid, stimulating the binding of RA to its reactive element (RARE). BIO was administered to *NPHS2.iCreERT2; mT/mG* transgenic mouse models; and *Pax2.rtTA; TetO.Cre; mT/mG* in which adriamycin damage from nephropathy was induced. In both models, after 14 days of drug treatment, a reduction of proteinuria was reported accompanied to the regeneration of 32% of lost podocytes by RPC versus 11% observed in the models stimulated with DMSO. Authors therefore demonstrated that an efficient differentiation of RPC into podocytes leads to a positive outcome of glomerular disorders and that this process can be pharmacologically enhanced (29) (Fig. 8).

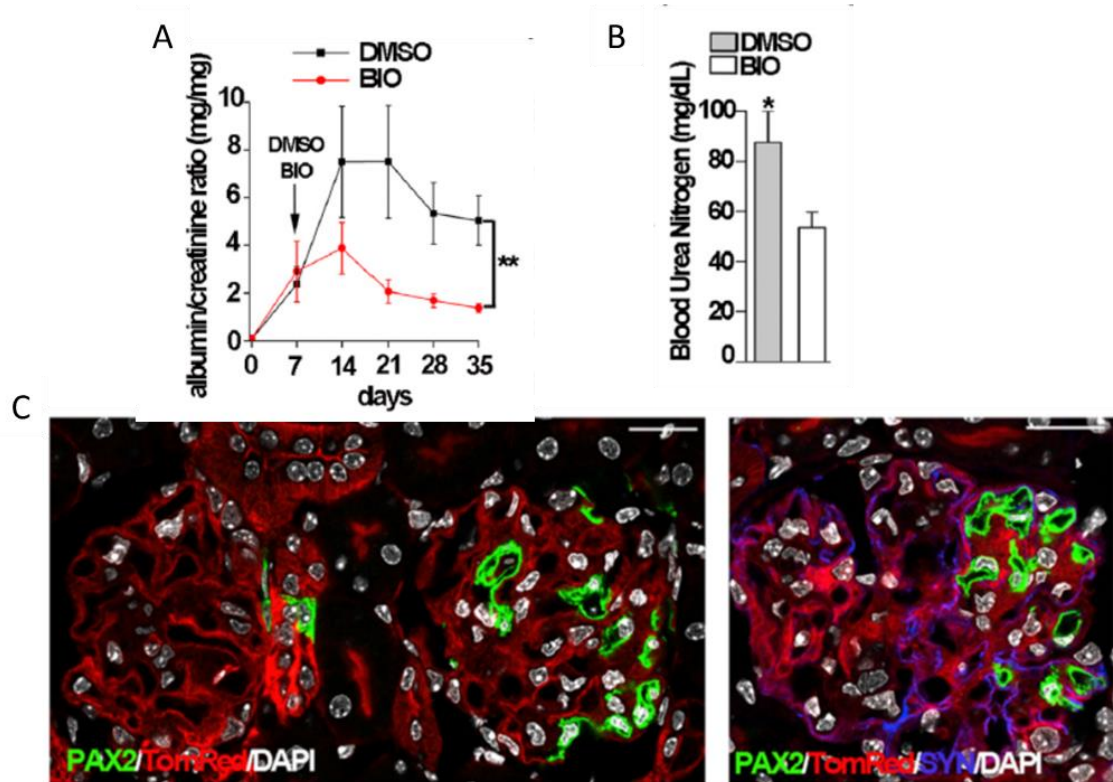


Fig. 8. GSK3s Inhibition Induces Remission of Glomerular Disease and Is Associated with the Generation of Novel Podocytes.

(A) Albumin/creatinine levels in DMSO and BIO treated *Pax2.rtTA;TetO.Cre;mT/mG* mice with Adriamycin nephropathy; day 0 corresponds to the time of second doxorubicin injection. $**p < 0.001$ (day 35) by Mann-Whitney test. (B) Blood urea nitrogen levels in DMSO and BIO treated mice at day 28; $*p < 0.05$ versus BIO-treated mice by MannWhitney test. (C) Representative glomeruli of BIO-treated *Pax2.rtTA;TetO.Cre;mT/mG* mouse (left) with PAX2+ cells inside the glomeruli express SYN (blue) (right).

In support of the increase in the regeneration of podocytes shown by RPC following pharmacological treatment, a recent work of Romoli and colleagues emerges, in which the inhibition of the chemokine CXCL12 would lead to an increase in the differentiation of renal progenitors into podocytes. Adriamycin nephropathy was induced in the *Pax2.rtTA; TetO.Cre; mT/mG* mouse model. Pharmacological inhibition of CXCL12 by NOX-A12 significantly reduced proteinuria levels and induced podocyte regeneration by PEC Pax2+ in 52.46% of damaged glomeruli, limiting residual podocyte loss to a small severely damaged cluster of juxtamedullary glomeruli. Furthermore, Romoli and collaborators observed that the *in vitro* inhibition of CXCL12 involves the expression of Notch in RPC treated with adriamycin, stimulating its activation. These data propose a

possible mechanism of the functioning of the glomerular niche, in which the constant secretion of SDF-1 by the podocytes in conditions of homeostasis contributes to the maintenance of the stem characteristics of the podocyte progenitors through the inhibition of the Notch pathway (43).

The works of Lasagni and Romoli thus open the way to the search for new potential therapeutic strategies capable of promoting the regeneration of lost podocytes by renal progenitor cells for the treatment of patients with CKD (chronic kidney disease).

1.11 Role of PEC in the genesis of glomerular pathologies

Although the data discussed are consistent in representing PEC as cells responsible for normal development and renal regeneration, paradoxically they also have a "negative side" in certain diseases, in which their responses directly contribute to the formation of glomerular diseases and, in certain circumstances, including the deterioration of renal function (44). In addition to all this, many studies have shown that the regenerative capacity of renal progenitors has limits. Podocyte regeneration occurs in the early stages of the disease, where there is less than 20% loss of podocytes, while with damage between 20% and 40% a poor response to damage is observed; for damage over 60% of lost podocytes, on the other hand, there is the formation of sclerotic lesions and glomeruli no longer able to carry out filtration (45,46). In conclusion, the regenerative potential of renal progenitors also varies according to the person's stage of life, exhibiting the highest degree during adolescence; for this reason, during the first years of a patient's life, glomerular disorders have a better prognosis and for this reason the presence of FSGS and crescentic glomerulonephritis is more frequent in the elderly, where this mechanism no longer works or in any case to a much lesser extent (47).

Regarding the "negative side" of PEC, Moeller's group, working on a mouse model of selective depletion of PEC with diphtheria toxin, showed that necrosis of PEC (caused by the toxin itself) is sufficient for the development of a crescentic lesion within the glomerulus; this is probably due to an "overcompensating" endothelial repair phenomenon driven by the progenitors that survived the damage (48). Although this study demonstrates the ability of PEC to create hyperplastic lesions, necrosis of this type of cells is not a typical feature of common crescent glomerulopathies, which, instead, show necrotic lesions of the clump of glomerular capillaries. Rupture of the capillary bundle leads to glomerular vascular damage and this leads to the leakage of plasma into the Bowman's space, providing mitogenic stimuli that drive PEC hyperplasia and crescent formation. PEC (like other epithelial cells) usually live in an environment devoid of plasma exposure and rupture of the capillaries causes a 20-40% increase in plasma concentration in Bowman's capsule (14); many plasma components could induce PEC hyperplasia but at the moment only fibrinogen (fundamental element of the coagulation cascade) has been considered as a target to consider. A depletion of fibrinogen or fibrinolysis, in fact, does not induce PEC hyperplasia in several rodent models with crescent glomerulonephritis (49). It has also been observed that glomerular crescents can evolve into fibrocellular lesions, due to the potentially irreversible accumulation of extracellular matrix; this process could be the result of the epithelium-mesenchymal transition operated by the PEC, characterized by a loss of epithelial polarity and an increase in the secretion of the components of the extracellular matrix (14).

Over the years, many studies have focused on evaluating whether PEC actually produced these lesions; in a first study in mice it was shown that the cells constituting the first hypercellular lesions were positively labeled for Pax2, CK8 (cytokeratin-8) and PAN-cadherin and did not express podocyte markers such as synaptopodin or VEGF. However, this did not give the researchers total confidence, as it had already been shown that during

the development of immature renal podocytes these are Pax2 positive, making it difficult to distinguish between mature PEC and dedifferentiated podocytes. Therefore, this group of researchers used a series of other markers (CK8, PAN-cadherin, synaptopodin and VEGF) and performed double labeling experiments (PAX-2 / synaptopodine and VEGF / CK8) obtaining results always in perfect agreement. The proliferating cells (identified by an immunofluorescence for Ki67) were always positive for all PEC markers and always negative for podocyte markers, thus identifying the person responsible for these lesions (50). Subsequent human studies have shown that within glomerular lesions present in different podocytopathies there are three main subgroups of progenitors with varying degrees of differentiation: undifferentiated renal progenitors CD133+CD24+podocalixin(PDX)-nestin-, a transitional population CD133+CD24+podocalixina (PDX) + nestin +, and differentiated progenitors to podocytes CD133- CD24-podocalixina(PDX)+nestin+ (24); in addition to this, immunofluorescent markings were made with an anti-Ki67 antibody (a nuclear protein closely associated with cell proliferation and found only in cells in an active phase of proliferation) and it was observed that within the lesion only the progenitors express this protein. Indeed, Smeets and collaborators have reported that renal progenitor cells, exposed to high concentrations of TGF- β , produced by podocytes following the increase in proteinuria, cause the deposition of a large amount of extracellular matrix which leads to the enlargement of the lesion within the glomerulus (24). Moreover, Lasagni *et al*, by using the *Pax2.rtTA; TetO.Cre; mT/mG* and *Pax2.rtTA, TetO.Cre, R26.Confetti* model, demonstrated that in the course of renal disease induced by adriamycin, the Pax2 positive cells of the Bowman's capsule originate hyperplastic lesions (29). These results indicate that hyperplastic lesions derive from the proliferation of renal progenitors, reinforcing the hypotheses that place these cells as responsible for the formation of crescents (24).

1.12 Molecular pathways of parietal epithelial cell hyperplasia in crescentic glomerulonephritis

Activation of PEC is an important pathomechanism and prime therapeutic target in crescentic glomerulonephritis, given its association with cellular crescent formation (23). Several molecular pathways are involved in PEC hyperplasia and the best known are listed below.

1.12.1 CD44 and CD9

A recent study in experimental CGN found that CD44 glycoprotein is expressed in active PEC and that its association was associated with a reduced presence of PEC in the Bowman space (30). CD44 is a surface glycoprotein that plays a key role in various cellular processes, such as differentiation, migration, extracellular matrix deposition, leukocyte trafficking and scar formation (51). CD44 is not expressed in PEC of healthy glomeruli, but its expression has been seen to increase significantly in models of focal segmental glomerulonephritis and crescentic glomerulonephritis and this has revealed that CD44 plays a fundamental role in the pathogenesis of these glomerular diseases (52). To underestimate the role of this glycoprotein, many studies have been carried out on the mouse; crescentic glomerulonephritis was induced in both wild type and CD44 deficient mice (CD44 $-/-$) and various physiological parameters were evaluated. First, it was observed that between the two models there was no difference in the histology of the kidney or in the number of immunity cells present within the glomerulus. However a significant difference was found in the albumin/creatinine ratio following a urine test; in fact, in CD44 $-/-$ mice, this ratio was 4 times lower compared with wild type mice, indicating an improvement in renal function in this group. In addition, it was observed that far fewer glomeruli with crescent formations were present in CD44-deficient mice

than in controls, reinforcing the hypothesis that this molecule played a key role in the lesion (Fig. 9).

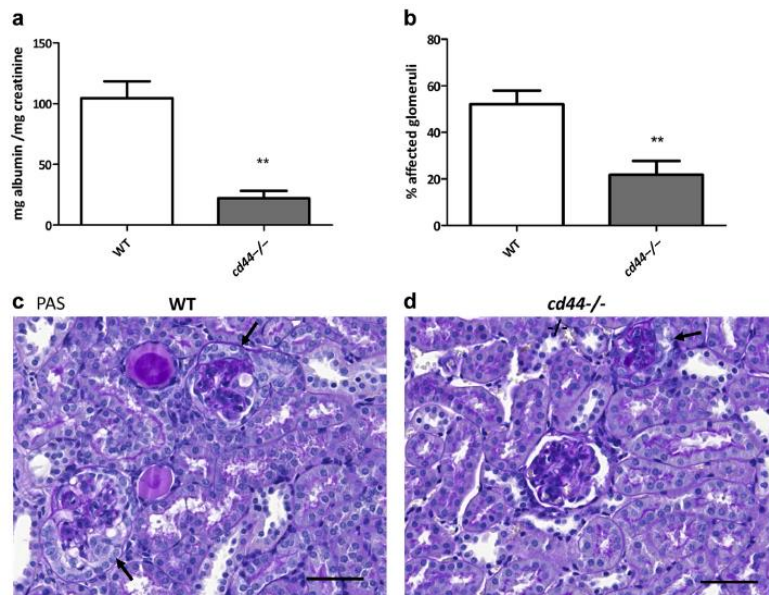


Fig. 9. Reduction of proteinuria and formation of crescentic lesions in CD44 $-/-$ mice. Proteinuria expressed as mg albumin / mg creatinine in wild-type (WT) and CD44 $-/-$ mice on day 14 after nephrotoxic serum injection (NTS) (a). The formation of crescent or hyalinosis in the glomeruli was determined by analysis of at least 50 glomeruli per mouse and expressed as a percentage of affected glomeruli in WT and CD44 $-/-$ mice on day 14 after NTS injection (b). Representative images of periodic-Schiff acid stained sections of WT and CD44 $-/-$ control mice (c, d). Eymael *et al.*, *Kidney International* (2018) 93, 626–642.

In conclusion, in the study of Eymael *et al.* it was shown that the CD44 deficiency is reflected in a smaller number of PEC in the crescentic lesions and in a reduction of proteinuria and cell proliferation within the glomerulus (30).

Another fundamental molecule studied in the crescent formation process is CD9, or Tetraspanin. CD9 expression has been extensively studied in cancer, where it facilitates proliferation, migration, adhesion and survival. The cellular functions of this molecule depend directly on its cellular expression and vary according to its association with other proteins; in fact, thanks to its specific structure, CD9 has the ability to interact with different partners. Moreover, CD9 has been described in association with CD44 in both humans and mice. This association causes a worsening of the crescentic lesion,

aggravating all the parameters seen previously, while its deletion, as already found for CD44, affects the proliferation and migration capacity of PEC, also placing this protein as a central point in the molecular mechanisms involved in the progression of the disease (53).

1.12.2 Glucocorticoids

Glucocorticoids have remained in use for the treatment of glomerulonephritis since decades. A recent study investigated the effects of glucocorticoids in glomerulonephritis and found that glucocorticoid receptor inhibition was associated with decreased cellular crescent formation and inhibition of proliferation and migration of PECs (54). This therapeutic approach also reduced the inflammatory infiltrate within the kidney, suggesting intracellular steroid receptors may contribute to inflammation in CGN (54).

1.12.3 Heparin-binding epidermal growth factor-like growth factor

Heparin-binding epidermal growth factor-like growth factor (HB-EGF), a member of the EGF family, increases phosphorylation of the EGFR. In an animal model of CGN, proHB-EGF was induced in PECs and podocytes even before the first appearance of crescents (55). Similar results were obtained in kidney biopsies from subjects with crescentic RPGN, in which HB-EGF staining was noted in all epithelia of the nephron, that is, podocytes, PECs, and tubules (55). HB-EGF deficiency attenuated CGN as did conditional deletion of EGFR only in podocytes, suggesting autocrine and paracrine feedback loops. Indeed, even delayed pharmacological inhibition of the EGFR mice could still attenuate CGN, which may be of translational relevance for human RPGN.

1.13 Therapeutic strategies in use for the treatment of RPGN

In all extracapillary proliferative glomerulonephritis, but especially in rapidly progressive glomerulonephritis, it is necessary to practice drug therapy with a certain timeliness (i.e. when serum creatinine is <5 mg/dL) and before renal biopsy shows the formation of crescent in all the glomeruli. It consists of boluses of corticosteroids, for example methylprednisone 1g/day for 3 days, plasmapheresis (every other day in the first two weeks of treatment) and immunosuppressive drugs including cyclophosphamide, azathioprine and mycophenolate mofetil. Aggressive immunosuppressive therapy may also be helpful in patients with higher creatinine levels. Plasma exchange combined with prednisone and cyclophosphamide benefited patients with renal involvement who did not require immediate renal replacement therapy, even if creatinine levels were elevated above 5-7 mg / dL (56). In any case, the response to therapy is very disappointing in these patients, who become safe candidates for dialysis and kidney transplantation.

The identification of PECs as responsible for the genesis of crescentic lesions within the glomerulus, and the definition of the molecular processes that regulate their aberrant activation, could lead to the identification of new therapeutic strategies aimed at slowing down or even reverting the disease. For this purpose, transgenic mouse models are needed on which to perform efficacy and safety tests of new molecules and drugs.

2. Study design

The formation of crescents is the consequence of various pathogenetic mechanisms upstream that feed into a shared response that provides for the specific activation of PEC. PEC normally reside peacefully along Bowman's capsule and partly represent renal progenitor cells (RPC), kept in quiescence via a humoral feedback loop by the differentiated podocytes of the intact glomerular filtration barrier (1, 2, 29, 43). Lesion of podocytes interrupts this feedback loop and activates PEC via surface glycoproteins, such as CD44 (30) and CD9 (53,54), which promote their activation, migration and proliferation (39, 57). RPC have a high survival capacity (58) and proliferative potential (58) and RPC markers are observed in the crescents of patients with different types of glomerulonephritis (24).

Based on the similarities between the bone marrow and kidney stem cell niches (59) we hypothesized that crescents result from the monoclonal expansion of a single clone of RPC conceptually similar to monoclonal diseases originating from hematopoietic stem cells (29,60,61). We further hypothesized that drugs known to treat monoclonal hematopoietic stem cell diseases may have an effect on renal progenitors by blocking proliferation by attenuating crescentic glomerulonephritis (25, 30, 53,54). In this work, a rapidly progressive glomerulonephritis model was developed in transgenic mice which, together with the use of high-resolution microscopy techniques, made it possible to perform lineage tracing experiments on Pax2+ capsular renal progenitor cells and to correlate data obtained with our findings in human biopsies of crescentic glomerulonephritis affected patients.

Therefore, the purpose of this study was to examine the contribution of renal progenitors among the PEC to the generation of crescents and to identify the mechanism involved in this process. These objectives were addressed by: (i) evaluating renal progenitors as the

cell of origin of crescents in transgenic mouse models and evaluating crescent clonality, (ii) analyzing the effect of drugs currently used in haematological stem cell disorders on crescentic glomerulonephritis outcome in mouse models, (iii) identifying the crescent-forming PEC subset in human by single cell RNA seq and immunofluorescence analysis on human biopsies of crescentic glomerulonephritis patients (iv) evaluating the mechanisms of panobinostat effects on human renal progenitors.

3. Materials and methods

3.1 Human kidney biopsies

A total of 22 native kidney biopsies of patients with SLE (8 women and 1 men, mean age 33.5 ± 13.3 years) and with AAV (9 women and 4 men, mean age 47.5 ± 20.7 years), were selected for the analysis and retrospectively reviewed in agreement with the Ethical Committee on human experimentation of the Meyer Children University Hospital and of the Careggi University Hospital, Florence, Italy (Table 2 and 3). As controls, normal kidney fragments were obtained from three patients who underwent nephrectomy for localized renal tumors (1 woman and 2 men, mean age 64.67 ± 8.45 years). These fragments were obtained from the pole opposite to the tumor. All biopsies had multiple levels cut and were stained with Jones methenamine silver, periodic acid Schiff (PAS), hematoxylin and eosin (H&E) and trichrome for clinical purposes. The cohort size was limited by the availability of both clinical data and representative kidney biopsy material, therefore sample size calculation was not applicable. Initial (time of biopsy) and 2 years follow-up clinical data were recorded (Table 2 and 3), and the outcome was assigned based on the estimated GFR at 2 years ($eGFR < 15$ ml/min/1.73m², ESKD; $eGFR > 15$ ml/min/1.73m², non ESKD).

3.2 Animal studies

Mice were randomly assigned to experimental and control groups, but investigators were not blinded. Sample size was calculated on the basis of the primary endpoint rate of crescent formation and other assumptions based on preliminary experiments. No data were excluded from studies in this manuscript. Pathology analysis was performed in a blinded fashion. All procedures were performed in accordance with institutional protocols

approved by the Institutional Animal Care and Use Committee of the University of Florence, Italy.

3.3 Transgenic mouse models

The *Pax2.rtTA;TetO.Cre;R26.Confetti* mice or *Pax2.rtTA;TetO.Cre;R26.mT/mG* or mice were developed on a full C57Bl/6 background by crossing the *Pax2.rtTA* mouse (6, 11) (kind gift from Dr. Beat Schäfer, Department of Oncology and Children's Research Center, University Children's Hospital, Zurich, Switzerland) with the TetO.Cre strain *B6.Cg-Tg(TetO-Cre)1Jaw/J* (IMSR Cat# JAX:006234, RRID:IMSR_JAX:006234) purchased from the Jackson Laboratory (Bar Harbor, ME, USA). Double transgenic mice were then crossed either with the Confetti strain *Gt(ROSA)26Sor^{tm1(CAG-Brainbow2.1)Cle/J}* (IMSR Cat# JAX:017492, RRID:IMSR_JAX:017492) or with the mT/mG strain *B6.129(Cg)-Gt(ROSA)26Sor^{tm4(ACTB-tdTomato,-EGFP)Luo/J}* (IMSR Cat# JAX:007676, RRID:IMSR_JAX:007676) (both from Jackson Laboratory), to obtain a triple transgenic inducible mouse model.

Mice were genotyped as reported below and triple homozygous mice were used. Transgene recombination was induced at 6 weeks of age by administration of 4 mg/mL (*Pax2.rtTA;TetO.Cre;R26.Confetti*) or 2 mg/mL (*Pax2.rtTA;TetO.Cre;R26.mT/mG*) doxycycline hyclate (Sigma-Aldrich, St.Louis, MO, USA) in drinking water supplemented with 2.5% sucrose (Sigma-Aldrich) for 10 days, followed by a 7-day washout. Uninduced animals showed no leakage nor non-specific transgene expression. The Confetti reporter, upon induction, allowed the stochastic labeling of the cells, by permanent recombination of a single color-encoding gene (red, yellow, green or cyan fluorescent proteins, RFP, YFP, GFP or CFP), with GFP cells occurring at lower frequency than other colors and being extremely rare (59, 62) (Fig. 10A-B). In homozygous animals, the combination of two color-encoding genes located on the two

homologous alleles is possible (red/yellow, red/cyan, red/green, yellow/yellow, yellow/cyan, etc.) and the resulting outcomes are shown in Fig.13Q. This technique allowed us to evaluate the clonal composition of the lesions, as all labeled cells will generate same color labeled cells following proliferation (58).

In the mT/mG reporter, following doxycycline administration, membrane-targeted EGFP genetically labels Pax2-expressing cells in green, while all the other kidney cells are labeled in red by the membrane-targeted tdTomato fluorescent protein (Fig. 10C-D).

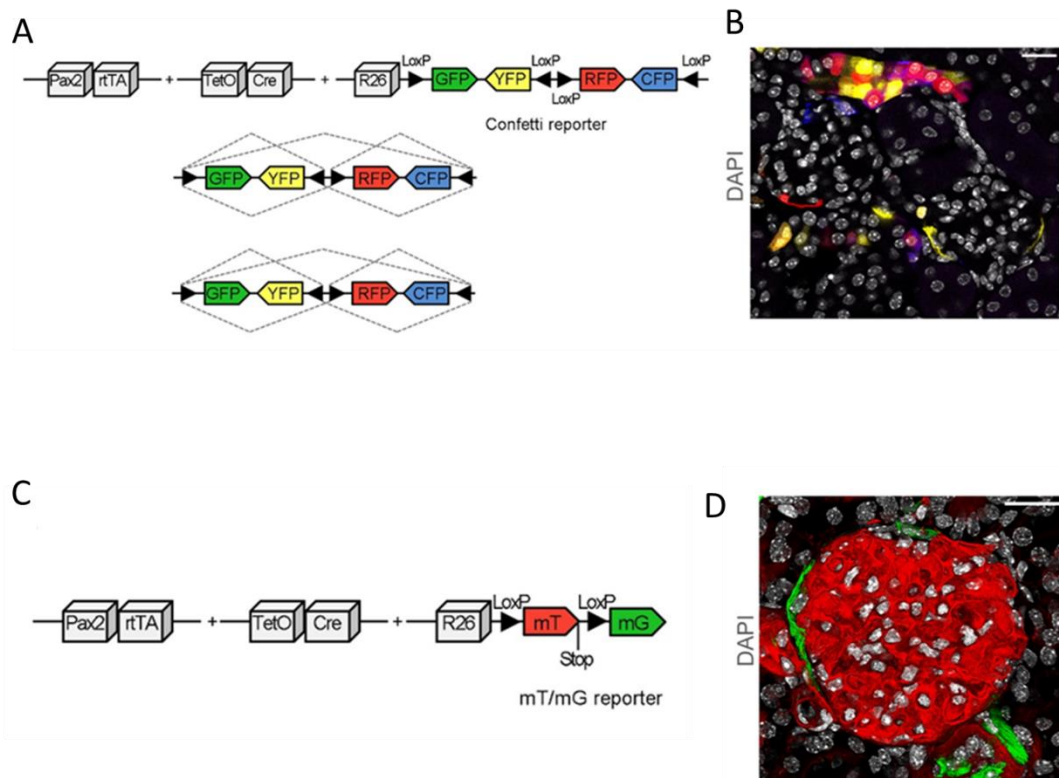


Fig. 10. *Pax2.rtTA;TetO.Cre;R26.Confetti* and *Pax2.rtTA; TetO.Cre; Rosa26.mT/mG* mouse models. (A) Scheme depicting the triple transgenic mouse model *Pax2.rtTA;TetO.Cre;R26.Confetti*. Confetti construct inserted in the Rosa26 locus. Upon doxycycline induction, recombination occurs across different pairs of loxP sites and results in expression of one out of the four possible fluorescent reporter proteins (nuclear GFP, membrane associated CFP, cytoplasmic RFP, cytoplasmic YFP). Recombination in homozygous mice for the R26R-Confetti allele allows up to ten different fluorescent proteins combinations. (B) Representative image of a healthy glomerulus in the Pax2/Confetti mouse model. Bar=20 uM. (C) Scheme depicting the triple transgenic mouse model *Pax2.rtTA;TetO.Cre;R26.mT/mG*. (D) A 3D reconstruction of a healthy glomerulus in the Pax2/mT;mG mouse model. Bar= 20 μm. DAPI, 4',6-diamidino-2-phenylindole.

Anti-GBM serum was injected in 57 male mice (uninduced mice: $n=23$, *Pax2.rtTA;TetO.Cre;R26.Confetti* mice: $n=6$; *Pax2.rtTA;TetO.Cre;R26.mT/mG* mice: $n=28$) by an intravenous injection of 150 μL of anti-GBM serum (PTX-001 sheep anti-rat GBM serum; Probetex, Inc., San Antonio, TX). Animals were sacrificed 7 days after anti-GBM serum injection. Healthy male mice (uninduced mice: $n=3$, *Pax2.rtTA;TetO.Cre;R26.Confetti* mice $n=9$; *Pax2.rtTA;TetO.Cre; R26.mT/mG* mice: $n=5$) were sacrificed at the same time point and used as control.

In addition, in drug administration experiments, mice were randomly assigned to various groups following anti-GBM injection: 1) vehicle (distilled water, uninduced mice: $n=7$, *Pax2.rtTA;TetO.Cre;R26.mT/mG* mice: $n=7$); 2) 15 mg/kg panobinostat (LBH-589, MedChemExpress, Solluntuna, Sweden; uninduced mice: $n=5$, *Pax2.rtTA;TetO.Cre;R26.mT/mG* mice: $n=10$), 3) 10 mg/kg givinostat (ITF2357, Selleckchem, Munich, Germany; uninduced mice: $n=5$); 4) 60 mg/kg ruxolitinib (INCB18424, MedChemExpress; uninduced mice: $n=6$). Drugs were administered daily, by oral gavage. In a group the treatment was administrated daily starting from 18 hours after anti-GBM injection and animals were sacrificed 7 days after anti-GBM serum injection and kidney collected. Another group received a daily treatment starting from day 4 and animals were sacrificed at day 10. For longterm experiments a third experimental group received the treatment for 30 days starting from day 4 and animals were sacrificed at day 90.

3.4 Genotyping

Tail biopsies were incubated overnight at 55°C in lysis reagent (1 M TrisHCl pH 8.5, 0.5 M EDTA, 20% SDS, 4 M NaCl, 0.1 mg/mL proteinase K neutralized with 40 mM TrisHCl, all from Sigma-Aldrich), centrifuged and DNA extracted using isopropanol

(Sigma-Aldrich). Primers and PCR parameters were obtained from Jackson Laboratory online resources of the relative strain purchased or previously reported experimental procedure (29).

3.5 Blood urea nitrogen measurement

Blood was collected from submandibular plexus at different time points and BUN measured in heparin anticoagulated plasma samples using the Reflotron System (Roche Diagnostics, Risch-Rotkreuz, Switzerland), according to the manufacturer's protocols. The number of mice used and statistical values (where applicable) are provided in the figure legends.

3.6 Albumin and Creatinine excretion measurement

Urine spot samples were collected for each mouse at different time points. Urine albumin (Mouse Albumin ELISA, Albuwell M, Exocell, Philadelphia, PA, USA) and urine creatinine (Creatinine urinary Colorimetric Assay kit, Cayman Chemical, Ann Arbor, MI, USA) concentrations were determined according to the manufacturer's protocol. The number of mice used and statistical values (where applicable) are provided in the figure legends.

3.7 Transcutaneous measurement of glomerular filtration rate

Measurement of the glomerular filtration rate (GFR) was done as described elsewhere (58). In brief, mice ($n=5$ anti-GBM treated mice, $n=5$ healthy mice) were anesthetized with isoflurane and a miniaturized imager device built from two light-emitting diodes, a photodiode and a battery (Mannheim Pharma and Diagnostics GmbH, Mannheim,

Germany) were mounted via a double-sided adhesive tape onto the shaved animals' neck. For the duration of recording (~1.5 h) each animal was conscious and kept in a single cage. Prior to the intravenous injection of 150 mg/kg FITC-sinistrin (Mannheim Pharma and Diagnostics GmbH), the skin's background signal was recorded for 5 min. After removing the imager device, the data were analyzed using MPD Studio software ver.RC12 (MediBeacon GmbH Cubex41, Mannheim, Germany) (63). The GFR [$\mu\text{l}/\text{min}$] was calculated from the decrease of fluorescence intensity over time (i.e., plasma half-life of FITC-sinistrin) using a two-compartment model, the animal's body weight and an empirical conversion factor.

3.8 Histological analysis

Kidney tissues were fixed in 10% neutral-buffered formalin overnight at room temperature, dehydrated in graded alcohols and embedded in paraffin. For histologic and morphometric analysis 5 μm sections were stained with periodic acid–Schiff (PAS) reagents and analyzed under the optical microscope Leica DM750 (Leica Microsystems, Mannheim, Germany). Cellular crescents were assessed when more than a single layer was present around the inner circumference of Bowman capsule.

Glomerular injury was scored in 150 glomeruli per section by a blinded observer. The following criteria were assessed in each of the glomeruli: mesangial matrix expansion, mesangial proliferation, focal necrosis, cellular crescents and tuft retraction.

These glomeruli were further classified as having no injury, mild injury (<25% of glomerulus), moderate injury (25%- 50% of glomerulus) or severe injury (>50% of glomerulus).

3.9 Immunofluorescence and confocal microscopy

Confocal microscopy was performed on 10 μm sections of renal tissues or on human renal progenitor cells cultured in multi-chamber slides by using a Leica SP5 AOBS confocal microscope equipped with a Chameleon Ultra-II two-photon laser (Coherent, Santa Clara, CA, USA) or a Leica SP8 STED 3X confocal microscope (Leica Microsystems). To generate 3D images, we used the image processing software Leica Application Suite X (Leica Microsystems). Z-series stacks were obtained from 30 μm kidney slices. Images were collected at 0.3 μm intervals.

For the mice with mT/mG reporter, the acquisition was set in the green and red wavelengths using 488 and 543 nm wavelength excitation, respectively. For the mice with Confetti reporter, the acquisition was set in the cyan, green, yellow, and red wavelengths using 405, 488, 514, and 543 nm wavelength excitation, respectively. Nuclei were counterstained with DAPI (Thermo Fisher Scientific, Waltham, MA, USA) excited with UV laser at 405 nm.

For immunofluorescence, the following antibodies were used: anti-synaptopodin (Progen Biotechnik, Heidelberg, Germany Cat# 65194, clone G1D4), anti-CD133/2 (Miltenyi Biotec S.r.l., Bergisch Gladbach, Germany, Cat# 130-090-851, clone 293C3), and anti-SFN (Thermo Fisher Scientific, USA, Cat# MA5-11663), anti-NPHS1 (Novus Biologicals, Centennial, CO, USA, Cat# NBP1-30130), anti-NPHS2 (Abcam, Cambridge, UK, Cat# ab50339), anti-histone H3 (acetyl K9) (Abcam, Cat# ab32129, clone Y28), anti-phospho-STAT3 (Tyr705) (Cell signaling, Danvers, Massachusetts, USA, Cat# 4113, clone M95C) and anti-fibrinogen (FITC conjugate) (Agilent Santa Clara, CA, Cat# F0111) primary antibodies. Alexa Fluor secondary antibodies were obtained from Molecular Probes (Thermo Fisher Scientific) and used at a dilution 1:1000 (Alexa Fluor 488- and 546-coniugated) or 1:400 (Alexa Fluor 647-coniugated). Staining with Alexa Fluor546 Phalloidin (Molecular Probes) was performed following manufacturer's instructions.

3.10 Optical tissue clearing and confocal 3D reconstruction

For the 3D reconstruction of the whole glomeruli and for quantification of filtration slit density, optical clearing of the kidneys was performed. Briefly, kidneys were dissected and immediately incubated at 4 °C in hydrogel solution (4% v/v acrylamide, 40.025% v/v bisacrylamide, 0.25% w/v VA-044 initiator, 4% PFA, 1X phosphate buffered saline (PBS)) for 1 day. The gel was polymerized at 37 °C for 3 h, and the presence of oxygen was minimized by filling tubes to the top with hydrogel solution. Samples were removed from the hydrogel solution, immersed in clearing solution (200 mmol/l boric acid, 4% SDS, pH 8.5) and incubated at 50°C for 1 day. Kidneys were cut in 300 µm thick slices using a Vibratome and incubated at 50 °C for 4 days with clearing solution changed every day. Before immunolabeling, samples were incubated in PBST (0.1% Triton-X in 1 × PBS) for 1 day. During immunolabeling, PBST was used as diluent in all steps. Samples were incubated in primary antibody for 24 h at 37 °C and then washed in PBST for 4 h at 37 °C followed by secondary antibody incubation for 24 h at 37 °C and washed for 4 h at 37 °C prior to mounting. Following primary antibodies were used: anti-NPHS2 (Sigma-Aldrich, Cat# P0372), anti-GFP (Abcam, Cat# ab6556) and anti-synaptopodin (Progen Biotechnik, Heidelberg, Germany Cat# 65194, clone G1D4). Secondary antibodies were obtained from Molecular Probes (Thermo Fisher Scientific). Samples were mounted in 80,2% fructose with 0.5% (v/v) 1-thioglycerol.

To generate 3D reconstructions of glomeruli, Z- series stacks were obtained from 300 µm kidney slices. Images were collected at 1µm intervals by using a Leica SP8 confocal microscope and de-convolved with Huygens Professional software (Scientific Volume Imaging B.V., Hilversum, The Netherlands). We used image processing software from Leica Microsystems “Leica Application Suite X” for 3D reconstruction.

3.11 STED microscopy and slit diaphragms density quantification

STED xyz images (i.e., z-stacks acquired along 3 directions: x, y, and z axes) were acquired by using SP8 STED 3X confocal microscope (Leica Microsystems). Alexa Fluor TRITC-secondary antibody was excited with a 555 nm tuned white light laser (WLL) and emission collected from 565 to 605 nm. 660 nm pulsed-depletion laser was used with a gating between 0.7 to 6 ns. Images were acquired with Leica HC PL APO CS2 100x/1.40 oil STED White objective.

Collected images were de-convolved with Huygens Professional software version 18.04. For the quantification of filtration slit coverage, z stacks of NPHS2 signal were acquired (at least 5 μm thick). All the images of each z stack were merged, and the foot process length and the area of the field were manually dissected and measured with Image J. The total length of the foot processes was divided by the total area of interest. The analysis was carried out in 8 mice (4 anti-GBM mice and 4 panobinostat treated mice); 5 randomly selected areas for each glomerulus of at least 5 glomeruli per mouse were evaluated.

For STED acquisition on progenitor cells culture, the following antibodies were used: anti- α -Tubulin (Sigma-Aldrich, Cat# T6074), goat anti mouse IgG1 546 secondary antibody (Thermo Fisher Scientific).

3.12 Clone frequency analysis

Single-cell clones and clones with two or more cells were counted within the inner circumference of Bowman capsule in 3D reconstructed glomeruli of healthy and crescentic glomerulonephritis *Pax2.rtTA;TetO.Cre;R26.Confetti* mice at time point 7 days. For each clone size, clone frequency analysis showed in Fig.1N, was assessed by calculating the relative frequency $F_{(i)}$ as followed:

$$F_{(i)} = \text{Clone frequency (\%)} = \frac{\text{n}^\circ \text{ of clones of } n \text{ cells}}{\text{total n}^\circ \text{ of clones}} \times 100$$

where $1 \leq n \leq 24$ in *Pax2.rtTA;TetO.Cre;R26.Confetti* mice because this is the maximum clone size observed.

In order to simplify the large data set, the clones which contains more than 5 cells were grouped in class intervals and then cumulative frequency $F_{(k)}$ was calculated for each group by using the following formula:

$$F_{(k)} = \sum_{i \in S} f_{(i)}$$

where cumulative frequency $F_{(k)}$ is the sum of overall relative frequency $f_{(i)}$ in the set S; were S is the class interval.

Reconstructed glomeruli were analyzed in blinded manner (78 glomeruli from 9 healthy mice; 32 glomeruli from 6 crescentic glomerulonephritis mice). Clone size was established by counting the nuclei counterstained with DAPI.

3.13 Calculating observed and theoretical distribution of crescent colors

To estimate Confetti reporter color distribution in affected glomeruli, the number of clones with different colors were counted for each 3D reconstructed glomerulus. Only clones with more than 5 cells were included in the analysis, as these were not observed in healthy animals. To compare the observed distribution of colors per glomerulus to what would be expected if lesions were generated from proliferation of 1, 2, 3 or 4 cells, we calculated the theoretical distribution as follow. First, we calculated the recombination frequency of each color on healthy mice glomeruli (72 glomeruli, n= 4 mice). A total of 10 colors were expected from the combination of the fluorescent protein YFP, RFP, CFP

and GFP (possible outcomes are reported in Fig.13Q). Resulted frequency of each color is shown in Fig.13R.

Since GFP cells occur at low frequency (frequency = 0.01), thus, to simplify the analysis, the green color and its combinations with the other colors were not considered, as they would have contributed only marginally and for the analysis a total of 6 colors were evaluated. All possible combinations of colored cells were considered (e.g. if 3 cells proliferate there are $6^3= 216$ possible color combinations: red-red-red, red-red-yellow, red-yellow-red, red-yellow-blue,...). To calculate the probability of each color combination, we applied the known recombination frequency of each color (for example: red-red-red= $0.24 \times 0.24 \times 0.24$, red-red-yellow= $0.24 \times 0.24 \times 0.48$, red-yellow-red = $0.24 \times 0.48 \times 0.24$, red-yellow-blue = $0.24 \times 0.48 \times 0.12$, ...). The frequencies for color combinations of 1, 2, 3, and 4 colors were summed; for example, out of 216 possible combinations of 3 cells there are 6 yielding one color (red-red-red etc.) with a summed frequency of 0.13, 90 x two color combinations (summed frequency=0.59), 120 x three color combinations (summed frequency=0.28) and 0 x four color combinations (Fig.13P). We then compared the observed distribution of colors per crescent to the expected distributions of colors in crescents derived from the hypothetical proliferation of 1, 2, 3 or 4 cells.

3.14 Crescent quantification and podocyte regeneration

In the *Pax2.rtTA;TetO.Cre; R26.mT/mG* mice, the percentage of the glomeruli presenting crescents was assessed by confocal microscopy and results were expressed as percentage of glomeruli presenting a crescent derived from PAX2+ cells over the number of glomeruli presenting a Pax2+ PEC in the Bowman capsule.

Quantification of glomeruli with Pax2+-derived podocytes in *Pax2.rtTA;TetO.Cre; R26.mT/mG* mice was performed on 30 μ m sections of renal tissues. Pax2+-derived

podocytes were detected as green cells within glomerular tuft in 3D reconstructed glomeruli. Results were expressed as percentage of glomeruli presenting Pax2+-derived podocyte over the number of Pax2+ glomeruli in the Bowman capsule.

3.15 Analysis of glomerular damage in kidney sections upon optical tissue clearing

To evaluate the percentage of glomeruli with no sign of damage, 3D reconstructions of confocal microscopy images of entire glomeruli stained for NPHS2 were analyzed. For each section, 10 glomeruli were acquired, and the integrity of the slit diaphragm was evaluated by two independent blinded observers.

Glomeruli without defects in coverage representing denudated areas with podocyte loss and without foot process effacement in podocytes surrounding these gaps were considered “uninjured”.

3.16 Single cell RNA sequencing

Single cell RNA sequencing was performed on human PEC derived from whole glomeruli culture prepared as previously described (38), in agreement with the Ethical Committee on human experimentation of the Azienda Ospedaliero-Universitaria Careggi, Florence, Italy. Briefly, human kidney fragments were minced and glomeruli isolated by standard sieving technique through graded mesh screen (60, 80 and 150 mesh). The glomerular suspension was collected, washed and plated on fibronectin-coated dishes. After 4-5 days of culture, isolated glomeruli adhered to the plate, resulting in cellular outgrowth. Glomeruli were detached and adherent cells were characterized for CD133 and CD24 expression and differentiation potential following 0.2 μ M panobinostat (LBH-589, MedChemExpress) stimuli at passage 1.

For Single cells RNA sequencing, adherent cells were harvested and filtered using the Flowmi™ Tip strainer (Miltenyi Biotec) to remove clumps and debris, followed by viability assessment with trypan blue (Sigma-Aldrich) staining.

The single cell suspension with 98% viability was run on a 10x Chromium Single Cell instrument (10x Genomics, Pleasanton, CA) following Manufacturer's instructions, as previously described (64). 3' gene expression libraries were constructed as previously described (64) and were sequenced on an Illumina NextSeq550 (Illumina Inc., San Diego, CA).

Healthy *Pax2.rtTA;TetO.Cre; R26.mT/mG* mouse (n=2) was anesthetized with ketamine/xylazine solution and perfused via the left heart ventricle with 40 mL cold D-PBS via intracardiac persusion. Kidneys were transferred into 50 mL EBM medium containing 1 % (v/v) penicillin-streptomycin solution, cut into small fragments and incubated 30 min at 37 °C with 1 mg/mL collagenase Type IV. The glomerular suspension was gently pressed and sieved through a 70 µm mesh cell strainer. Strainer was repeatedly rinsed with cold D-PBS and the filtrate was collected, washed and resuspended in RPMI-1640 medium (Sigma-Aldrich) supplemented with 20% FBS (Hyclone, GE Healthcare Life Sciences, Logan, UT, USA) and containing 1% penicillin-streptomycin solution. Primary murine glomeruli were cultured in their medium at 37 °C in a humidified atmosphere containing 95 % air 5 % CO₂. After 5 days glomerular cell outgrowths were trypsinized, and the cells were resuspended in D-PBS and sorted for endogenous expression of GFP by using the FACS Aria III BD (Becton Dickinson, Franklin Lakes, NJ, USA). Cells were then plated in 6 well dishes at a density of 80,000 cell/well in RPMI supplemented with 20% FBS. Following 16 hours of starvation, cells were stimulated for 48 hours with 0.2 µM panobinostat, or DMSO (Sigma-Aldrich) in DMEM-F12 medium (D2906, Sigma-Aldrich) containing 10% FBS (Hyclone, GE Healthcare Life Sciences). For Single cells RNA sequencing, following 48 h stimuli adherent cells were harvested

and processed as previously described for the run on the 10x Chromium Single Cell instrument (10x Genomics) and the subsequent sequencing on the Illumina NextSeq550 (Illumina Inc).

Pax2.rtTA;TetO.Cre;R26.Confetti mice injected with anti-GBM serum and treated with vehicle ($n=2$), panobinostat ($n=2$), givinostat ($n=2$) or ruxolitinib ($n=2$) were sacrificed 7 days after injury. Kidneys were minced into 1-mm pieces with a razor blade, incubated at 37°C in enzyme dissociation buffer containing 250 U/ml Liberase (Roche) and 40 U/ml DNase I (Sigma-Aldrich) for 10 minutes, following by a mechanical dissociation by using gentleMACS tissue dissociator (Miltenyi Biotec). The reaction was stopped by adding 10% FBS and then passed through a 40µm cell strainer. The dissociated cells were then incubated with RBC lysis buffer. We then proceeded to remove the dead cells employing the dead cell removal kit (Miltenyi Biotec) according to manufacturer's instruction. Cells were then filtered using the Flowmi™ Tip strainer and run on a 10x Chromium Single Cell instrument (10x Genomics). This method generated single cell suspension with greater than 95% viability.

3.17 Bioinformatic Analysis on mouse samples

Raw sequencing data for kidney samples and for Pax2-labelled renal progenitors were processed using the 10x Genomics Cell Ranger pipeline (version 3.0.1). First, cellranger mkfastq demultiplexed libraries based on sample indices and converted the barcode and read data to FASTQ files. Next, cellranger count performed alignment to the GRCh38 human reference genome (STAR) (65), filtering and unique molecular identifier (UMI) counting.

Next, we performed the quality control on both datasets to remove poor-quality cells and badly detected genes. For in vitro data we filtered out cells with a mitochondrial read rate > 10% and expressed < 1700 genes, for in vivo > 40% and < 100 respectively. Cell-

specific biases were normalized through the `scrn computeSumFactors` method and all counts were log-transformed after addition of a pseudocount of 1.

Next we mitigated the batch effect through the `ComBat` (66) and `MNN` methods for *in vitro* and *in vivo* data respectively to later proceed with feature selection to keep “informative” genes only used for dimensional reduction through PCA. The first 50 PCs were used to construct a neighborhood graph of observations through the `pp.neighbors` function, which relies on the UMAP algorithm to estimate connectivity of data points.

Once visualized data, for *in vitro*, we assessed the localization and the expression of interesting markers such as the EGFP and the podocyte, progenitor and tubular cells markers, for *in vivo* we clustered data at different resolutions and obtained the marker genes for produced clusters. Based on results we kept data at resolution 1 and relying on the expression of tissue specific markers we gathered clusters with similar signatures. Next, we isolated the immune line clusters in order to subset them in their subtypes to then proceed with the comparison between panobinostat treated and vehicle samples in order to define the most differential expressed genes between these two groups to study their trend in all treatments. Finally, we evaluated the expression of genes related to crescentic glomerulonephritis in mouse in each immune subtype.

3.18 Bioinformatic Analysis on human samples

Raw sequencing data for human PEC and RPC samples were processed in the same way as those from mouse experiments except for alignment that was performed to the GRCh38 human reference genome (STAR) (65).

The resulting count matrices have undergone quality control to remove poor-quality cells by selecting those with a mitochondrial read percentage $< 20\%$ and a number of expressed genes > 350 . Cell-specific biases were normalized by dividing the measured counts by the size factor obtained through the `scrn computeSumFactors` method, which

implements the deconvolution strategy for scaling normalization (67), and log-transformed after addition of a pseudocount of 1. Looking for highly variable genes, through the scanpy (68) `pp.highly_variable_genes` function with default parameters, we noticed a high expression of renal progenitor cell markers, in particular *CD44*, *CD9*, *CD24* and *PROM1*. In order to confirm the progenitor signature of our cells, we matched this dataset with a previous one containing renal progenitors, already used in (69).

We took the union of highly variable genes whose expression was common across both datasets, thus resulting in 4000 genes that were used for the matching mutual nearest neighbors (MNN) batch correction (70), performed through the python `mnnpy` package (<https://github.com/chriscainx/mnnpy>).

Then we used these genes to perform the dimension reduction on the MNN batch corrected data (7443 cells) through principal component analysis (PCA) and the first 40 principal components (PCs) were used to construct a neighborhood graph of observations through the `pp.neighbors` function, which relies on the Uniform Manifold Approximation and Projection (UMAP) algorithm to estimate connectivity of data points. Lastly, we clustered data by `tl.louvain` function with a resolution of 0.3, obtaining 5 clusters, identified the marker genes by the function `tl.rank_genes_groups` and plotted them as a hierarchically clustered heatmap, focusing on the cluster 2 main markers, in the order *CD9*, *EPCAM*, *SFN*, *PROM1*, *CD24*.

3.19 Differentiation of murine bone marrow-derived macrophages

Bone marrow was isolated from C57BL/6J mice. Briefly, both hind limbs per mouse were removed. Under sterile conditions, the ends of the bones were snipped and the bone marrow flushed into a 50 ml FALCON tube using a 25G needle and a 5 ml syringe

containing DMEM with GlutaMAX™ I (Gibco, Thermo Fisher Scientific). The cells were centrifuged at 1500 rpm for 7 minutes, the supernatant discarded and the cell pellet resuspended in 8 ml fresh differentiation medium (40 ml DMEM with 10% FBS (Biochrom, Merck Millipore, Burlington, MA, USA), 1% Pen/Strep (PAN-Biotech, Aidenbach, Germany), and 50 µM β-Mercaptoethanol (Gibco, Thermo Fisher Scientific), and 20% L929 supernatant and 5% Horse Serum. Cell suspension was placed through a 70 µm filter and transferred into a non-treated 10 cm polystyrene petri dish. On day 4, 6 and 8, remove 50% old medium and add 50% fresh differentiation medium. If macrophages are confluent on day 9, remove medium and add cold D-PBS for 10 minutes at 4°C and pipette up and down to detach macrophages. This step was repeated if not all macrophages were detached. Cell suspension was centrifuged at 1500 rpm for 7 minutes, resuspended in fresh differentiation medium, cells counted and transferred into non-treated 12-well plates (300.000 cells per well in 1 ml medium, Costar, US) or non-treated 6-well plates (1x10⁶ cells per well in 3 ml medium, Thermo Scientific, Roskilde, Denmark) followed by priming with 50 pg/ml LPS (Sigma-Aldrich) for 16 or 24 hours.

3.20 Generation of necrotic soups

The kidneys were harvested from C57BL/6J mice, cut into half (longitudinal) and the medulla and papilla removed using a scalpel. Only the cortex containing glomeruli was used and cut into small pieces using a scalpel and placed into 1 ml D-PBS (1 kidney in 1 ml D-PBS). Necrotic soups were generated by 4-5 freezing and thawing cycles (-80°C for 30 minutes, then water bath (37°C), -80°C and so on. A 1 ml syringe was used to make a suspension and placed through a 70 µm filter to remove tissue. Afterwards, the necrotic soups were stored at -20°C until usage.

3.21 Stimulation of bone marrow-derived macrophages

After LPS priming, macrophages were treated with or without 400 nM panobinostat (LBH-589, MedChemExpress), 800 nM givinostat (ITF2357, Selleckchem) or 800 nM ruxolitinib (INCB18424, MedChemExpress) for 30 minutes prior to activation with 20% necrotic soups or 100 ng/ml LPS (Sigma-Aldrich) or vehicle (DMSO, Sigma-Aldrich) for 24 hours (71-73). After stimulation, supernatants were collected for ELISA and macrophages detached for flow cytometry analysis. For RT-qPCR, macrophages were stimulated for 16 hours.

3.22 Flow cytometry analysis of macrophages

Macrophages were detached from the 12-well plates using cold D-PBS for 10 minutes at 4°C and by pipetting up and down. Cells were transferred into collecting tubes, centrifuged and then washed with wash buffer (0.1% BSA, 0.01% sodium azide in D-PBS), and blocked with anti-mouse CD16/32 (2.4G2) for 5 minutes. After blocking, cells were stained with the surface antibodies FITC anti-mouse MHCII, FITC anti-mouse CD40, FITC anti-mouse CD80, PerCP anti-mouse CD86, and APC anti-mouse F4/80 (all from BioLegend, San Diego, CA, USA) for 30 minutes at 4°C in the dark. After incubation, cells were washed with wash buffer and reconstituted in 200 µl of fresh wash buffer. Flow cytometry analysis was performed on a FACSCalibur (Becton Dickinson) and the data analyzed with FlowJo 8.7 (Tree Star Inc., Ashland, OR, USA).

3.23 ELISA

Concentrations of IL-6 in the cell culture supernatants were measured using the mouse IL-6 ELISA Set (BD Biosciences) according to the manufacturer's protocol. The

absorbance was measured on a Multiskan Ex reader (Thermo Electron Corporation, Germany).

3.24 RPC cultures

Human RPCs were obtained from the pole opposite to the tumor of 3 patients who underwent nephrectomy for localized renal tumors in agreement with the Ethical Committee on Human Experimentation of the Careggi University Hospital, Florence, Italy. Written informed consent was received from participants prior to inclusion in the study. hRPCs were cultured as previously described (30).

3.25 MTT assay

80,000 RPCs were seeded on 6-well plate (Corning Incorporated, Corning New York, USA) in EGM-MV medium (Lonza, Basel, Switzerland) supplemented with 20% FBS (Hyclone, GE Healthcare Life Sciences, Logan, UT, USA). Following 16 hours starvation, cells were treated for 48 hours with 0.2 μ M panobinostat (LBH-589, MedChemExpress), 2 μ M givinostat, (ITF2357, Selleckchem) 20 μ M ruxolitinib (INCB18424, MedChemExpress) (or vehicle, DMSO, Sigma-Aldrich). For cell proliferation experiments, after 48 hours cells were detached with trypsin-EDTA solution 0,25% (Sigma-Aldrich) and counted. Cell viability and metabolism was assessed by MTT assay (Thermo Fisher Scientific) following manufacturer's instructions.

3.26 Annexin-V/ Propidium Iodide staining and cell cycle analysis

Following 48h stimuli with the different compounds, single cell suspensions were prepared and washed with cold D-PBS containing 0.1% sodium azide. Apoptosis and/or necrosis were evaluated using propidium iodide (PI) (Miltenyi Biotec) and the Annexin

V-APC (Thermo Fisher Scientific). For cell cycle analysis, cells were fixed in 2% paraformaldehyde, then, incubated with DAPI (Thermo Fisher Scientific) to perform the DNA content analysis.

Samples were acquired using MACS Quant Analyzer instrument and then analyzed with the Flowlogic software (both from Miltenyi Biotec). Annexin-APC was excited by a 635 nm laser line, Propidium Iodide was excited by a 488 nm laser line and DAPI was excited by a violet laser line at 408 nm (Fig.11).

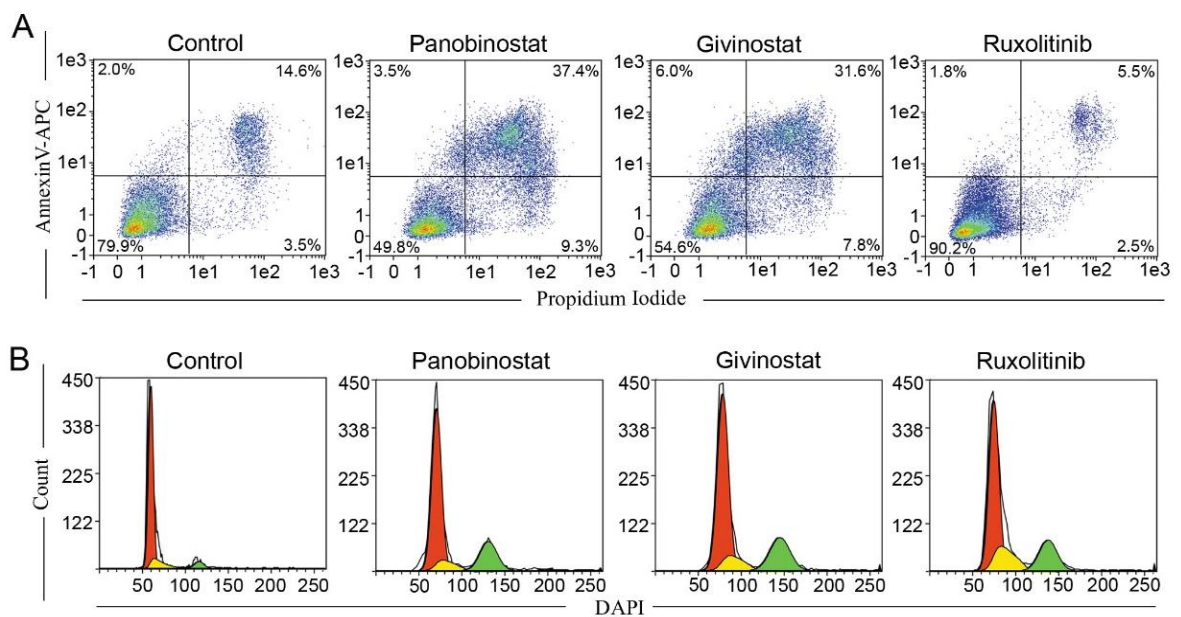


Fig. 11. Drugs influence RPC viability and proliferation.

(A) Representative gating strategy of Annexin-V/Propidium Iodide FACS staining for assessment of apoptosis induction. (B) Flow cytometry cell cycle analysis. Representative curve fitting used in order to calculate the distribution of the different phases of cell cycle in RPC measured by FlowLogic Software.

3.27 *In vitro* differentiation

RPC were plated in 6 well dishes at a density of 80,000 cell/well in EGM-MV 20% FBS. Following 16 hours of starvation, cells were stimulated for 48 hours with panobinostat, givinostat, ruxolitinib or 100 μ M retinoic acid (RA) (R2625, Sigma-Aldrich) in DMEM-F12 medium (D2906, Sigma-Aldrich) containing 10% FBS (Hyclone, GE Healthcare Life

Sciences). At the end of the differentiation period, cells were collected, counted, mRNA extracted using RNeasy Microkit (Qiagen, Hilden, Germany) and retrotranscribed using TaqMan Reverse Transcription Reagents (Thermo Fisher Scientific). TaqMan RT-PCR for GAPDH, NPHS1 and NPHS2 was performed using commercially available Assay on Demand kits (Thermo Fisher Scientific).

4 Results

4.1 Crescents derive from Pax2+ progenitors of the Bowman capsule

To evaluate the contribution of renal progenitors among the PEC to the generation of crescents, we employed *Pax2.rtTA;TetO.Cre;mT/mG* conditional transgenic reporter mice that allow to genetically label progenitors with enhanced green fluorescent proteins (EGFP) and perform lineage tracing (29). Following transgene induction by doxycycline administration, all Pax2+ progenitors among the PEC were marked in green (Fig. 12A). Following a washout period, we induced crescentic glomerulonephritis by intravenous injection of sheep anti-GBM serum (Fig. 12B). On day 7 we observed sheep IgG deposits in the glomeruli (Fig. 12C).

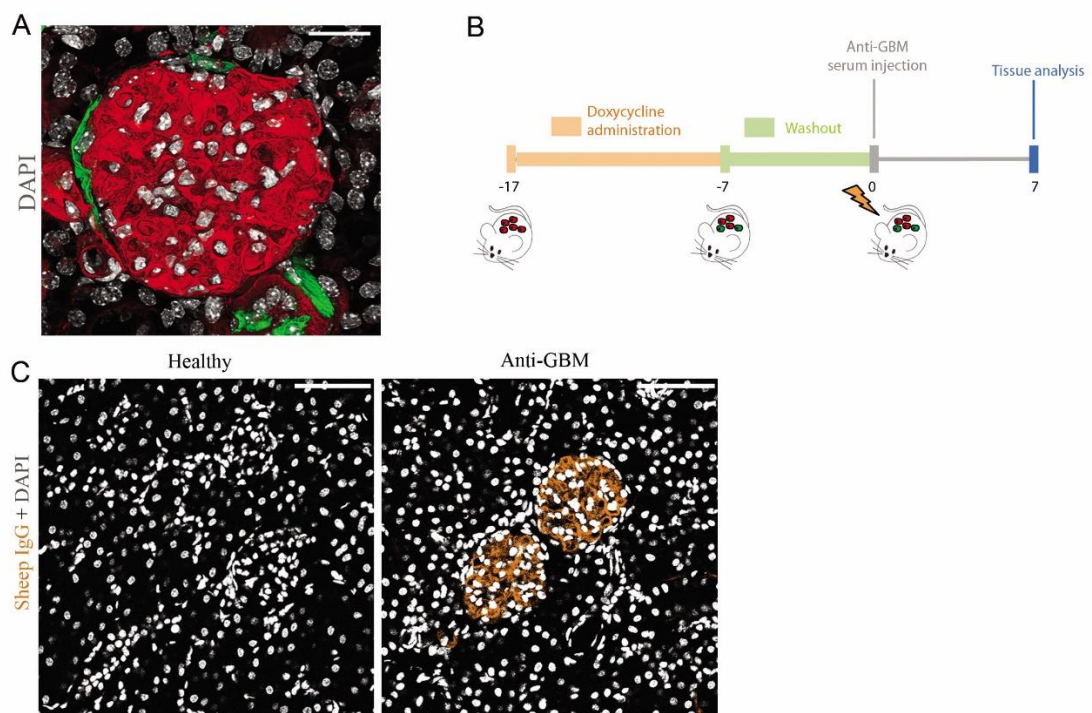


Fig. 12. Induction of anti-GBM disease in the *Pax2.rtTA;TetO.Cre; R26.mT/mG* mouse model. (A) 3D reconstruction of a healthy glomerulus in the *Pax2.rtTA;TetO.Cre;R26.mT/mG* mouse model. Bar=20 μ m. **(B)** Experimental scheme of crescentic glomerulonephritis induction. **(C)** Representative images of sheep IgG immunofluorescence performed at day 7 in healthy and

anti-GBM mouse respectively, demonstrating that mice mounted an immune response to sheep IgG. Bar=75 μ m.

DAPI, 4',6-diamidino-2-phenylindole; GBM, glomerular basement membrane.

PAS staining revealed focal segmental capillary loop necrosis and crescent-like proliferation of PEC in the Bowman space (Fig. 13A) in 37.7 ± 3.0 % of the glomeruli (Fig. 13B). Glomerular damage was associated with a rapid increase in albuminuria at day 1, that decline in the following days remaining higher than in healthy mice at day 7 (Fig. 13C). Proteinuria was accompanied by a loss of kidney function, shown by drop of glomerular filtration rate (GFR) (Fig. 13D) and by an increase in blood urea nitrogen (BUN) (Fig. 13E), i.e. altogether severe glomerulonephritis. Lineage tracing experiments and 3D confocal analysis showed that the Pax2⁺ subset of PEC expanded circumferentially among the Bowman capsule and largely constituted the glomerular crescents (Fig. 13F-H). Taken altogether, crescents originate from immature Pax2⁺ cells among the PEC that expand massively.

4.2 Crescents originate from clonal expansion of single Pax2⁺ progenitors

The origin of crescents from proliferation of Pax2⁺ progenitors suggested possible similarity to disorders induced by uncontrolled clonal proliferation and/or differentiation arrest of subpopulation of hematopoietic stem cells such as myelodysplastic syndrome, leukemia or myelofibrosis (77,78). In order to evaluate the possibility that also crescents could be clonal lesions, we employed the *Pax2.rtTA; TetO.Cre; Rosa26.Confetti* conditional transgenic mouse model that allowed clonal lineage tracing by genetical labelling of individual Pax2⁺ cells with one of the four fluorescent proteins (Fig. 10A,B) (29). To detect the entire crescentic lesion, we performed Z-stack analysis and 3D

reconstructions of glomeruli in 30 μm -thick sections (43) (Fig. 13I-L). Quantification of 3D analysis showed that in healthy mice, the number of Pax2+ cells per glomerulus was 4.6 ± 0.2 , while in mice with crescentic glomerulonephritis Pax2+ cells expanded to 18.9 ± 1.8 per glomerulus (Fig. 13M). Clone frequency analysis revealed that over 60% of clones were longer than 5 cells with a maximum clone size of 25 cells (Fig. 13N). In particular, 50% of crescents showed a single color, 36% two colors, and only 13% three colors (Fig. 1O). The observed color frequency matched the theoretically expected color pattern generated if no more than 1-2 Pax2+ cells proliferate to generate a crescent (Fig. 13P), calculated on the basis of the recombination frequency of each color observed in glomeruli of healthy mice (Fig. 13Q, R). Taken together, these results show that crescents derive from clonal proliferation of single Pax2+ PEC conceptually like in stem cell-related proliferative disorders.

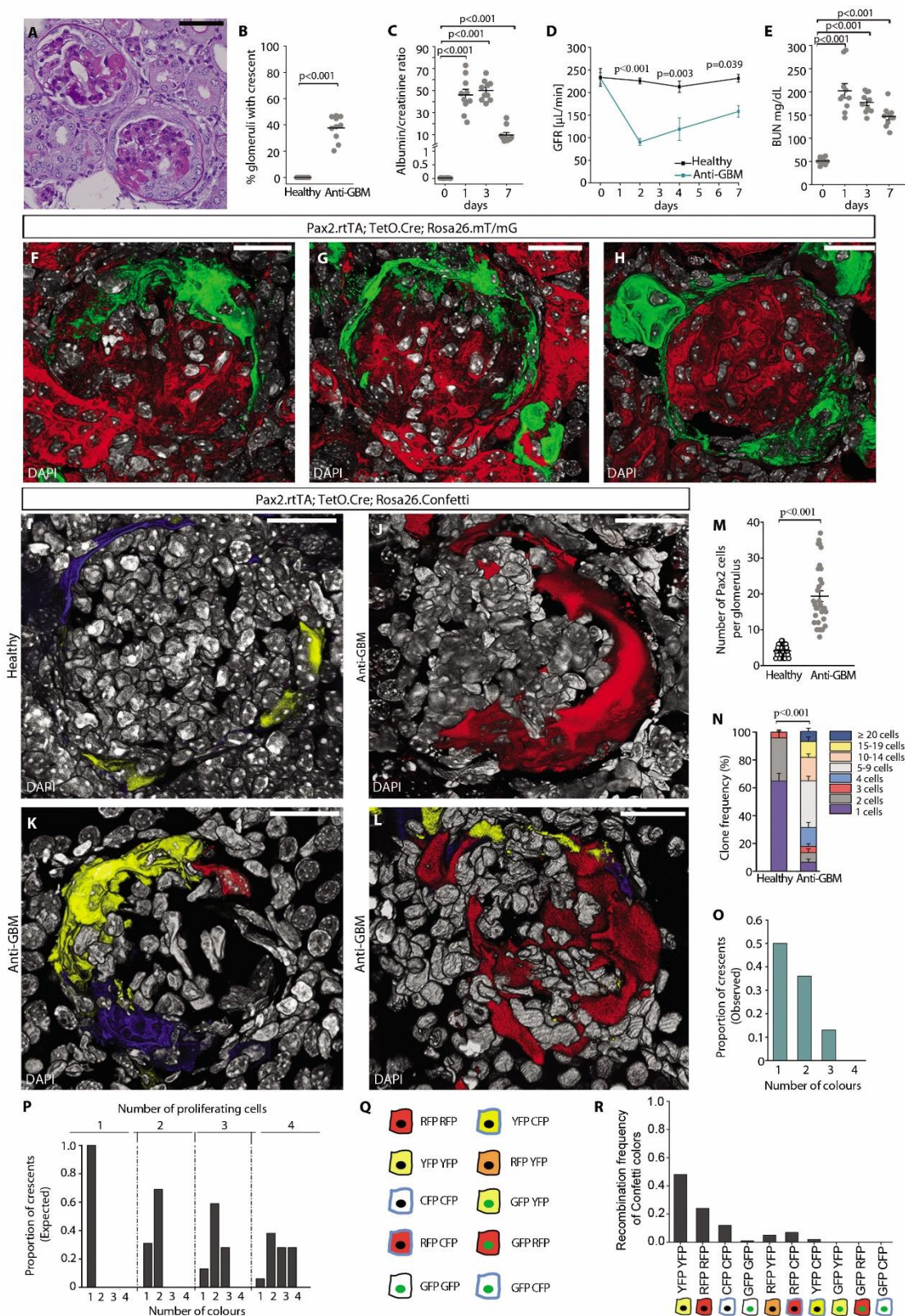


Fig.13. Crescents are generated by clonal proliferation of single RPCs.

(A) Representative image of a PAS-stained kidney section showing crescents and glomerulosclerosis in anti-GBM treated mice. Bars=50 μ m. (B) Quantification of glomeruli with crescent at day 7 on PAS-stained sections ($n=10$). (C) Assessment of urine albumin/creatinine ratio in anti-GBM treated mice ($n=10$). (D) GFR monitored over time in healthy mice and in mice following anti-GBM serum injection. Data are mean \pm SEM

(healthy $n=5$ and anti-GBM $n=5$). **(E)** BUN monitored over time in anti-GBM mice ($n=10$). **(F-H)** 3D reconstruction of glomeruli showing Pax2-tracked hyperplastic lesions (green) in *Pax2.rtTA;TetO.Cre;Rosa26.mT/mG* at day 7. DAPI (white) counterstains nuclei. Bars=20 μm . **(I-L)** 3D reconstruction of representative glomeruli of healthy *Pax2.rtTA;TetO.Cre;Rosa26.Confetti* (I) and of anti-GBM mice (J-L). DAPI (white) counterstains nuclei. Bars=20 μm . **(M)** Dot plot showing the number of Pax2+ cells per glomerulus in healthy mice ($n=9$) and in anti-GBM mice ($n=6$) at 7 days observed in 3D analysis. **(N)** Clone frequency analysis of Pax2+ cells in glomeruli of healthy ($n=9$) and anti-GBM mice ($n=6$) at day 7. Data are mean \pm SEM. **(O)** Bar chart showing the number of colours observed per crescent in anti-GBM mice ($n=6$). **(P)** Bar chart showing the theoretical distribution of colours per crescents resulting from proliferation of 1, 2, 3 or 4 Pax2+ cells labelled at the recombination frequency observed in induced animals. **(Q)** Colour combinations generated by recombination of the four possible fluorescent reporter proteins (nuclear GFP, membrane associated CFP, cytoplasmic RFP, cytoplasmic YFP) in homozygous mice for the R26R-Confetti allele, upon doxycycline induction (64). **(R)** Bar chart showing the proportion of each Confetti colour in 3D reconstructed glomeruli of healthy mice following induction period ($n=9$ mice).

Signals for fluorescent *mT/mG* proteins are GFP, green, and tdTomato, red. Signals for fluorescent *Confetti* proteins are GFP, green, CFP, cyan, RFP, red and YFP, yellow.

In dot plots (B, C, E and M) bars indicate mean values. Individual scores are shown. Statistical significance was calculated by Mann-Whitney test (B, C, E, M and N) or two-way ANOVA with Bonferroni post hoc test (D); numbers on graph represent p-values.

4.3 Panobinostat attenuates crescentic glomerulonephritis

The origin of crescents from clonal proliferation of single progenitors suggested a possible pathogenic similarity to proliferative hematopoietic stem cell disorders (79). Therefore, we examined the effect of three drugs successfully used for treatment of acute myeloid leukemia and primary myelofibrosis to inhibit the clonal expansion of the pathogenic hematopoietic stem cell clone, the two histone deacetylase inhibitors panobinostat and givinostat and the Jak1/2 inhibitor ruxolitinib (79-81). We treated *Pax2.rtTA;TetO.Cre;mT/mG* and *Pax2.rtTA;TetO.Cre;Rosa26.Confetti* mice with crescentic glomerulonephritis with the three compounds for 6 days starting 18 hours after anti-GBM serum injection. Animals were sacrificed at day 7. Panobinostat treatment decreased the number of crescents in comparison to the vehicle-treated group at day 7 after treatment (Fig. 14A, B, E, F), while no effects were observed in animals receiving givinostat and ruxolitinib (Fig. 14C-F). Consistently, the albumin/creatinine ratio was significantly improved in animals treated with panobinostat in comparison to the vehicle-treated group, at both day 3 and day 7 (Fig. 14G). Likewise, panobinostat ameliorated excretory kidney function, and a small effect was observed with givinostat, as shown by improvement of BUN levels (Fig. 14H). By contrast, no effect was observed with ruxolitinib (Fig. 14H). The doses of givinostat and ruxolitinib were sufficient to block their targets as demonstrated respectively by increase in lysine 9-acetylated histone H3 (Fig. 14I) and reduction in phosphorylated STAT3 (Fig. 14J) in comparison to vehicle-treated mice. These results show that panobinostat can attenuate crescent formation and ameliorate proteinuria and excretory kidney function.

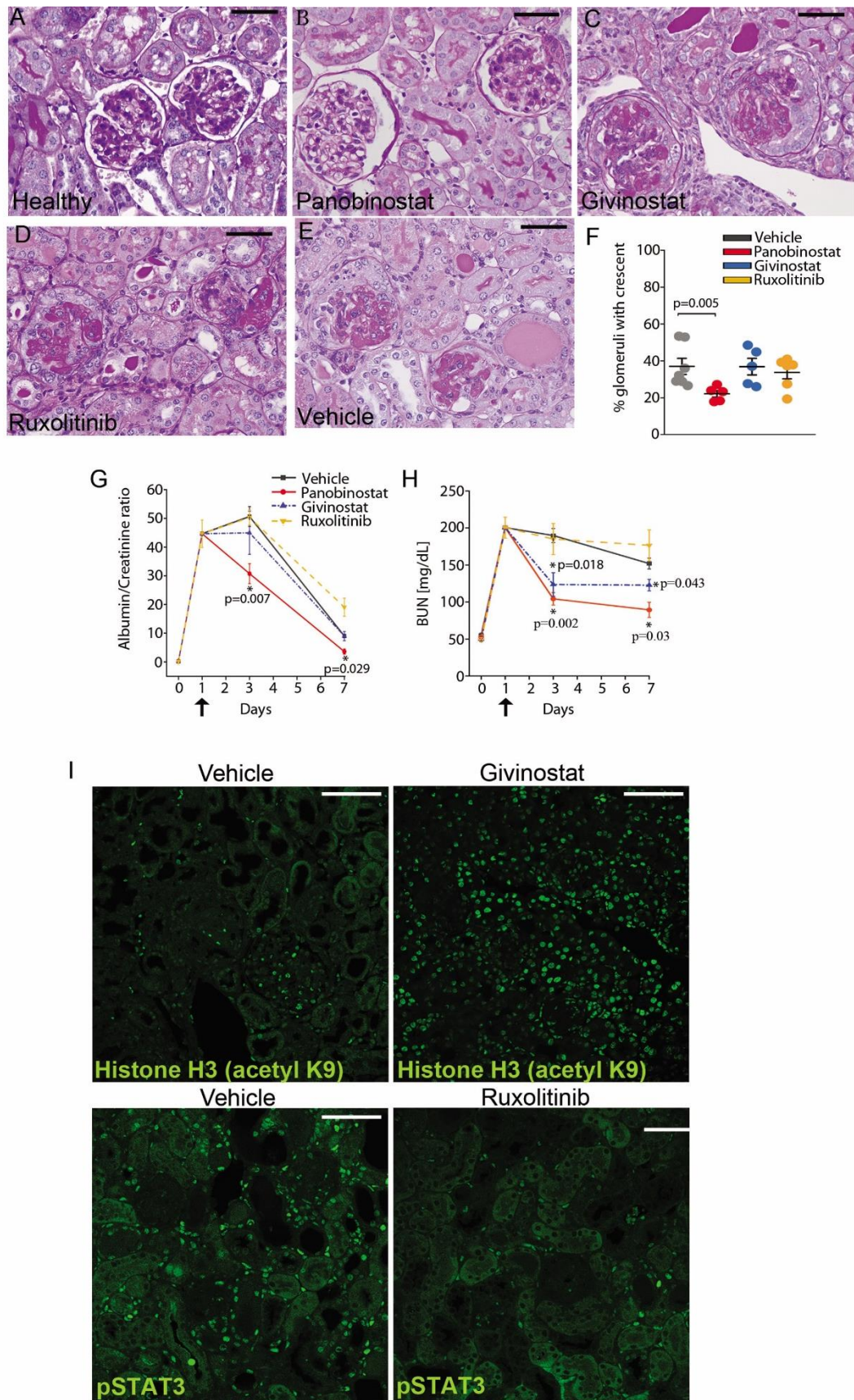


Fig. 14. Panobinostat ameliorates crescentic glomerulonephritis.

(A-E) Representative images of PAS-stained kidney sections at 7 days in the four experimental groups of mice and in healthy mice. Bars= 50 μ m. (F) Percentage of glomeruli presenting crescents at day 7 in the four experimental groups of mice (vehicle $n=7$, panobinostat $n=5$,

givinostat $n=5$, ruxolitinib $n=6$). **(G)** Time course of urine albumin/creatinine ratio and **(H)** BUN determined in the four experimental groups of mice (vehicle $n=7$, panobinostat $n=5$, givinostat $n=5$, ruxolitinib $n=6$). Data are mean \pm SEM. Black arrows indicate the starting point for drug treatment. **(I)** Representative image of lysine 9-acetylated histone H3 staining pattern in vehicle and givinostat treated mice. **(J)** Representative image of phospho-STAT3 staining pattern in vehicle and ruxolitinib treated mice.

In dot plots (F) bars indicate mean values. Individual scores are shown. Statistical significance was calculated by Mann-Whitney test; numbers on graph represent exact p-values. BUN, blood urea nitrogen. pSTAT3, phospho-STAT3.

4.4 Panobinostat promotes the generation of new podocyte

To establish the mechanisms how panobinostat could improve proteinuria and BUN, we performed single cell RNAseq on kidney samples obtained from mice with crescentic glomerulonephritis treated with panobinostat and compared it with those treated with givinostat and ruxolitinib. Therefore, we first characterized the different types of cell populations (Fig. 15A-E).

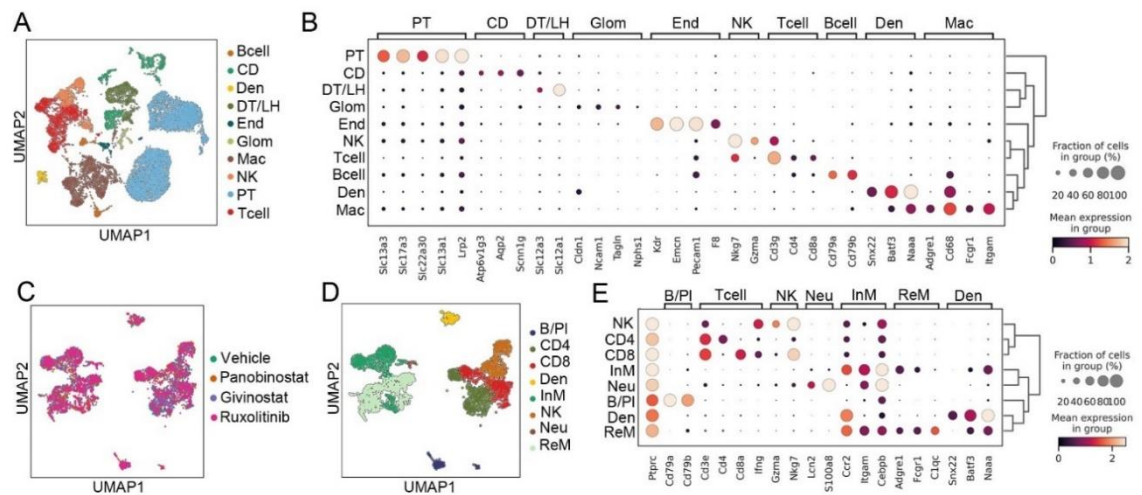
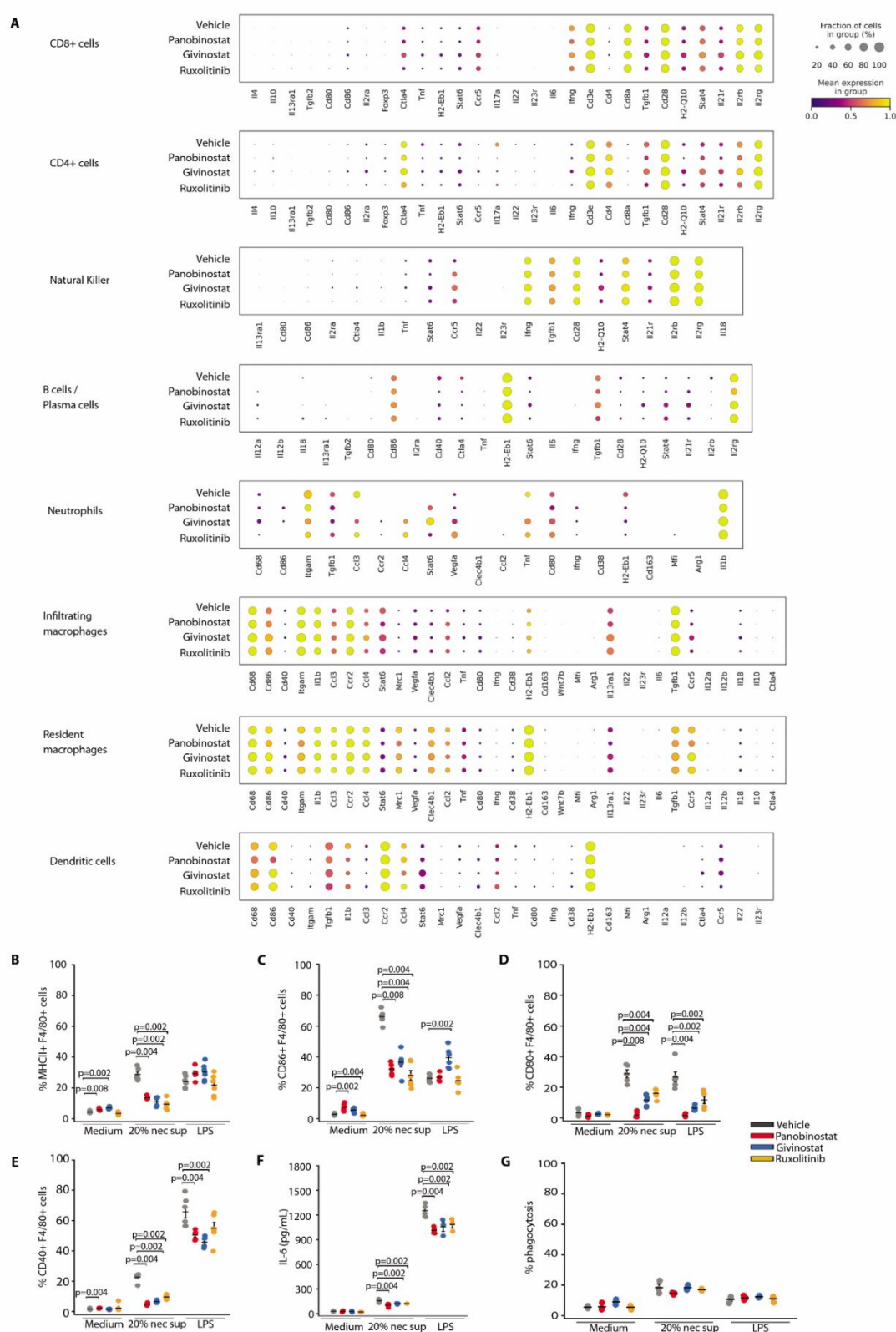


Fig. 15. Panobinostat, givinostat and ruxolitinib similarly modulate genes expression in immune system cells inside the kidney.

(A) UMAP projection of mouse kidney cells scRNA-seq dataset coloured by cluster. (B) Dot plot cluster characterization. (C) UMAP showing cluster distribution of immune system cells in mouse kidneys. (D) Dot plot cluster characterization of immune system cells in mouse kidneys. (E) UMAP showing cluster distribution of immune system cells in mouse kidneys derived from vehicle ($n=2$), panobinostat ($n=2$), givinostat ($n=2$) and ruxolitinib ($n=2$) treated mice.

UMAP, uniform manifold approximation and projection; CD, collecting ducts; Den, dendritic cells, DT/LH, distal tubule and loop of Henle; End, endothelial cells; Glom, glomerular cells; Mac, macrophages; NK, natural killer cells; PT, proximal tubule; B/PI, B cells and plasma cells; InM, Infiltrating macrophages; Neu, neutrophils; ReM, resident macrophages.

We then evaluated the expression on molecules reported in the context of crescentic glomerulonephritis in the literature (Fig. 16A) (1, 15, 82) and we observed no panobinostat-specific effect. Since macrophages have important roles in the pathogenesis of crescentic glomerulonephritis, we further analyzed the effect of panobinostat, givinostat or ruxolitinib on the expression of MHCII, CD86, CD80 and CD40, the level of IL6 and the phagocytic capacity in murine bone marrow-derived macrophages (Fig. 16B-G). We did not observe any effect specific to panobinostat suggesting that all the three drugs elicit similar anti-inflammatory properties. However, only panobinostat strongly reduces proteinuria and improves excretory kidney function in vivo, so their consistent anti-inflammatory effects cannot serve as an explanation and other unique properties of panobinostat must apply.



100 ng/ml). MHCII (B), CD86 (C), CD80 (D), CD40 (E) expression was evaluated on F4/80+ macrophages by FACS analysis. Data were obtained from 6 different murine bone marrow-derived macrophage preparations. (F) IL-6 production determined by ELISA. Data were obtained from at least 3 different murine bone marrow-derived macrophage preparations. (G) Phagocytosis rates determined by FACS. Data were obtained from 3 different murine bone marrow-derived macrophage preparations.

In dot plots (B-G), bars indicate mean values. Individual scores are shown. Statistical significance was calculated by Mann-Whitney test; numbers on graph represent p-values. LPS, lipopolysaccharide.

Finally, we explored the effects of panobinostat on resident glomerular cells. In the glomerulus, panobinostat reduced fibrin deposition at day 7, whereas no effect was observed at day 3 (Fig. 17A, B). Consistently, quantification of glomerular injury in PAS-stained sections demonstrated that panobinostat treatment reduced the percentage of injured glomeruli at day 7 in comparison to vehicle treated mice.

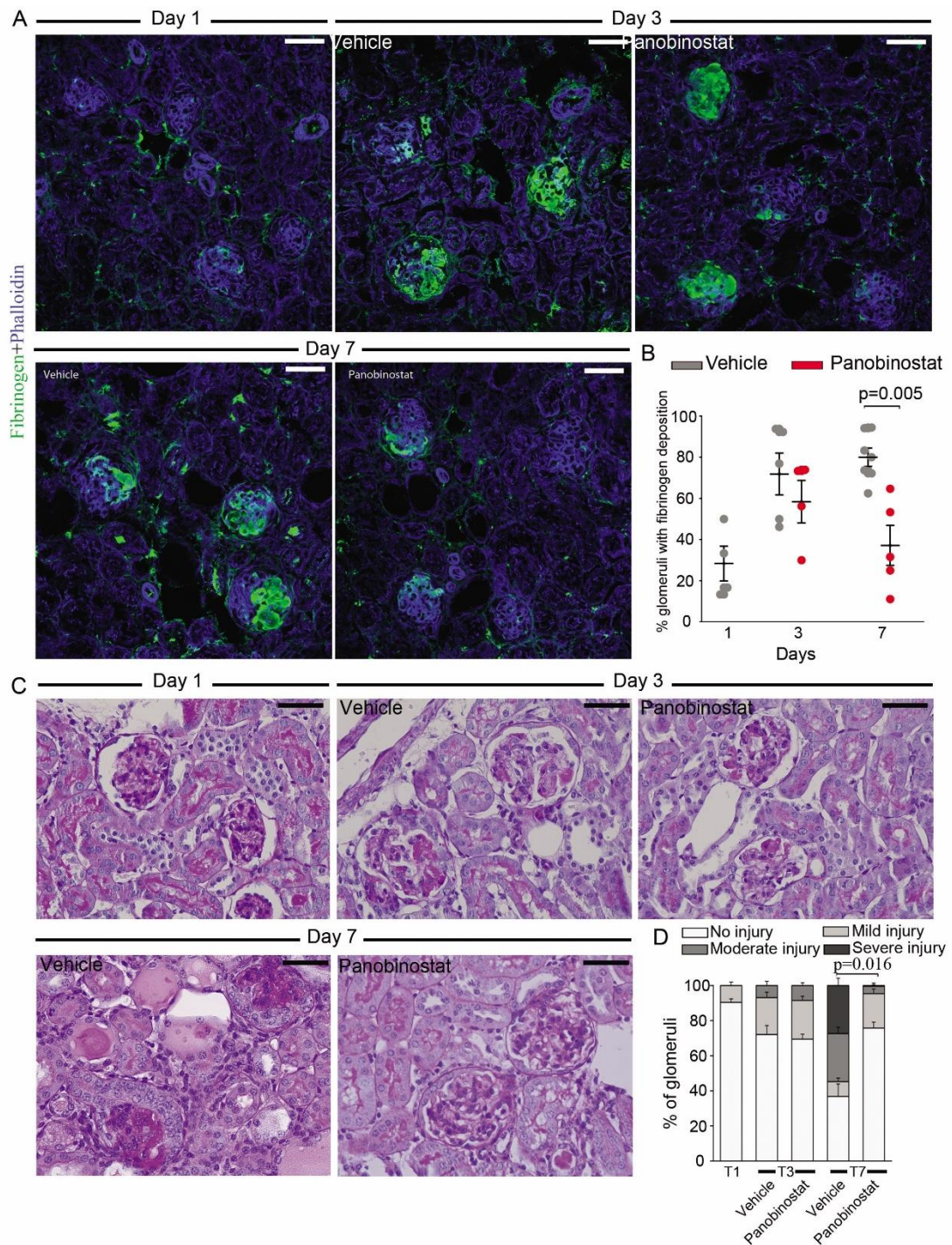


Fig. 17. Panobinostat reduces glomerular injury only at day 7.

(A) Representative images of fibrinogen staining patterns at different time points in vehicle and panobinostat treated mouse tissues. Phalloidin highlight the appearance of the surrounding tissues. Bars= 50 μ m. **(B)** Dot plot showing the percentage of glomeruli with fibrinogen deposition in vehicle and panobinostat treated mice at day 1 ($n=4$), at day 3 (vehicle $n=5$, panobinostat $n=4$) and at day 7 (vehicle $n=7$, panobinostat $n=5$) following anti-GBM injection. **(C)** Representative images of PAS-stained kidney sections at day 1 (before treatment starting), at day 3 and at day 7 in vehicle and in panobinostat treated group. Bars= 50 μ m. **(D)** Bar plot reporting percentage of glomerular injury quantified on PAS-stained renal sections in vehicle and panobinostat treated mice at day 1 ($n= 4$), at day 3 (vehicle $n=5$, panobinostat $n=4$) and at day 7 (vehicle $n=7$, panobinostat $n=5$) following anti-GBM injection.

In dot plots (B), bars indicate mean values. Individual scores are shown. Statistical significance was calculated by Mann-Whitney test; numbers on graph represent p-values.

By performing 3D analysis on kidneys *Pax2.rtTA;TetO.Cre;R26.mT/mG* mice, we observed smaller crescents in those treated for 7 days with panobinostat in comparison to vehicle (Fig. 18A-C). This associated with the appearance of Pax2-derived GFP+ cells inside the glomerular tuft showing morphological features of podocytes, such as primary and secondary foot processes (Fig. 18B, b'). Upon tissue clearing and staining with synaptopodin and anti-GFP, we confirmed the reduction in crescent dimensions (Fig. 18C-E) and observed a specular increase of glomeruli containing Pax2-derived podocytes clearly engrafted within the tuft after treatment with panobinostat, (Fig. 18E-G). Overall, panobinostat treatment resulted in a reduction in the ratio between glomeruli with crescent over glomeruli containing new podocytes (Fig. 18H).

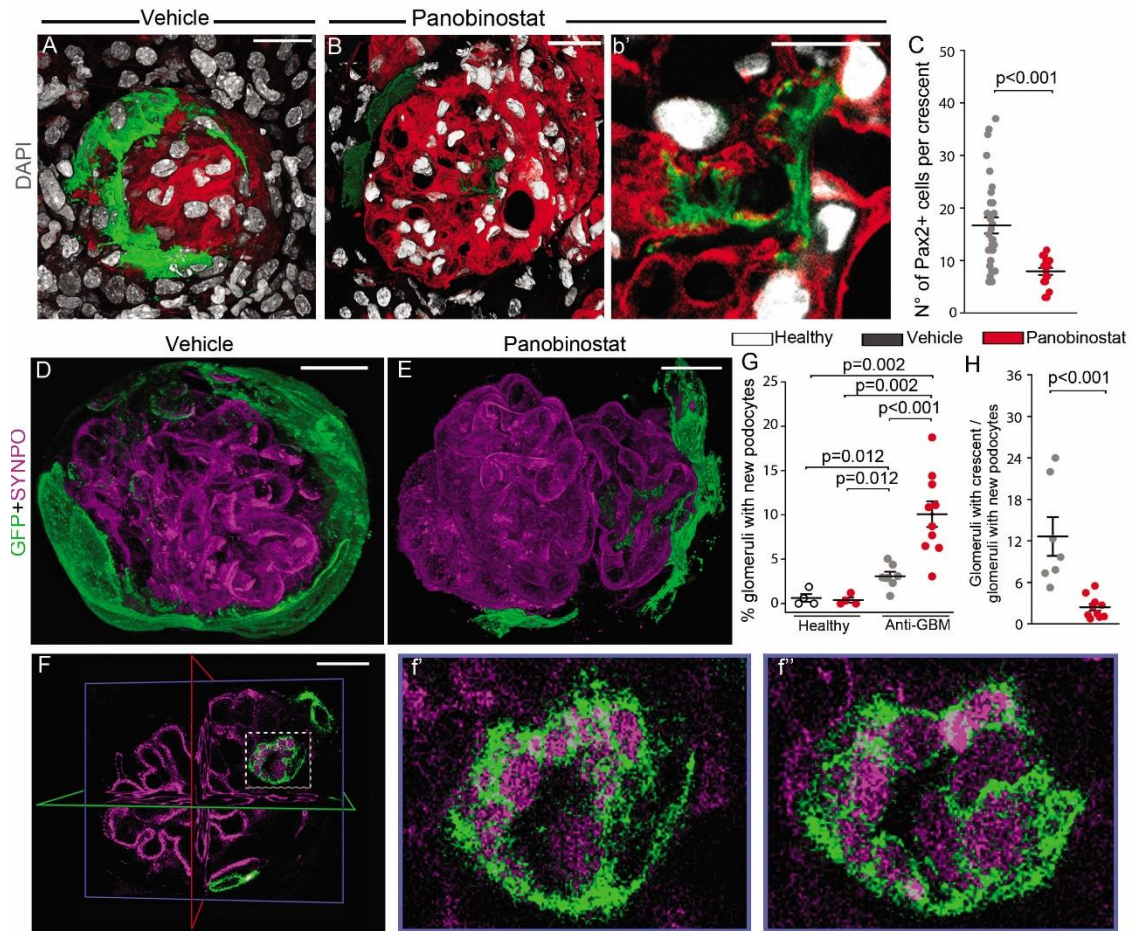


Fig. 18. Panobinostat enhances generation of new podocytes.

(A) Representative glomerulus of crescentic glomerulonephritis showing a Pax2+ positive hyperproliferative lesion in vehicle group. (B) Representative image of a glomerulus showing Pax2+ derived cells inside the glomerular tuft in panobinostat treated *Pax2.rtTA;TetO.Cre;R26.mT/mG* mouse. Bars = 20 μm (b') Higher magnification showing foot processes of the Pax2+ derived cell in (J) showing formation. DAPI counterstains nuclei (white). Bar = 10 μm . (C) Dot plot showing the number of Pax2+ cells within the crescent in vehicle ($n=6$) and panobinostat treated mice ($n=4$) in 3D analysis. (D-E) 3D reconstructions of whole glomeruli using optical tissue clearing in *Pax2.rtTA;TetO.Cre;R26.mT/mG*. The panel shows main patterns of glomerular lesion based on GFP and synaptopodin (SYNPO) expression (magenta) in anti-GBM injected mice treated with vehicle (D) or panobinostat (E). (F) A z-plane within the glomerulus in M showing a de novo formed green podocyte. The position of x (green), y (red) and z (blue) axis are reported. Bar = 20 μm . (f' and f'') Higher magnifications of the boxed area in (N). Different planes along Z axis show foot processes of the Pax2+ derived podocyte (green) interdigitating with those of preexisting podocytes (magenta). (G) Percentage of glomeruli with new podocyte over total number of glomeruli in vehicle ($n=4$) and panobinostat treated healthy mice ($n=4$) and in vehicle ($n=7$) and panobinostat treated anti-GBM mice ($n=10$). New podocytes were identified as GFP+ cells within the tuft presenting feature of podocyte cells. (H) Dot plot showing ratio of glomeruli with crescent to glomeruli with new podocytes in vehicle ($n=7$) and panobinostat treated mice ($n=10$). Signals for fluorescent *mT/mG* proteins are EGFP, green, and tdTomato, red. In dot plots (C, G and H) bars indicate mean values. Individual scores are shown. Statistical significance was calculated by Mann-Whitney test; numbers on graph represent p-values. BUN, blood urea nitrogen; DAPI, 4',6-diamidino-2-phenylindole; GFP, green fluorescent protein; SYNPO, synaptopodin;

Finally, we obtained pure primary cultures of mouse Pax2-labelled renal progenitors by sorting GFP+ cells from *Pax2.rtTA;TetO.Cre;R26.mT/mG* mice (Fig. 19A-C). Single cell RNAseq showed that after treatment with panobinostat primary cultures of mouse GFP+ renal progenitors upregulated podocyte markers (Fig. 19 E,F). These data suggest that panobinostat reduces crescent formation and promotes de novo generation of lost podocytes.

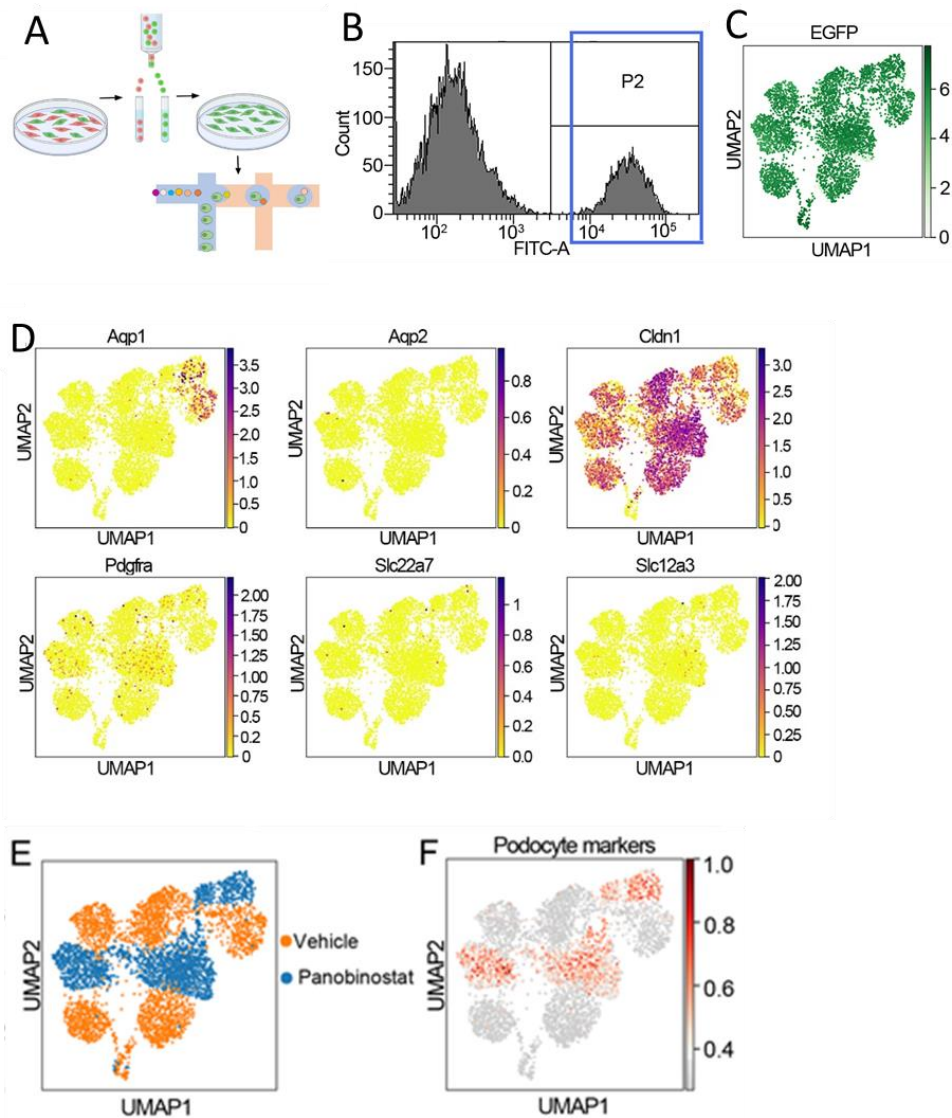


Fig. 19. Pax2+ cells isolated from *Pax2.rtTA;TetO.Cre;R26.mT/mG* mice express the progenitor marker *Cldn1* and upregulate podocyte markers following panobinostat treatment.

(A) Schematic representation of experimental setting used to perform single cell RNAseq on Pax2+ sorted cells. (B) Gating strategy to isolate Pax2+ cells from renal cells of the Pax2.rtTA;TetO.Cre;R26.mT/mG mouse. The far right peak (P2) containing EGFP+ cells was isolated by cell sorting. (C) UMAP visualization of GFP expression in Pax2+ isolated cells. (D) UMAP visualization of expression of the progenitor marker *Cldn1* and absence of expression of differentiated cells markers (*Pdgfra* for endothelial cells, *Aqp1*, *Aqp2*, *Slc22a7* and *Slc12a3* for tubular cells) in isolated Pax2+ cells. (E) UMAP projection of control and panobinostat treated Pax2+ cell scRNA-seq dataset splitted by treatment. (F) UMAP visualization of podocyte marker expression.

UMAP, uniform manifold approximation and projection; *Aqp1*, aquaporin1; *Aqp2*, aquaporin2; *Cldn1*, claudin1; *Pdgfra*, platelet derived growth factor receptor alpha; *Slc22a7*, solute carrier family 22 member 7; *Slc12a3*, solute carrier family 12 member 3.

4.5 Panobinostat improves 3D glomerular structure and restores slit diaphragm integrity

In order to gain further insight into how panobinostat influenced the integrity of the glomerular filtration barrier, we used STED super-resolution microscopy imaging for NPHS2, a slit diaphragm component, in optically cleared kidney tissues to produce volumetric representations of the glomerular slit ultrastructure at the nanometer scale (83). Three-dimensional rendering of confocal z-stacks showed the complex slit diaphragm structure with interdigitating foot processes in healthy glomeruli (Fig. 20A, a'), but simplified structure in mice treated with GBM antiserum (Fig. 20B, b'), consistent with foot process effacement or podocyte loss in crescent areas and in areas of podocytes surrounding the crescents. Podocyte loss as well as reduction of foot process density were less evident in panobinostat-treated animals (Fig. 20C, c'). Overall, panobinostat treatment resulted in a high increase of glomeruli with no sign of damage ("uninjured glomeruli") from 25.0 ± 7.6 to 85.4 ± 8.6 (Fig. 3D). Quantitative analysis showed that panobinostat treatment increased the filtration slit density as a marker of podocyte foot process density in comparison to vehicle-treated mice (Fig. 20E-G). These results show that panobinostat turns the uncontrolled hyperplasia of immature PEC into a coordinated differentiation into new mature podocytes that restore the injured glomerular filtration barrier in crescentic glomerulonephritis.

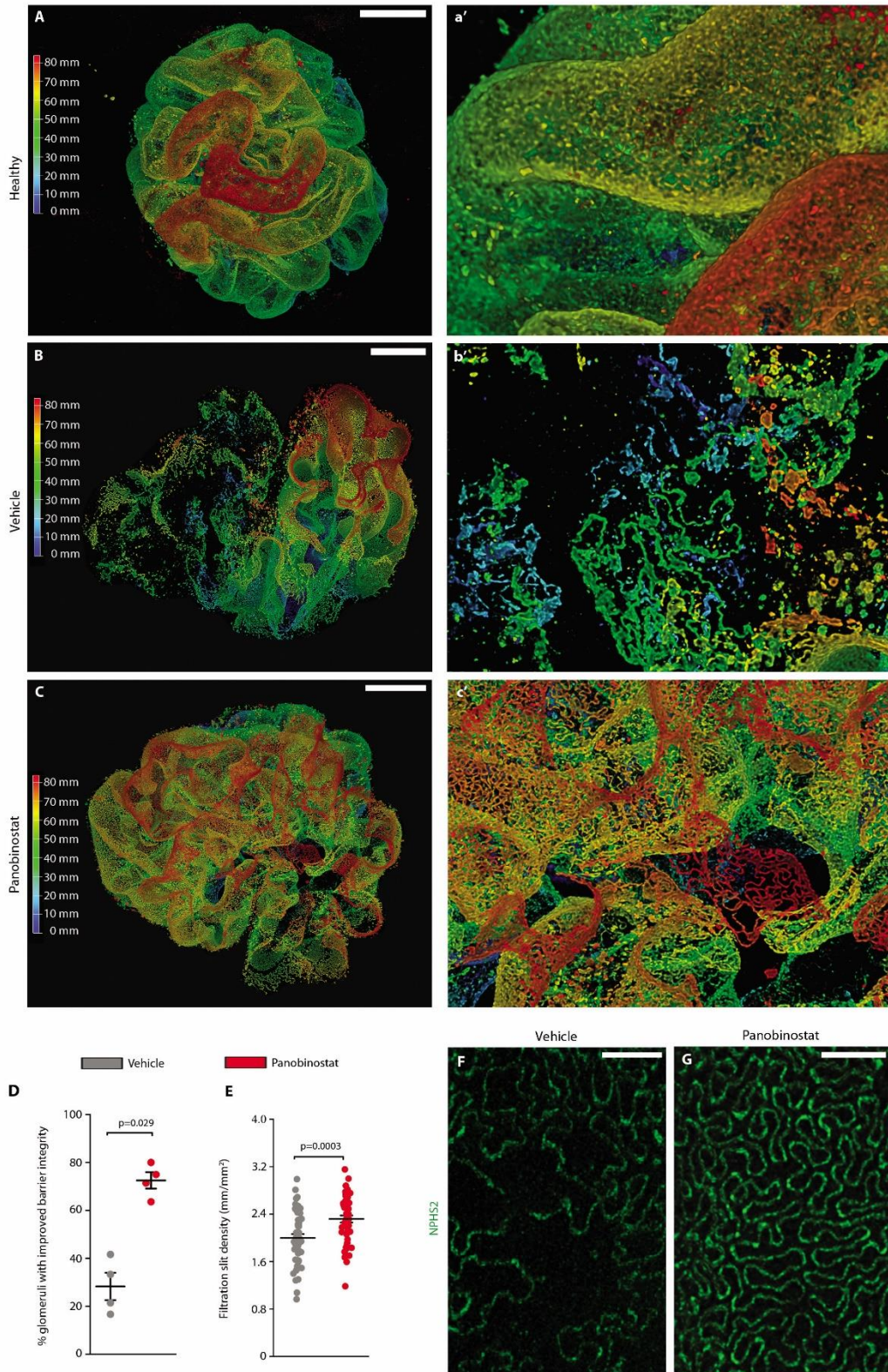


Fig. 20. Panobinostat improves 3D glomerular structure and slit diaphragm integrity.

(A-C, a'-c') 3D reconstructions of whole glomeruli using optical tissue clearing. The panel shows main patterns of glomerular lesion based on NPHS2 expression in healthy mice (A, a') and in crescentic glomerulonephritis mice treated with vehicle (B, b') or panobinostat (C, c'). NPHS2 expression is shown with a depth coding profile to preserve z-information. Bars=20 μ m. (D) Percentage of uninjured glomeruli presenting slit diaphragms integrity in vehicle ($n=4$) and panobinostat treated mice ($n=4$), assessed on fluorescently labeled optically cleared kidney tissue. (E) Density of slit diaphragm was assessed as a marker of terminal podocyte differentiation by

using STED-super resolution microscopy. The quantification was carried for 5 randomly selected areas for each glomerulus in at least 5 glomeruli per mouse (vehicle $n=4$ and panobinostat $n=4$ mice for group). **(F-G)** Representative images of podocytes foot processes by using STED-super resolution microscopy upon tissue clearing. NPHS2 is stained in green. Bars= 2 μm . In dot plots (D and E) bars indicate mean values. Individual scores are shown. Statistical significance in D and E was calculated by Mann-Whitney test; numbers on graph represent p-values. GBM, glomerular basement membrane. NPHS2, podocin.

4.6 Delayed treatment with panobinostat maintains renoprotective capacity and avoids chronic kidney disease

We then evaluated the capacity of panobinostat to exert a renoprotective effect even once the injury had already established and prevent kidney failure, even after apparent acute phase remission. To this aim, we administered the drug to mice on day 4 after induction of injury, and we followed-up mice for 90 days measuring proteinuria and kidney function at different time points (Fig. 21A-C). Starting treatment with panobinostat at day 4, i.e. once the peak of proteinuria had passed and crescents were already present, maintained its efficacy in reducing proteinuria and improving kidney function (Fig. 21A-C). The difference was already visible at day 10, 1 week after the start of treatment (Fig. 21A-C) confirming that this was not related to suppression of the injury phase.

At day 90, mice treated with vehicle achieved a partial remission, but with persistent proteinuria, elevated BUN and reduced GFR, i.e., CKD. In contrast, mice treated with panobinostat underwent complete remission of proteinuria and BUN levels showing normal GFR (Fig. 21A-C), hence, did not develop kidney failure (Fig. 21A-C).

Analysis of the kidneys showed a reduction of the percentage of glomeruli with crescent at day 10 and an almost total disappearance at day 90 (Fig. 21D). This associated with a significant increase in the percentage of glomeruli with new podocytes at day 10 that had further increased at day 90 (Fig. 21E). Strikingly, we also observed a significant increase of the number of newly generated podocytes per glomerulus in panobinostat-treated mice in comparison to vehicle at day 90, but also to panobinostat-treated mice at day 10 (Fig. 21F), suggesting a persistently active repair process with time. Indeed, at day 90, glomeruli with newly generated podocytes represented 60.7% of glomeruli presenting crescents on day 4 (at start of treatment) in panobinostat treated mice vs. only 24.3% in vehicle-treated mice (Fig. 21G). Representative pictures are shown in Fig. 21H-M. Taken altogether, these results show that panobinostat exerts long-term nephroprotective effects

by persistently promoting the production of new podocytes for a continued glomerular repair.

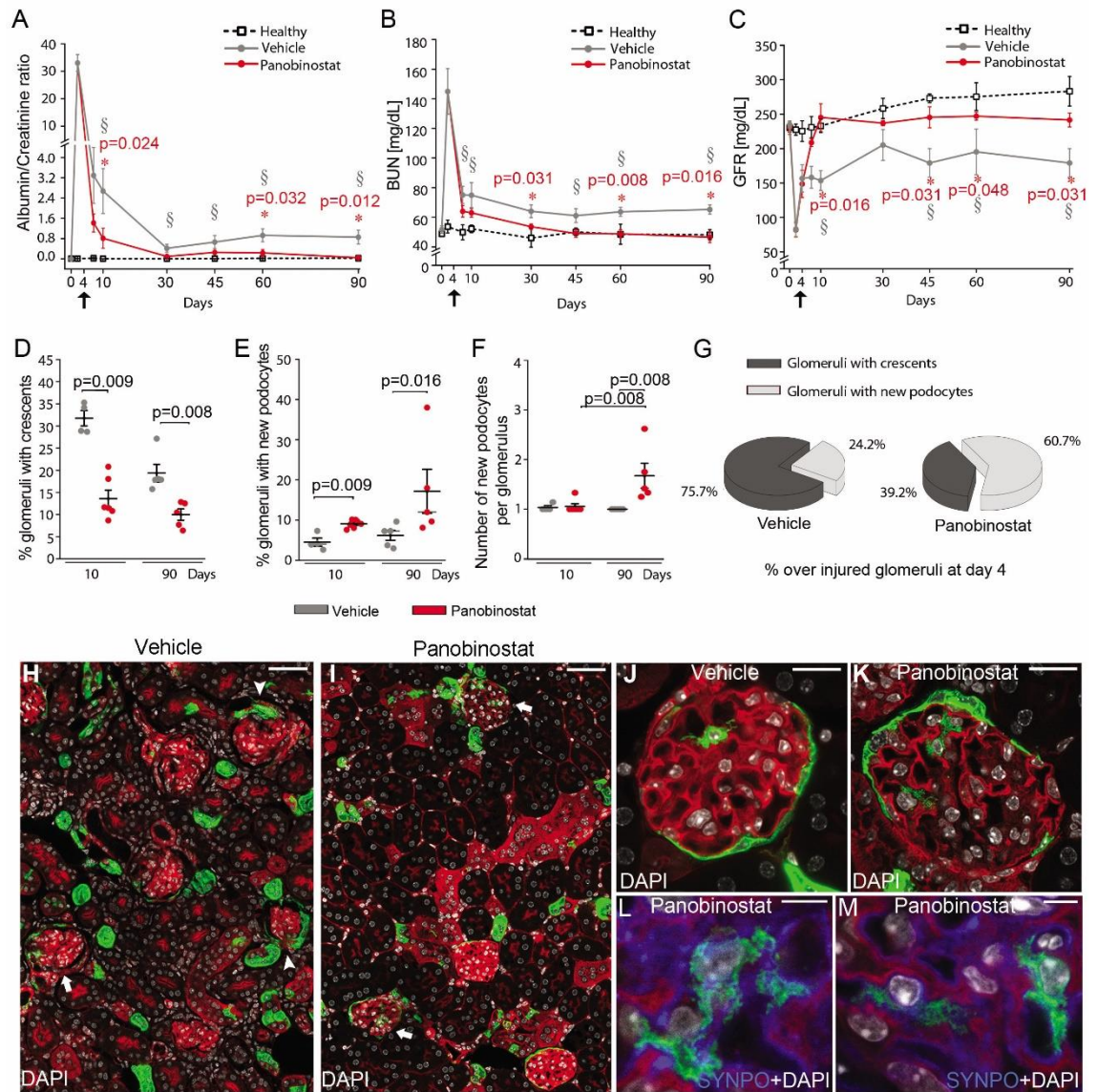


Fig. 21. Panobinostat ameliorates crescentic glomerulonephritis and prevents kidney failure progression.

(A) Time course of urine albumin/creatinine ratio determined in healthy ($n=4$), vehicle ($n=9$ at day 4 and 10, $n=5$ at day 30, 45, 60 and 90) and panobinostat ($n=11$ at day 4 and 10, $n=5$ at day 30, 45, 60 and 90) treated mice. (§) Significance of vehicle versus healthy mice: day 10 $p=0.004$, day 30, 45, 60 and 90 $p=0.016$. (*) Significance of panobinostat versus vehicle. (B) Time course of BUN determined in healthy ($n=4$), vehicle ($n=9$ at day 4 and 10, $n=5$ at day 30, 45, 60 and 90) and panobinostat ($n=11$ at day 4 and 10, $n=5$ at day 30, 45, 60 and 90) treated mice. (§) Significance of vehicle versus healthy mice: day 7, 10 $p=0.019$, day 45, 60 and 90 $p=0.032$. (*) Significance of panobinostat versus vehicle. (C) GFR determined in healthy ($n=4$), vehicle ($n=5$) and panobinostat ($n=4$) treated mice. Black arrows indicate the starting point for drug treatment. Data are mean \pm SEM. (§) Significance of vehicle versus healthy mice: day 10, 45 and 90 $p=0.016$, day 60 $p=0.032$. (*) Significance of panobinostat versus vehicle. (D) Percentage of glomeruli

presenting crescents at day 10 (vehicle $n=4$, panobinostat $n=6$) and day 90 (vehicle $n=5$, panobinostat $n=5$). **(E)** Percentage of glomeruli with new podocyte(s) over total number of glomeruli at day 10 (vehicle $n=4$, panobinostat $n=6$) and day 90 (vehicle $n=5$, panobinostat $n=5$). **(F)** Dot plot showing the mean number of Pax2+ cells observed within glomeruli at day 10 (vehicle $n=4$, panobinostat $n=6$) and day 90 (vehicle $n=5$, panobinostat $n=5$). **(G)** Percentage of glomeruli with crescent and glomeruli with new podocytes observed at day 90 (vehicle $n=5$, panobinostat $n=5$). Percentages were calculated among glomeruli presenting crescent at day 4 after injury. **(H, I)** Representative images of kidneys from vehicle (H) and panobinostat (I) treated *Pax2.rtTA;TetO.Cre;R26.mT/mG* mice sacrificed at day 90, showing the presence of Pax2+ derived cells inside the glomerular tuft in panobinostat treated mice (arrows) and the presence of crescent in vehicle treated mice (arrowheads). Bars=50 μm . **(J, K)** Representative image of a glomerulus showing Pax2+ derived cells inside the glomerular tuft in vehicle (J) and panobinostat (K) treated *Pax2.rtTA;TetO.Cre;R26.mT/mG* mice sacrificed at day 90. Bars=20 μm . **(L, M)** Higher magnification showing foot processes and synaptopodin (SYNPO) expression (blue) in the Pax2+ derived cell in panobinostat treated *Pax2.rtTA;TetO.Cre;R26.mT/mG* mice sacrificed at day 90. DAPI counterstains nuclei (white). Bars=5 μm .

Signals for fluorescent mT/mG proteins are GFP, green, and tdTomato, red. In dot plots (D-F) bars indicate mean values. Individual scores are shown. Statistical significance in A-F was calculated by Mann-Whitney test. Numbers on graph represent p-values.

BUN, blood urea nitrogen; DAPI, 4',6-diamidino-2-phenylindole; SYNPO, synaptopodin.

4.7 Expansion within crescents of a PEC subset expressing CD133 and stratifin associates with patient outcome

To identify the cell subset generating crescents also in human, we obtained PEC cultures from outgrowth of glomeruli of healthy human kidney (38) and processed them by 10X Genomics Chromium system combined with Illumina sequencing. Clustering of the entire pooled dataset identified seven transcriptionally distinct populations (Fig. 22A) and for each of them we looked for the 50 most differentially expressed genes (Table 1). By cross-referencing genes that were enriched in these clusters with the published literature, we observed that cluster 4 and 5 were highly enriched in previously reported crescent markers (53) (Fig. 22B). In addition, cluster 4 was enriched for genes with roles in cellular pathways intimately linked to crescents, stem cell niches (29,84,85) and cancer-stem cell (86,87, 88) such as *EPCAM*, *CD9*, *CD24*, *SFN*, *LAMC2*, *CRNDE*, *HOXB9*, *CDA* (Table 1).

0_n	1_n	2_n	3_n	4_n	5_n	6_n
TFPI2	CKS2	NEAT1	LDHA	PDLIM4	IGFBP2	CCT6A
HSPD1	CENPF	S100A6	ENO1	GSTP1	SRGN	GLRX3
HSPE1	HMGB2	FTH1	SRGN	CD24	SPARC	CYCS
HSP90AA1	TPX2	TUBA1A	PGK1	KRT7	TPM2	PPA1
NASP	UBE2S	RPS18	LGALS1	CAPG	BGN	PCBD1
PTMA	MKI67	S100A10	VIM	TPM2	PDLIM4	GHITM
HNRNPM	PLK1	MALAT1	CKB	HOXB9	SELENOM	SSBP1
MCM3	ASPM	RPL34	TPI1	CDA	TAGLN	CHCHD2
MCM4	AURKA	PDZK1IP1	TMSB10	CRNDE	THY1	GAL
SLBP	CENPE	MXD4	TFPI	UCHL1	CPA4	AK5
SSRP1	HMMR	SERF2	PLIN2	ACTG1	KRT19	NUDT5
HNRNPA2B1	DEPDC1	RPL3	TIMP1	PMEPA1	COL8A1	EEF1A2
MSH6	GTSE1	IL32	TINAGL1	LGALS3	IFITM2	PDAP1
CDCA7	CCNA2	FN1	LTBP1	TMSB4X	LYPD1	VDAC2
HMG2	ARL6IP1	ITGA3	CYGB	IFITM2	EDIL3	AP1S1
CCT6A	NUSAP1	TGFBI	SLC16A3	EVA1B	A1BG	RHEB
H2AFZ	KIF23	PRDX5	FAM162A	FSTL1	CTGF	ODC1
RANBP1	SGO2	FBN1	ANGPTL4	DMKN	INHBA	RAC1
DUT	CKS1B	S100A13	SELENOM	PDXK	DSTN	CDC123
HMGB1	CKAP2	WSB1	ITGA5	HOXB-AS3	CKAP4	RPA3
PSMD2	CDC20	ABCC3	ANXA2	RHOBTB3	FKBP10	MT1M
NOP56	TOP2A	RPL39	CAVIN3	LAMC2	CTSC	CBX3
HNRNPF	CCNB1	TPT1	LOX	KRT19	HHIP	ECHS1
XRCC6	NUF2	TMSB10	CA9	COL4A1	UPK1B	ATP5F1C
MCM6	KPNA2	RRAS	SLC20A1	HSPG2	MYL9	BUD31
MCM7	KIF20B	TPM1	CAV1	APOL1	GJA1	ATP5MD
C1QBP	CENPA	OST4	SUB1	TAGLN	ESAM	MRPS16
NCL	TACC3	IGFBP7	COL6A2	HOXB3	ACTG1	RPS24
ANP32B	ANLN	RPS27	PGAM1	COL8A1	TMSB4X	CRNDE
SRSF7	SMC4	TNS1	GAPDH	FKBP10	PLOD2	ATP6V1F
CCT5	DLGAP5	PLOD2	LY6E	TCIM	FGB	GNG11
GIN52	CDCA8	TRAM1	ABI3BP	COL4A2	RGS4	GGCT
FAM111B	CDCA3	EEF1A1	EMP3	S100A11	IGFBP4	HNRNPF
ODC1	KNSTRN	RNASET2	ARHGAP22	CDKN2A	CALU	PRDX3
HNRNPR	KIF2C	C4orf3	GYPC	CD9	DPYSL3	FUOM
PRELID1	NDC80	CST3	RRAGA	TNFSF10	FHL1	GDI2
PNN	BIRC5	MT-CO1	RPL15	SFN	TRAM1	SBDS
PCNA	CEP55	EEF2	RNASET2	CXCL1	COL4A1	PA2G4
HELLS	UBE2C	RPL37	NR2F2	GSN	COL5A1	TFPI2
TYMS	H2AFX	FTL	CYBA	FAM84B	NECTIN2	MCM7
MCM5	KIF14	S100A11	EFHD2	BST2	MRPS6	CISD1
RPL22L1	BUB1	PNRC1	YBX1	IGFBP7	SLC5A3	PPIA
SIVA1	HJURP	OPTN	LOXL2	KITLG	MLLT11	NOLC1
SERBP1	CDCA2	RPS19	C4orf3	SPINT2	AMIGO2	VIM
HNRNPD	AURKB	FLNA	TRNP1	SOX4	LMO7	H2AFV
HSP90AB1	CCNB2	RPL10	ANXA5	FARP1	DOK1	ARPC1B
PA2G4	CKAP5	ZFP36L1	RBPJ	IGFBP2	CXCL8	OAZ1
SLC3A2	NEK2	DUSP1	BNIP3	FOXC1	SFRP1	CAPG
MGST1	ARHGAP11A	CRYAB	VCAM1	NR2F6	CSRP1	HSPD1
CLSPN	PBK	RPLP2	NPM1	BRI3	CD9	PLPP2

Table 1. List of most differentially expressed genes in PEC clusters.

Table shows the 50 most differentially expressed genes for each transcriptionally distinct population identified in the entire PEC dataset generated by unbiased clustering.

To verify the progenitor signature of cluster 4, we analyzed the PEC outgrowth dataset together with a previously described renal progenitor dataset (89) (Fig. 22C-E). By matching them through the mutual nearest neighbors (MNN) batch correction algorithm, we obtained a matrix of 7443 cells that showed a high correspondence between some PEC clusters and RPC. Consistently, cluster 2 was enriched for genes with roles in cellular pathways linked to crescents such as *CD44*, *CD9*, to cancer-stem cells, such as *EPCAM* and *SFN* (85) as well as the RPC markers *CD133* (*PROM1*) and *CD24* (Fig. 20F) revealing a large overlap between the cluster 4 present in PEC dataset and cluster 2 of RPC/PEC dataset. Interestingly, stratifin, encoded by *SFN*, is a cell cycle checkpoint protein involved in stem cell proliferation/differentiation (90) that showed a virtually selective expression in cluster 2 of RPC/PEC. We then analyzed stratifin expression in healthy human glomeruli and in the glomeruli of 22 patients with crescents at kidney biopsies, 9 patients with lupus nephritis and 13 patients with ANCA-associated vasculitis (AAV) selected following the flow chart shown in Fig. S11. Tables S2 and S3 list the clinical characteristics of these patients, respectively. Double immunolabeling for CD133 and stratifin in glomeruli of healthy patients confirmed the existence of a subset of CD133+ progenitors of Bowman capsule expressing stratifin and representing the $15.0 \pm 1.5\%$ of CD133+ PEC (Fig. 22G), while in crescents they were enriched to $64.3 \pm 2.5\%$ (Fig. 22H, I). Comparison between patients that on the basis of their progression or not to ESKD after two years of follow-up (Table 2 and 3) showed that while the percentage of glomeruli with crescents, crescent dimension and percentage of CD133+SFN- was similar (Table 2, 3 and Fig. 22J-K), the percentage of CD133+stratifin+ cells constituting the crescents was lower in the group with a good outcome (Table 2,3 and Fig. 22L). In

addition, patients with a good prognosis showed a higher percentage of CD133-stratificin-cells (Fig. 22M), which was at least in part related to a higher podocyte amount within the crescents (Fig. 22N-P). Although in a small number of patients, these results suggest that crescents mostly result from the amplification of CD133+stratificin+ PEC, and that the extent of involvement of this cell population associates with clinical outcome.

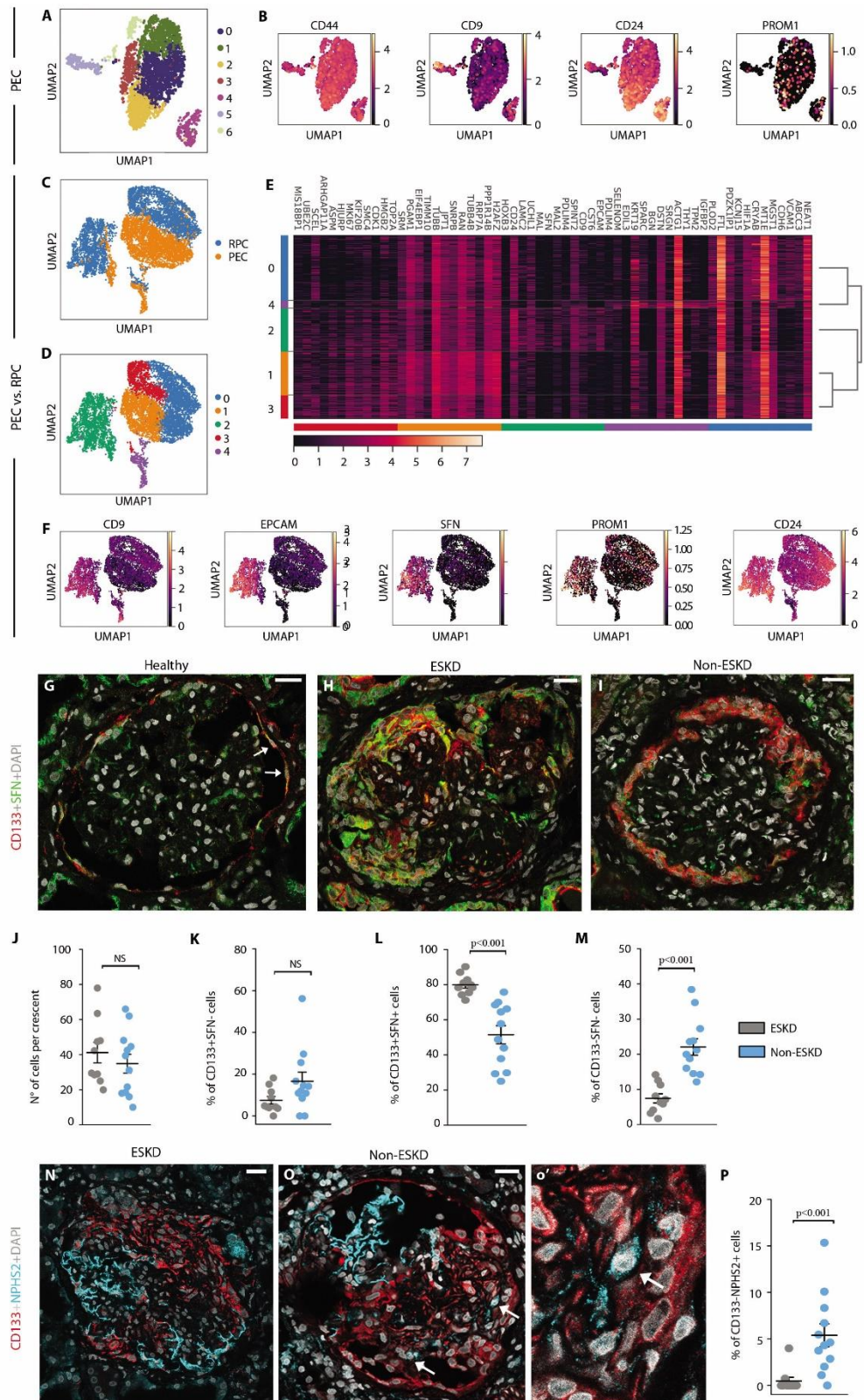


Fig. 5. Expansion within crescents of a PEC subset expressing CD133 and stratifin associates with patient outcome. (A) UMAP projection of PEC culture single cell RNAseq dataset colored by cluster. (B) UMAP visualization of expression of progenitor and crescent main markers. (C, D) UMAP projection of matched RPC/PEC dataset splitted and colored by sample (C) and cluster (D), respectively. (E) Heatmap representing the expression of the first 12 main markers for each cluster. (F) UMAP visualization of stem cell and cancer-stem cell marker expression. Color bar indicates log2 normalized expression. (G-I) Representative images showing CD133 (red) and SFN (green) expression and localization in healthy (G) and pathological human tissues obtained

from patients with diagnosis of ANCA-associated vasculitis and progressing (H) or not to ESKD (I). Arrows indicate region with CD133 and SFN co-expression. h' depicts a magnification of the splitted channels of H. DAPI (white) counterstains nuclei. Bars=25 μ M. **(J)** Graph representing the number of cells per crescent in patients progressing (grey dots, $n=10$) or not progressing (blue dots, $n=12$) to ESKD. **(K-M)** Graphs representing the percentage of CD133+SFN+ cells (K), CD133+SFN- cells (L) and CD133-SFN- cells (M) over the total number of cells within the crescent of patients progressing ($n=10$) or not progressing to ESKD ($n=12$). **(N, O)** Representative images showing CD133 (red) and NPHS2 (cyan) expression and localization in pathological tissues obtained from patients with AAV from the ESKD (N) and the non ESKD group (O). A detail is shown in o'. Arrows point CD133-NPHS2+ cells in a crescent. DAPI (white) counterstains nuclei. Bars=25 μ M. **(P)** Quantification of percentage of CD133- NPHS2+ cells over the total number of cells within the crescent in ESKD ($n=10$) and not ESKD patients ($n=12$).

In dot plots (J-M and P) bars indicate mean values. Individual scores are shown. Statistical significance was calculated by Mann-Whitney test; numbers on graph represent p-values. PEC, parietal epithelial cells; UMAP, uniform manifold approximation and projection; PROM1, prominin 1 (CD133); RPC, renal progenitor cell; EPCAM, epithelial cell adhesion molecule; SFN, stratifin, NPHS2, podocin; DAPI, 4',6-diamidino-2-phenylindole, ESKD, end-stage kidney disease.

Table S2. Comparison of demographic, laboratory and crescent characteristics of AAV patients divided based on outcome (ESKD) at two years post-renal biopsy.

	ESKD (n=7)	non-ESKD (n=6)	P
<i>Demographic and clinical characteristics at biopsy</i>			
Sex (F/M)	5/2	4/2	
Age at biopsy(years)	51.0 ± 20.7	54.2 ± 21.2	0.73
Creatinine at biopsy (mg/dL)	3.5 ± 2.2	3.5 ± 2.2	0.95
eGFR at biopsy (mL/min/1.73m²)	22.9 ± 17.1	30.9 ± 31.7	0.95
Proteinuria at biopsy (grams/24h)	3.4 ± 3.2	1.4 ± 0.5	0.041
<i>Demographic and clinical characteristics two years after the biopsy</i>			
Creatinine after 2 years (mg/dL)	8.5 ± 3.2	1.6 ± 0.8	0.002
eGFR after 2 years (mL/min/1.73m²)	5.4 ± 2.8	54.2 ± 38.4	0.002
<i>Crescents' characteristics and cell counts</i>			
Glomeruli with crescents (%)	59.2 ± 26.5	59.0 ± 28.4	0.93
Total cells per crescent (number)	37.9 ± 14.0	36.4 ± 17.9	1.0
CD133+ cells (%)	83.9 ± 13.4	71.4 ± 16.2	0.035
CD133+SFN+ cells (%)	79.3 ± 6.3	49.4 ± 20.1	0.008
CD133+SFN- cells (%)	8.8 ± 6.5	22.0 ± 18.4	0.18
CD133-SFN+ cells (%)	4.3 ± 3.3	7.4 ± 9.0	0.63
CD133-SFN- cells (%)	7.6 ± 4.5	21.3 ± 8.1	0.005
CD133+NPHS2+ cells (%)	19.6 ± 14.6	12.8 ± 11.8	0.63
CD133+NPHS2- cells (%)	68.1 ± 15.2	66.5 ± 18.7	1.0
CD133-NPHS2+ cells (%)	0.1 ± 0.3	4.7 ± 5.4	0.014
CD133-NPHS2- cells (%)	12.1 ± 7.1	16.1 ± 11.5	0.63

All values are presented as mean ± SD. Glomeruli with crescents and cell counts are expressed as percentage (over the total glomeruli and over total cells per crescent). Between-groups comparison using Mann-Whitney test for continuous variables is shown (p values ≤0.05 in bold). ESKD is defined as eGFR <15 ml/min/1.73m² at two years post-renal biopsy.

F, female; M, male; eGFR, estimated glomerular filtration rate; ESKD, end stage kidney disease; SFN, stratipin; NPHS2, podocin.

Table S3. Comparison of demographic, laboratory and crescent characteristics of LES patients divided based on outcome (ESKD/CKD-IV) at two years post-renal biopsy.

	ESKD/CKD-IV (n=3)	non-ESKD (n=6)	P
<i>Demographic and clinical characteristics at biopsy</i>			
Sex (F/M)	2/1	6/0	
Age at biopsy(years)	30.0 ± 18.4	35.6 ± 11.3	0.79
Creatinine at biopsy (mg/dL)	1.8 ± 1.0	0.9 ± 0.35	0.048
eGFR at biopsy (mL/min/1.73m ²)	54.7 ± 48.2	90.9 ± 30.9	0.26
Proteinuria at biopsy (grams/24h)	3.5 ± 0.28	2.4 ± 1.16	0.14
<i>Demographic and clinical characteristics two years after the biopsy</i>			
Creatinine after 2 years (mg/dL)	6.0 ± 4.0	0.8 ± 0.1	0.024
eGFR after 2 years (mL/min/1.73m ²)	13.3 ± 12.9	97.9 ± 18.8	0.024
<i>Crescents' characteristics and cell counts</i>			
Glomeruli with crescents (%)	30.0 ± 0.0	22.0 ± 16.2	0.64
Total cells per crescent (number)	31.4 ± 14.7	33.3 ± 20.7	0.91
CD133+ cells (%)	85.6 ± 5.5	64.8 ± 19.6	0.024
CD133+SFN+ cells (%)	81.3 ± 5.0	53.5 ± 11.2	0.024
CD133+SFN- cells (%)	4.3 ± 0.6	11.2 ± 10.0	0.55
CD133-SFN+ cells (%)	7.2 ± 3.2	12.4 ± 10.9	1.0
CD133-SFN- cells (%)	7.2 ± 4.0	22.9 ± 8.9	0.024
CD133+NPHS2+ cells (%)	9.4 ± 12.8	4.4 ± 4.6	0.55
CD133+NPHS2- cells (%)	77.7 ± 19.4	74.2 ± 14.2	0.71
CD133-NPHS2+ cells (%)	1.3 ± 2.3	6.1 ± 3.1	0.048
CD133-NPHS2- cells (%)	7.4 ± 10.5	15.4 ± 13.2	0.43

All values are presented as mean ± SD. Glomeruli with crescents and cell counts are expressed as percentage (over the total glomeruli and over total cells per crescent). Between-groups comparison using Mann-Whitney test for continuous variables is shown (p values ≤0.05 in bold). ESKD is defined as eGFR <15 ml/min/1.73m² at two years post-renal biopsy. CKD-IV is defined as eGFR between 15 and 30 ml/min/1.73m² at two years post-renal biopsy.

F, female; M, male; eGFR, estimated glomerular filtration rate; ESKD, end stage kidney disease; CKD, Chronic Kidney Disease; SFN, stratipin; NPHS2, podocin.

4.8 Panobinostat inhibits RPC proliferation and promotes their differentiation into podocytes also in humans

The results obtained in human biopsies, suggesting CD133+SFN+ PEC as the cells of origin of crescents prompted us to verify the effects of panobinostat observed in the mouse model of crescentic glomerulonephritis also in human cultures. Givinostat and ruxolitinib were tested as additional controls. All the three drugs reduced metabolic activity of RPC, with panobinostat being the most effective, as assessed by the MTT test (Fig. 23A). This associated with a sharp reduction in the number of cells, i.e., an anti-proliferative effect (Fig. 23B). Panobinostat and givinostat also induced a reduction in the percentage of live cells, as detected by the annexin-V/PI assay, while ruxolitinib had no effect (Fig. 23C). However, cell cycle analysis by flow cytometry also highlighted a doubling of the percentage of RPC in the G2/M phase following panobinostat, givinostat, and ruxolitinib treatment, suggesting all the three drugs promoted cell cycle arrest (Fig. 23D). Taken together, drugs that inhibit hematopoietic progenitor proliferation can also inhibit the proliferation of RPC. We then evaluated the capacity of the aforementioned compounds to modulate RPC differentiation into podocytes. We used all-trans retinoic acid as positive control given its well-defined effect as podocyte differentiation inducer (39, 91). Panobinostat was much more efficient than all-trans retinoic acid (89) in promoting RPC differentiation toward podocytes, as demonstrated by the change in cell morphology shown by tubulin staining and super-resolution microscopy (Fig. 22E), and the high expression of *NPHS2* and *NPHS1* mRNAs (Fig. 22F, G) as well as proteins (Fig. 22H, I). Givinostat only increased *NPHS1*, while *NPHS2* expression was not detectable, suggesting a limited effect of progenitor differentiation (Fig. 22F-I). Ruxolitinib did not induce *NPHS2* or *NPHS1* (Fig. 22F-I).

Comparison of the single-cell transcriptome of control- and panobinostat-treated PEC culture obtained from outgrowth of glomeruli of healthy human kidney (Fig. 22J), confirmed that panobinostat induced upregulation of podocyte-specific markers *NPHS1*, *NPHS2*, *MAFB*, *KFL14*, *KFL15*, *PLA2G7*, *PTPRO*, *SYNPO*, in different PEC subsets including stratifin-expressing RPC (Fig. 22K-M). Interestingly, panobinostat treatment also downregulated expression of stratifin as well as of genes of the Notch and of the β -catenin pathways (Fig. 22N), involved in promoting renal progenitor proliferation and inhibiting their differentiation into podocytes, respectively. Altogether, panobinostat is a powerful inhibitor of podocyte progenitor proliferation and inducer of their differentiation into podocytes also in humans with potential for treatment of rapidly progressive glomerulonephritis also in humans.

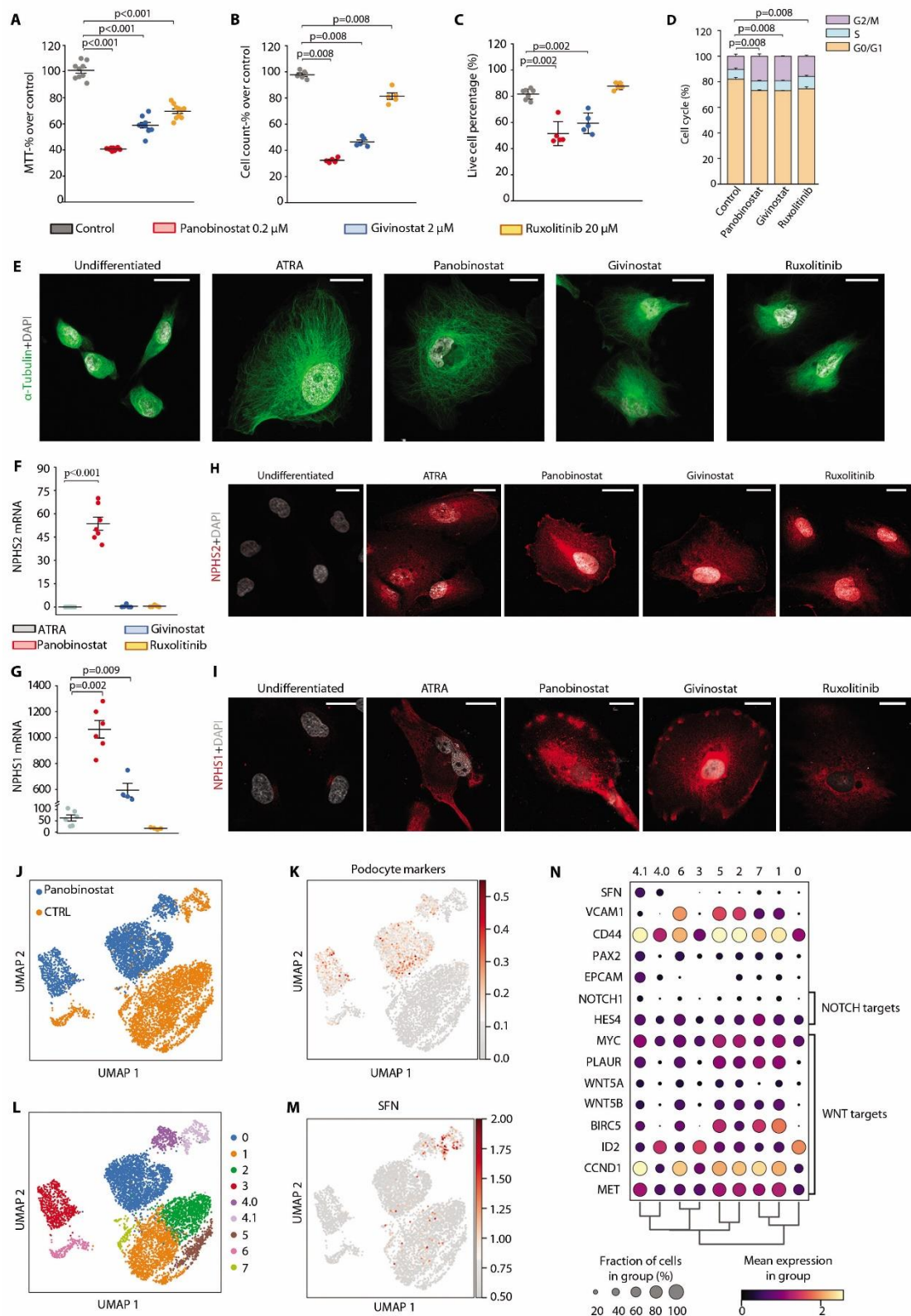


Fig. 23. Panobinostat inhibits RPC proliferation and promotes their differentiation also in humans.

(A-I) *In vitro* drugs screening on RPC following 48 hours stimuli with panobinostat, givinostat and ruxolitinib. Each dot represents the mean of technical triplicates. (A) MTT assay on primary human RPC treated with panobinostat, givinostat and ruxolitinib for 48 hours. Data were obtained from 3 different primary cultures in 3 independent experiments. (B) Cell count following 48 hours treatment. Data were obtained from 3 different primary cultures in 2 independent experiments. (C) Quantification of live cells of Annexin-V/Propidium Iodide FACS staining for assessment of

apoptosis induction after treatment with the three compounds. Data were obtained from 3 different primary cultures in 3 independent experiments. (D) Distribution of RPC in cell cycle phases assessed by flow cytometry. Data were obtained from 3 different primary cultures in 2 independent experiments. (E) Representative STED images showing cytoskeleton changes based on tubulin expression after treatment with the three compounds. Untreated cells and ATRA treated cells were used as negative and positive control, respectively. One representative of 3 independent experiments is shown. DAPI counterstains nuclei (white). Bars=20 μ m. (F, G) Podocyte marker expression in RPC after treatment with ATRA, panobinostat, givinostat and ruxolitinib. mRNA expression of NPHS2 (F) and NPHS1 (G) were determined by real-time RT-PCR and reported as fold increase over untreated cells. Data were obtained from 3 different primary cultures in 3 independent experiments. (H, I) Representative confocal microscopy images showing expression of podocyte markers (NPHS2 and NPHS1 in red) following treatment with the three compounds. Untreated and ATRA treated cells were used as negative and positive control, respectively. One representative of 3 independent experiments is shown. DAPI counterstains nuclei (white). Bars=25 μ m. (J) UMAP projection of control and panobinostat treated PEC culture scRNAseq dataset splitted by sample. (K) UMAP visualization of podocyte markers expression. (L) UMAP projection of control and panobinostat treated PEC culture scRNAseq dataset splitted by clusters. (M) UMAP visualization of stratifin expression. (N) Dot plot showing the expression of genes related to crescent, NOTCH or WNT pathways affected by panobinostat treatment.

In dot plots (A-C, F and G), bars indicate mean values. Individual scores are shown. Statistical significance was calculated by Mann-Whitney test; numbers on graph represent p-values. MTT, 3-(4,5-dimethylthiazol-2-yl)-2,5-diphenyltetrazolium bromide; ATRA, *all-trans* retinoic acid; DAPI, 4',6-diamidino-2-phenylindole; NPHS2, podocin; NPHS1, nephrin, UMAP, uniform manifold approximation and projection; SFN, stratifin.

5. Discussion

Crescent formation compromises glomerular filtration and outflow independent from the upstream pathomechanisms of loop necrosis and treatments specifically targeting the causative uncontrolled hyperplasia of PEC are not available. In this study we show that

1. Crescents form via clonal proliferation of single cells from a particular immature subset of PEC along Bowman capsule;
2. Panobinostat, an inhibitor of clonal proliferation used in primary myelofibrosis, successfully reduces proteinuria and improves kidney function in models of crescentic glomerulonephritis;
3. The beneficial effect of panobinostat relates to its capacity to turn the uncontrolled hyperplasia of immature RPC into a controlled differentiation into new podocytes and thereby restoring the injured glomerular filtration barrier.

According to the traditional concept, crescents represent an overshooting epithelial healing response of the PEC lining along Bowman capsule occurring in response to ruptures of the glomerular basement membrane during capillary loop necrosis (1,2). Using lineage tracing analysis of Pax2+ podocyte progenitors, clonal analysis with the Confetti reporter and scRNAseq we show that a distinct PEC subpopulation forms the crescent. This reflects heterogeneity among PEC in terms of both differentiative potential and proliferative capacity, as known for other stem cell compartments (59, 92). We identified the subset of PEC that forms the crescent by clonal expansion by an expression pattern similar to stem cells of other organs and tissues, including the hematopoietic stem cells. This further underlines the similarities between the stem cells of the kidney and of the bone marrow, as already previously suggested (92,93). Indeed, the bone marrow stem cell niche of hematopoietic stem cells involves endothelial cells producing CXCL12, which keeps hematopoietic stem cells largely in an immobile and quiescent state (59). The glomerulus where RPC reside among the PEC along the inner aspect of Bowman's

capsule has a similar structure. Of note, in healthy conditions podocytes produce high levels of CXCL12 to keep RPC among the PEC quiescent and undifferentiated (43). Other similarities relate to the expression of CD44 (94) and VCAM1 (40) by RPC and their role in RPC activation. In addition, the local presence of high levels of VEGF (95) and TGF- β (24), also contribute to RPC quiescence and survival, like in the bone marrow stem cell niche (96). The results of this study add another crucial similarity. Crescents develop from a clonal proliferation of an immature PEC subset, a podocyte progenitor, that expands but without differentiating into podocytes conceptually like other diseases driven by clonal proliferation of resident progenitor or stem cell populations not only in the bone marrow (77,78) but also in the gut or the skin (97,98). Of note, we recently reported that injury of kidney tubules stimulates progenitors scattered within such tubules to also undergo hyperplasia and form papillary adenomas and carcinomas in a similar clonal fashion (69). As such tubule adenomas may be the tubular equivalent to glomerular crescents. In the crescent, stimuli for PEC proliferation likely include mitogenic serum factors reaching Bowman space upon capillary loop necrosis and GBM rupture and the consequent inflammation (14). Even if all PEC are similarly exposed to this mitogenic micromilieu, a particular PEC subset with phenotypic and functional features of podocyte progenitors has a higher capacity to proliferate consistent with its stem cell features, becoming the cell of origin for a clonal crescent. The crescent-forming PEC subset is characterized by expression of stratifin, also known as 14-3-3 σ . The 14-3-3 proteins are 28- to 33-kDa polypeptides found in all eukaryotic organisms (99). Seven members (b, c, e, g, s, h/t and f) are found in mammals (100). Through binding to at least 200 proteins including enzymes, transcription factors, cytoskeletal proteins, signaling molecules, apoptosis factors and tumor suppressors (100), 14-3-3 proteins are pivotal drivers of proliferation and differentiation (100) and essential regulators of stem cell function (101-103) and cancer development (85,104) in multiple organs and tissues. For example, 14-3-3

interfere with the adaptor protein LNK, a critical inhibitor of JAK2, thereby limiting hematopoietic stem and progenitor cell self-renewal (102). LNK deficiency promotes myeloproliferative neoplasm development in mice (105), and LNK loss-of-function mutations are found in human myeloproliferative disorders (106), proposing 14-3-3 as crucial players in these diseases (102). The 14-3-3 protein stratifin expression determines the choice between proliferation and differentiation also in embryonic stem cells (101). In particular, it induces PI3K/Akt activation and triggers dissociation from the APC/axin/GSK-3b complex of β -catenin, which translocates into the nucleus to drive the transcription of mitogenic genes (101). Interestingly, β -catenin induces PEC proliferation, while its deletion promotes PEC differentiation into podocytes (107). In addition, retinoid acid, a crucial driver of progenitor differentiation into podocytes (89), selectively suppresses stratifin (101). Finally, stratifin+ RPC show a low expression of VCAM1. Similar to hematopoietic cells (108), VCAM1 expression characterizes immature RPC that exhibit stem cell potential and are quiescent in the glomerular niche (40). Once VCAM1+ RPC are committed to podocyte differentiation they first start to express podocalyxin (40) and then downregulate VCAM1 before upregulating podocyte markers and differentiating into podocytes (40). The results of this study suggest that stratifin expression characterizes a VCAM1^{low} RPC subset functionally committed to proliferate that undergo clonal expansion like bone marrow myeloproliferative disorders (Fig. 24). Stratifin+RPC are characterized also by expression of CD44 (30) and CD9 (53), crucial drivers of crescent formation (30,53). Clonal amplification of this subset promotes crescent formation, as confirmed also by the association between the percentage of stratifin-expressing PEC within crescents and a poor outcome in patients with crescentic glomerulonephritis.

Patients with crescentic glomerulonephritis have a high risk of progressing toward ESKD, despite therapy (1-3). Current treatments target upstream autoimmune and inflammatory

pathways but do not directly target crescent formation itself (3), albeit cyclophosphamide that is used for some of these diseases elicits antiproliferative effects not only on immune cells but also on PEC (1). These results provided the rationale for the evaluation of drugs already in use for disorders of uncontrolled stem cell hyperplasia, such as myeloma or primary myelofibrosis (80,81,109,110), in crescentic glomerulonephritis. All the three drugs showed anti-inflammatory effects and inhibited the proliferation of RPC, suggesting common mechanisms mediating clonal amplification in stem cell disorders across different organs, including the kidney. However, when administered to models of crescentic glomerulonephritis *in vivo*, only panobinostat promoted crescent and proteinuria reduction as well as kidney function improvement, an effect that was consistent with its strong and unique capacity to promote differentiation into podocytes of a PEC subset with phenotypic and functional features of podocyte progenitors. Consistently, the reduction in crescent number associated with a downregulation of stratifin as well as β -catenin target genes in stratifin expressing human PEC and with their shift from crescent formation to generation of new podocytes *in vivo*. These results suggest that inhibition of crescent formation alone cannot efficiently treat crescentic glomerulonephritis because it does not bring back the lost podocytes. By contrast, drug-induced differentiation of podocyte progenitors into podocytes can solve two problems a) hyperplasia of the immature PEC, b) repair of visceral filtration barrier, and is therapeutically more efficient. Strikingly, delayed treatment with panobinostat administered only upon the peak of proteinuria and crescents had formed still induced proteinuria remission and avoided longterm development of kidney failure, an effect related to a continued generation of new podocytes and crescent regression over time. Taken altogether, these results offer mechanistic insights into crescent formation suggesting that this lesion is caused by fast clonal proliferation of single immature PEC and by a lack of its differentiation toward a fully differentiated podocyte phenotype upon

severe glomerular injury. More importantly, in analogy with other disorders caused by dysregulation of the stem cell response, development of this lesion can be interrupted by using drugs that have already been developed and successfully used to block abnormal clonal stem cell growth in other organs and tissues.

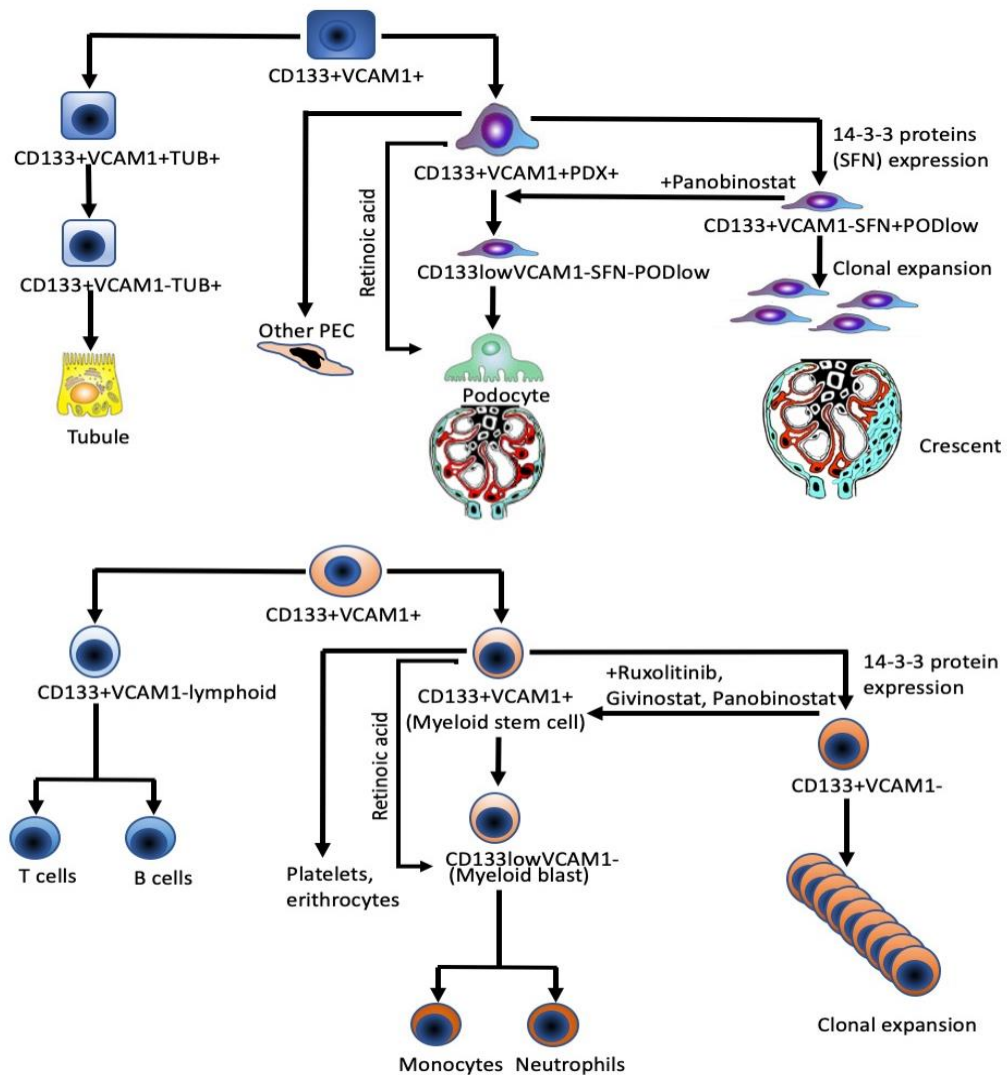


Fig. 24. Similarities between the hematopoietic system and the pathogenesis of myeloproliferative disorders with renal progenitors and the pathogenesis of crescent.

Similar to hematopoietic stem cells (108), renal progenitor hierarchy starts from a multipotent quiescent stem cell expressing CD133 and VCAM1 that can generate podocytes as well as tubular cells (40). VCAM1+ RPC can generate tubular progenitors or podocyte progenitors that in turn generate mature tubular cells or podocytes through a series of intermediate steps characterized by progressive upregulation of differentiative markers and downregulation of CD133 and VCAM1 (40), similar to lymphoid or myeloid commitment within the bone marrow (74). Intermediate steps of podocyte differentiation consist of a podocyte progenitor that first starts to express podocalyxin remaining quiescent on the Bowman capsule (40) and then downregulates VCAM1

before upregulating podocyte markers and differentiating into podocytes (40), similar to the myeloid stem cell ultimately generating monocytes and neutrophils. The choice between proliferation and differentiation in the podocyte progenitor is determined by expression of the 14-3-3 protein stratifin, promoting clonal expansion, or by retinoic acid promoting differentiation (89), similar to hematopoietic progenitors (102, 75). Persistent activation of 14-3-3 proteins promotes crescent formation as well as myeloproliferative neoplasm development (102) from the CD133+ progenitor (76). Treatment with drugs (Panobinostat) that inhibit clonal expansion of podocyte progenitor and promote differentiation into podocytes can reverse crescent formation, similar to drugs used for treatment of myeloproliferative disorders (79,80).

References

1. L. Anguiano, R. Kain, H. J. Anders, The glomerular crescent: triggers, evolution, resolution, and implications for therapy. *Curr Opin Nephrol Hypertens* 29, 302-309 (2020).
2. S. K. Singh, M. Jeansson, S. E. Quaggin, New insights into the pathogenesis of cellular crescents. *Curr Opin Nephrol Hypertens* 20, 258-262 (2011).
3. D. Nakazawa, S. Masuda, U. Tomaru, A. Ishizu, Pathogenesis and therapeutic interventions for ANCA-associated vasculitis. *Nat Rev Rheumatol* 15, 91-101 (2019).
4. M. Segelmark, T. Hellmark, Anti-glomerular basement membrane disease: an update on subgroups, pathogenesis and therapies. *Nephrol Dial Transplant* 34, 1826-1832 (2019).
5. Chadban, S., & Atkins, R. (2005). Glomerulonephritis. *The Lancet*, 365(9473), 1797–1806
6. Thomas DB, Franceschini N, Hogan SL, et al. (2006). "Clinical and pathologic characteristics of focal segmental glomerulosclerosis pathologic variants". *Kidney Int.*69(5): 920–6
7. Kumar, Vinay, ed. (2007).Robbins basic pathology(8th ed.). Philadelphia: Saunders/Elsevier.
8. Schwimmer, J. A., Markowitz, G. S., Valeri, A., & Appel, G. B. (2003).Collapsing glomerulopathy. *Seminars in Nephrology*, 23(2), 209–218
9. Nicholas Cossey, L., Larsen, C. P., & Liapis, H. (2017). Collapsing glomerulopathy: a 30-year perspective and single, large center experience. *Clinical Kidney Journal*, 10(4), 443–449.
10. Stokes, M. B., Markowitz, G. S., Lin, J., Valeri, A. M., & D’Agati, V. D. (2004).Glomerular tip lesion: A distinct entity within the minimal change disease/focal segmental glomerulosclerosis spectrum. *Kidney International*, 65(5), 1690–1702.
11. Cotran, Ramzi S.; Kumar, Vinay; Fausto, Nelson; Nelso Fausto; Robbins, Stanley L.; Abbas, Abul K. (2005). Robbins and Cotran pathologic basis of disease. St. Louis, MO: Elsevier Saunders. pp. 976–8
12. Bajema IM,Wilhelmus S, Alpers CE, et al. Revision of the International Society of Nephrology/Renal Pathology Society classification for lupus nephritis:clarification of definitions, and modified National Institutes of Health activity and chronicity indices. *Kidney Int* 2018; 93:789–796
13. Sethi S, Fervenza FC. Standardized classification and reporting of glomerulonephritis.*Nephrol Dial Transplant* 2019; 34:193–199.
14. Ryu M, Migliorini A, Miosge N, et al. Plasma leakage through glomerular basement membrane ruptures triggers the proliferation of parietal epithelial cells and crescent formation in non-inflammatory glomerular injury. *J Pathol.* 2012; 228:482–494.
15. Chen A, Lee K, D’Agati VD, et al. Bowman’s capsule provides a protective niche

- for podocytes from cytotoxic CD8 β T cells. *J Clin Invest* 2018; 128:3413–3424.
16. Krebs CF, Schmidt T, Riedel JH, et al. T helper type 17 cells in immunemediated glomerular disease. *Nat Rev Nephrol* 2017; 13:647–659.
 17. Gan PY, Chan A, Ooi JD, et al. Biologicals targeting T helper cell subset differentiating cytokines are effective in the treatment of murine antimyeloperoxidase glomerulonephritis. *Kidney Int* 2019; 96:1047–1246.
 18. Klinge S, Yan K, Reimers D, et al. Role of regulatory T cells in experimental autoimmune glomerulonephritis. *Am J Physiol Renal Physiol* 2019; 316: F572–F581.
 19. Chen A, Lee K, Guan T, et al. Role of CD8 β T cells in crescentic glomerulonephritis. *Nephrol Dial Transplant* 2019; pii: gfz043. doi: 10.1093/ndt/gfz043. [Epub ahead of print] PMID: 30879039
 20. Thorner, P. S., Ho, M., Eremina, V., Sado, Y., & Quaggin, S. (2008). Podocytes Contribute to the Formation of Glomerular Crescents. *Journal of the American Society of Nephrology*, 19(3), 495–502.
 21. Bariéty, J., Bruneval, P., Meyrier, A., Mandet, C., Hill, G., & Jacquot, C. (2005). Podocyte involvement in human immune crescentic glomerulonephritis. *Kidney international*, 68(3), 1109–1119
 22. Lan, H. Y., Nikolic-Paterson, D. J., MU, W., & Atkins, R. C. (2007). Local macrophage proliferation in the pathogenesis of glomerular crescent formation in rat anti-glomerular basement membrane (GBM) glomerulonephritis. *Clinical & Experimental Immunology*, 110(2), 233–240.
 23. Smeets B, Uhlig S, Fuss A, et al. Tracing the origin of glomerular extracapillary lesions from parietal epithelial cells. *J Am Soc Nephrol* 2009; 20: 2604–2615.
 24. Smeets B, Angelotti ML, Rizzo P, et al. Renal progenitor cells contribute to hyperplastic lesions of podocytopathies and crescentic glomerulonephritis. *J Am Soc Nephrol* 2009; 20:2593–2603.
 25. Fogo AB, Lusco MA, Najafian B, et al. *AJKD atlas of renal pathology: pauciimmune necrotizing crescentic glomerulonephritis*. *Am J Kidney Dis* 2016; 68:e31–e32.
 26. Puelles VG, Fleck D, Ortiz L, et al. Novel 3D analysis using optical tissue clearing documents the evolution of murine rapidly progressive glomerulonephritis. *Kidney Int* 2019; 96:505–516.
 27. D’Agati, V. D., & Shankland, S. J. (2019). Recognizing diversity in parietal epithelial cells. *Kidney International*, 96(1), 16–19.
 28. Shankland SJ, Smeets B, Pippin JW, et al. Emergence of the glomerular parietal epithelial cell. *Nat Rev Nephrol*. 2014;10: 158–173.
 29. Lasagni, L., Angelotti, M. L., Ronconi, E., Lombardi, D., Nardi, S., Peired, A., ... Romagnani, P. (2015). Podocyte Regeneration Driven by Renal Progenitors Determines Glomerular Disease Remission and Can Be Pharmacologically Enhanced. *Stem Cell Reports*, 5(2), 248–263.
 30. Eymael, J., Sharma, S., Loeven, M. A., Wetzels, J. F., Mooren, F., Florquin, S., ... van der Vlag, J. (2018). CD44 is required for the pathogenesis of experimental crescentic glomerulonephritis and collapsing focal segmental glomerulosclerosis. *Kidney International*, 93(3), 626–642.
 31. Lee SJ, Sparke J, Howie AJ. The mammalian glomerulotubular junction studied

- by scanning and transmission electron microscopy. *J Anat.* 1993;182(pt 2): 177–185.
32. Kuppe C, Leuchte K, Wagner A, et al. Novel parietal epithelial cell subpopulations contribute to focal segmental glomerulosclerosis and glomerular tip lesions. *Kidney Int.* 2019;96:80–93
 33. Anglani F, Forino M, Gambaro G, D'Angelo A. Alla ricerca della cellula staminale renale [In search of renal stem cells]. *G Ital Nefrol.* 2002 Nov-Dec;19(6):607-16. Italian. PMID: 12508164.
 34. Kale S, Karihaloo A, Clark PR, Kashgarian M, Krause DS, Cantley LG. Bone marrow stem cells contribute to repair of the ischemically injured renal tubule. *J Clin Invest.* 2003 Jul;112(1):42-9. doi: 10.1172/JCI17856. Epub 2003 Jun 16. PMID: 12824456; PMCID: PMC162291.
 35. Lin F, Cordes K, Li L, Hood L, Couser WG, Shankland SJ, Igarashi P. Hematopoietic stem cells contribute to the regeneration of renal tubules after renal ischemia-reperfusion injury in mice. *J Am Soc Nephrol.* 2003 May;14(5):1188-99. doi: 10.1097/01.asn.0000061595.28546.a0. PMID: 12707389.
 36. Duffield JS, Park KM, Hsiao LL, Kelley VR, Scadden DT, Ichimura T, Bonventre JV. Restoration of tubular epithelial cells during repair of the postischemic kidney occurs independently of bone marrow-derived stem cells. *J Clin Invest.* 2005 Jul;115(7):1743-55. doi: 10.1172/JCI22593. Epub 2005 Jun 2. PMID: 16007251; PMCID: PMC1159124.
 37. Oliver JA, Maarouf O, Cheema FH, Martens TP, Al-Awqati Q. The renal papilla is a niche for adult kidney stem cells. *J Clin Invest.* 2004 Sep;114(6):795-804. doi: 10.1172/JCI20921. PMID: 15372103; PMCID: PMC516259.
 38. Sagrinati C, Netti GS, Mazzinghi B, Lazzeri E, Liotta F, Frosali F, Ronconi E, Meini C, Gacci M, Squecco R, Carini M, Gesualdo L, Francini F, Maggi E, Annunziato F, Lasagni L, Serio M, Romagnani S, Romagnani P. Isolation and characterization of multipotent progenitor cells from the Bowman's capsule of adult human kidneys. *J Am Soc Nephrol* 2006; 17: 2443-56.
 39. Ronconi, E., Sagrinati, C., Angelotti, M. L., Lazzeri, E., Mazzinghi, B., Ballerini, L., ... Romagnani, P. (2009). Regeneration of Glomerular Podocytes by Human Renal Progenitors. *Journal of the American Society of Nephrology*, 20(2), 322–332.
 40. Angelotti, M. L., Ronconi, E., Ballerini, L., Peired, A., Mazzinghi, B., Sagrinati, C., ... Romagnani, P. (2012). Characterization of Renal Progenitors Committed Toward Tubular Lineage and Their Regenerative Potential in Renal Tubular Injury. *STEM CELLS*, 30(8), 1714–1725.
 41. Appel D, Kershaw DB, Smeets B, Yuan G, Fuss A, Frye B, Elger M, Kriz W, Floege J, Moeller MJ. Recruitment of podocytes from glomerular parietal epithelial cells. *J Am Soc Nephrol.* 2009 Feb;20(2):333-43. doi: 10.1681/ASN.2008070795. Epub 2008 Dec 17. PMID: 19092119; PMCID: PMC2637040.
 42. Ryan, G., Steele-Perkins, V., Morris, J.F., Rauscher, F.J., 3rd, and Dressler, G.R. (1995). Repression of Pax-2 by WT1 during normal kidney development. *Development* 121, 867–875.
 43. Romoli S, Angelotti ML, Antonelli G, Kumar Vr S, Mulay SR, Desai J, Anguiano

- Gomez L, Thomasova D, Eulberg D, Klussmann S, Melica ME, Conte C, Lombardi D, Lasagni L, Anders HJ, Romagnani P. CXCL12 blockade preferentially regenerates lost podocytes in cortical nephrons by targeting an intrinsic podocyte-progenitor feedback mechanism. *Kidney Int.* 2018 Dec;94(6):1111-1126. doi: 10.1016/j.kint.2018.08.013. Epub 2018 Oct 29. PMID: 30385042; PMCID: PMC6251974.
44. Shankland, S. J., Anders, H.-J., & Romagnani, P. (2013). Glomerular parietal epithelial cells in kidney physiology, pathology, and repair. *Current Opinion in Nephrology and Hypertension*, 22(3), 302–309
 45. Wharram BL, Goyal M, Wiggins JE, Sanden SK, Hussain S, Filipiak WE, Saunders TL, Dysko RC, Kohno K, Hozman LB, Wiggins RC: Podocyte depletion causes glomerulosclerosis: Diphtheria toxin-induced podocyte depletion in rats expressing human diphtheria toxin receptor transgene. *J Am Soc Nephrol* 16: 2941–2952, 2005
 46. Wiggins RC: The spectrum of podocytopathies: A unifying view of glomerular diseases. *Kidney Int* 71: 1205–1214, 2007
 47. Lasagni, L., & Romagnani, P. (2010). Glomerular Epithelial Stem Cells: The Good, The Bad, and The Ugly. *Journal of the American Society of Nephrology*, 21(10), 1612–1619.
 48. Sicking EM, Fuss A, Uhlig S, et al. Subtotal ablation of parietal epithelial cells induces crescent formation. *J Am Soc Nephrol* 2012; 23:629– 640
 49. Drew AF, Tucker HL, Liu H, et al. Crescentic glomerulonephritis is diminished in fibrinogen-deficient mice. *Am J Physiol Renal Physiol* 2001; 281:F1157– F1163
 50. Dijkman H, Smeets B, van der Laak J, Steenberg E, Wetzels J. The parietal epithelial cell is crucially involved in human idiopathic focal segmental glomerulosclerosis. *Kidney Int.* 2005 Oct;68(4):1562-72. doi: 10.1111/j.1523-1755.2005.00568.x. PMID: 16164633.
 51. Cichy J, Pure E. The liberation of CD44. *J Cell Biol.* 2003;161:839–843.
 52. Nakamura H, Kitazawa K, Honda H, et al. Roles of and correlation between alpha-smooth muscle actin, CD44, hyaluronic acid and osteopontin in crescent formation in human glomerulonephritis. *Clin Nephrol.* 2005;64:401–411.
 53. Lazareth, H., et al. The tetraspanin CD9 controls migration and proliferation of parietal epithelial cells and glomerular disease progression. *Nature Communications*, 10(1).
 54. Kuppe C, van Roeyen C, Leuchtle K, Kabgani N, Vogt M, Van Zandvoort M, Smeets B, Floege J, Gröne HJ, Moeller MJ. Investigations of Glucocorticoid Action in GN. *J Am Soc Nephrol.* 2017 May;28(5):1408-1420. doi: 10.1681/ASN.2016010060. Epub 2016 Nov 28. PMID: 27895155; PMCID: PMC5407712.
 55. Bollée G, Flamant M, Schordan S, Fligny C, Rumpel E, Milon M, Schordan E, Sabaa N, Vandermeersch S, Galaup A, Rodenas A, Casal I, Sunnarborg SW, Salant DJ, Kopp JB, Threadgill DW, Quaggin SE, Dussaule JC, Germain S, Mesnard L, Endlich K, Boucheix C, Belenfant X, Callard P, Endlich N, Tharaux PL. Epidermal growth factor receptor promotes glomerular injury and renal failure in rapidly progressive crescentic glomerulonephritis. *Nat Med.* 2011 Sep 25;17(10):1242-50. doi: 10.1038/nm.2491. Erratum in: *Nat Med.* 2011

- Nov;17(11):1521. Erratum in: *Nat Med.* 2011 Oct;17(10):2 p following 1250. PMID: 21946538; PMCID: PMC3198052.
56. Levy JB, Turner AN, Rees AJ, et al: Long-term outcome of anti-glomerular basement membrane antibody disease treated with plasma exchange and immunosuppression. *Ann Intern Med* 134(11):1033-1042, 2001.
 57. H. Lazareth et al., The tetraspanin CD9 controls migration and proliferation of parietal epithelial cells and glomerular disease progression. *Nat Commun* 10, 3303 (2019).
 58. E. Lazzeri et al., Endocycle-related tubular cell hypertrophy and progenitor proliferation recover renal function after acute kidney injury. *Nat Commun* 9, 1344 (2018).
 59. H. J. Anders, P. Romagnani, A. Mantovani, Pathomechanisms: homeostatic chemokines in health, tissue regeneration, and progressive diseases. *Trends Mol Med* 20, 154-165 (2014).
 60. A. J. Mead, A. Mullally, Myeloproliferative neoplasm stem cells. *Blood* 129, 1607-1616 (2017).
 61. J. Chen et al., Myelodysplastic syndrome progression to acute myeloid leukemia at the stem cell level. *Nat Med* 25, 103-110 (2019).
 62. H. J. Snippert et al., Intestinal crypt homeostasis results from neutral competition between symmetrically dividing Lgr5 stem cells. *Cell* 143, 134-144 (2010).
 63. J. Friedemann et al., Improved kinetic model for the transcutaneous measurement of glomerular filtration rate in experimental animals. *Kidney Int* 90, 1377-1385 (2016).
 64. J. Park et al., Single-cell transcriptomics of the mouse kidney reveals potential cellular targets of kidney disease. *Science* 360, 758-763 (2018).
 65. A. Dobin et al., STAR: ultrafast universal RNA-seq aligner. *Bioinformatics* 29, 15-21 (2013).
 66. W. E. Johnson, C. Li, A. Rabinovic, Adjusting batch effects in microarray expression data using empirical Bayes methods. *Biostatistics* 8, 118-127 (2007).
 67. A. T. Lun, K. Bach, J. C. Marioni, Pooling across cells to normalize single-cell RNA sequencing data with many zero counts. *Genome Biol* 17, 75 (2016).
 68. F. A. Wolf, P. Angerer, F. J. Theis, SCANPY: large-scale single-cell gene expression data analysis. *Genome Biol* 19, 15 (2018).
 69. A. J. Peired et al., Acute kidney injury promotes development of papillary renal cell adenoma and carcinoma from renal progenitor cells. *Sci Transl Med* 12, (2020).
 70. L. Haghverdi, A. T. L. Lun, M. D. Morgan, J. C. Marioni, Batch effects in single-cell RNA-sequencing data are corrected by matching mutual nearest neighbors. *Nat Biotechnol* 36, 421-427 (2018).
 71. H. Wang et al., Histone deacetylase inhibitor LAQ824 augments inflammatory responses in macrophages through transcriptional regulation of IL-10. *J Immunol* 186, 3986-3996 (2011).
 72. A. M. Grabiec, O. Korchynskiy, P. P. Tak, K. A. Reedquist, Histone deacetylase inhibitors suppress rheumatoid arthritis fibroblast-like synoviocyte and macrophage IL-6 production by accelerating mRNA decay. *Ann Rheum Dis* 71, 424-431 (2012).

73. E. Huarte et al., Ruxolitinib, a JAK1/2 Inhibitor, Ameliorates Cytokine Storm in Experimental Models of Hyperinflammation Syndrome. *Front Pharmacol* 12, 650295 (2021).
74. G. Guo et al., Mapping cellular hierarchy by single-cell analysis of the cell surface repertoire. *Cell Stem Cell* 13, 492-505 (2013).
75. M. I. Dawson et al., Myeloid differentiation mediated through retinoic acid receptor/retinoic X receptor (RXR) not RXR/RXR pathway. *Blood* 84, 446-452 (1994).
76. I. Triviai et al., CD133 marks a stem cell population that drives human primary myelofibrosis. *Haematologica* 100, 768-779 (2015).
77. A. J. Mead, A. Mullally, Myeloproliferative neoplasm stem cells. *Blood* 129, 1607-1616 (2017).
78. J. Chen et al., Myelodysplastic syndrome progression to acute myeloid leukemia at the stem cell level. *Nat Med* 25, 103-110 (2019).
79. M. Schieber, J. D. Crispino, B. Stein, Myelofibrosis in 2019: moving beyond JAK2 inhibition. *Blood Cancer J* 9, 74 (2019).
80. E. Evrot et al., JAK1/2 and Pan-deacetylase inhibitor combination therapy yields improved efficacy in preclinical mouse models of JAK2V617F-driven disease. *Clin Cancer Res* 19, 6230-6241 (2013).
81. C. Harrison et al., JAK inhibition with ruxolitinib versus best available therapy for myelofibrosis. *N Engl J Med* 366, 787-798 (2012).
82. H. J. Anders, Diagnosis and management of crescentic glomerulonephritis: state of the art. *Saudi J Kidney Dis Transpl* 11, 353-361 (2000).
83. D. Unnersjo-Jess, L. Scott, H. Blom, H. Brismar, Super-resolution stimulated emission depletion imaging of slit diaphragm proteins in optically cleared kidney tissue. *Kidney Int* 89, 243-247 (2016).
84. S. Safarikia et al., Distinct EpCAM-Positive Stem Cell Niches Are Engaged in Chronic and Neoplastic Liver Diseases. *Front Med (Lausanne)* 7, 479 (2020).
85. A. Shiba-Ishii et al., High expression of stratifin is a universal abnormality during the course of malignant progression of early-stage lung adenocarcinoma. *Int J Cancer* 129, 2445-2453 (2011).
86. J. Lin et al., Regulation of Cancer Stem Cell Self-Renewal by HOXB9 Antagonizes Endoplasmic Reticulum Stress-Induced Melanoma Cell Apoptosis via the miR-765-FOXA2 Axis. *J Invest Dermatol* 138, 1609-1619 (2018).
87. S. Bhatlekar, J. Z. Fields, B. M. Boman, Role of HOX Genes in Stem Cell Differentiation and Cancer. *Stem Cells Int* 2018, 3569493 (2018).
88. M. Munz, P. A. Baeuerle, O. Gires, The emerging role of EpCAM in cancer and stem cell signaling. *Cancer Res* 69, 5627-5629 (2009).
89. A. Peired et al., Proteinuria impairs podocyte regeneration by sequestering retinoic acid. *J Am Soc Nephrol* 24, 1756-1768 (2013).
90. E. Lazzeri, M. L. Angelotti, C. Conte, H. J. Anders, P. Romagnani, Surviving Acute Organ Failure: Cell Polyploidization and Progenitor Proliferation. *Trends Mol Med* 25, 366-381 (2019).
91. Y. Dai et al., Retinoic acid improves nephrotoxic serum-induced glomerulonephritis through activation of podocyte retinoic acid receptor alpha. *Kidney Int* 92, 1444-1457 (2017).

92. P. Romagnani, Toward the identification of a "renopietic system"? *Stem Cells* 27, 2247-2253 (2009).
93. K. Sainio, A. Raatikainen-Ahokas, Mesonephric kidney--a stem cell factory? *Int J Dev Biol* 43, 435-439 (1999).
94. S. S. Roeder et al., Activated ERK1/2 increases CD44 in glomerular parietal epithelial cells leading to matrix expansion. *Kidney Int* 91, 896-913 (2017).
95. C. C. Estrada, A. Maldonado, S. K. Mallipattu, Therapeutic Inhibition of VEGF Signaling and Associated Nephrotoxicities. *J Am Soc Nephrol* 30, 187-200 (2019).
96. S. Saw, A. Weiss, R. Khokha, P. D. Waterhouse, Metalloproteases: On the Watch in the Hematopoietic Niche. *Trends Immunol* 40, 1053-1070 (2019).
97. H. J. Snippert, A. G. Schepers, J. H. van Es, B. D. Simons, H. Clevers, Biased competition between Lgr5 intestinal stem cells driven by oncogenic mutation induces clonal expansion. *EMBO Rep* 15, 62-69 (2014).
98. A. G. Schepers et al., Lineage tracing reveals Lgr5+ stem cell activity in mouse intestinal adenomas. *Science* 337, 730-735 (2012).
99. H. Fu, R. R. Subramanian, S. C. Masters, 14-3-3 proteins: structure, function, and regulation. *Annu Rev Pharmacol Toxicol* 40, 617-647 (2000).
100. D. K. Morrison, The 14-3-3 proteins: integrators of diverse signaling cues that impact cell fate and cancer development. *Trends Cell Biol* 19, 16-23 (2009).
101. T. C. Chang et al., 14-3-3sigma regulates beta-catenin-mediated mouse embryonic stem cell proliferation by sequestering GSK-3beta. *PLoS One* 7, e40193 (2012).
102. J. Jiang et al., 14-3-3 regulates the LNK/JAK2 pathway in mouse hematopoietic stem and progenitor cells. *J Clin Invest* 122, 2079-2091 (2012).
103. F. Cianfarani et al., Impaired keratinocyte proliferative and clonogenic potential in transgenic mice overexpressing 14-3-3sigma in the epidermis. *J Invest Dermatol* 131, 1821-1829 (2011).
104. X. Fan et al., 14-3-3 Proteins Are on the Crossroads of Cancer, Aging, and Age-Related Neurodegenerative Disease. *Int J Mol Sci* 20, (2019).
105. A. Bersenev et al., Lnk constrains myeloproliferative diseases in mice. *J Clin Invest* 120, 2058-2069 (2010).
106. F. Baran-Marszak et al., Expression level and differential JAK2-V617F-binding of the adaptor protein Lnk regulates JAK2-mediated signals in myeloproliferative neoplasms. *Blood* 116, 5961-5971 (2010).
107. S. Grouls et al., Lineage specification of parietal epithelial cells requires beta-catenin/Wnt signaling. *J Am Soc Nephrol* 23, 63-72 (2012).
108. T. Ulyanova et al., VCAM-1 expression in adult hematopoietic and nonhematopoietic cells is controlled by tissue-inductive signals and reflects their developmental origin. *Blood* 106, 86-94 (2005).
109. A. Rambaldi et al., Safety and efficacy of the maximum tolerated dose of givinostat in polycythemia vera: a two-part Phase Ib/II study. *Leukemia*, (2020).
110. J. Mascarenhas, Rationale for combination therapy in myelofibrosis. *Best Pract Res Clin Haematol* 27, 197-208 (2014).